A comparison of wave-dominated cross-shore sand transport models

Enschede, May 2010

W.H. Wong
Water Engineering & Management
University of Twente
The Netherlands

A COMPARISON OF WAVE-DOMINATED CROSS-SHORE SAND TRANSPORT MODELS

Enschede, May 2010

Master's Thesis of:
W.H. Wong
Water Engineering & Management
University of Twente

Supervisors:
Dr. ir. J.S. Ribberink
Water Engineering & Management
University of Twente

Drs. J.J.L.M. Schretlen
Water Engineering & Management
University of Twente

Dr. K.M. Wijnberg
Water Engineering & Management
University of Twente

UNIVERSITY OF TWENTE.

TABLE OF CONTENT

PREFACE

In front of you lies the final report that presents the results of my graduation assignment. This master thesis marks the end of my study Water Engineering & Management at the University of Twente.

I would like to thank my supervisors Jan, Jolanthe and Kathelijne for their patience and time. Thank you for your advices during the past year. Also, thank you for always having time to help me with my thesis. Furthermore, I would like to thank my roommates of the graduation room and the employees of the Water Engineering & Management department for contributing to a good working and social environment. I enjoyed spending my time in the graduation room and the group activities we had (especially the food related activities like the barbeques and the hot potting).

I hope you enjoy reading this thesis!

Wing Hong Wong
Enschede, May 2010

SUMMARY

Most of the existing cross-shore sand transport models for coastal areas are based on data measured in experiments conducted in oscillatory flow tunnels (OFT). In these experiments boundary layer streaming, which is a steady current near the bed induced by surface waves, does not occur. The boundary layer streaming can contribute to the sand transport. In the recent years, practical wave-dominated cross-shore sand transport models have been developed that include boundary layer streaming. These models are based on concepts of existing models that are developed with data from oscillatory flow tunnel experiments. To include the influences of the boundary layer streaming, the developers of the models modified the existing formulas by adding an additional streaming component into the models for surface wave conditions.

The objectives of this study are i) identifying which model is the most suitable for predicting wave dominated cross-shore sand transport and ii) gaining more understanding of the influences of the boundary layer streaming on the model performances under surface wave conditions. To reach the objectives, the sand transport predictions of the models of Nielsen (2006), Van Rijn (2007) and the recently developed SANTOSS model are compared with a large dataset of measured sand transports in OFT experiments and surface wave experiments. Furthermore, model intercomparisons are carried out to assess which model gives the best performance in cross-shore sand transport predictions under general wave dominated conditions.

This study shows that the streaming components of the model of Van Rijn (2007) and the SANTOSS model improve the model performances under surface wave conditions. Both models perform well under these conditions. The model of Nielsen (2006) performs better if the streaming component is not included. If streaming is included, the model overestimates the sand transport under surface wave conditions.

A comparison between the sand transport predictions and sand transport measured in a wide range of sediment and hydrodynamic conditions shows that the overall best performance is obtained by the SANTOSS model. The major differences between the SANTOSS model and the other two models are that the SANTOSS model is capable to account for influences of the phase-lag effects and for the influences of acceleration skewness. The better performance of the SANTOSS model is also partly caused by the fact that the model is calibrated with the datasets that are used for the comparisons. It may be noted that a small part of these datasets are also used for calibration and validation of the other two models.

An attempt is made to adjust the models of Nielsen (2006) and Van Rijn (2007). The approach of the SANTOSS model to account for the phase-lag effects is implemented into the two models. The model performances improve, but the good performance of the SANTOSS model still cannot be obtained by the other two models.

1 INTRODUCTION

1.1 NEW SAND TRANSPORT MODELS

Due to the increasing amount of activities in the coastal areas, it is becoming more and more important to be able to predict the morphological developments in these areas. For instance, it is important to predict if sand nourishments will bury the coastal habitats (due to the migration of sand), understand if a beach will grow or erode away, or predict how a navigational route will develop. Therefore, understanding of cross-shore sand transport is of importance for the safety, navigability and ecology in coastal areas.

To develop sand transport models, it is important to understand the sand transport under different conditions. During storm conditions, high flow velocities cause ripples to be washed out and, in a relative short period, large quantities of sand are transported across the bed in a thin layer (of millimetres-centimetres thick) with high sand concentrations. This is called the sheet flow regime. The sand transport in this regime is mostly determined by processes that occur close to the bed. It is difficult to perform detailed measurements of such high density sand transport in field conditions, especially at a few millimetres above the bed. Therefore, detailed measurements under controlled flow and sediment conditions in large-scale laboratories have been carried out.

Based on the knowledge obtained from these large-scale laboratory experiments many models for sand transport under waves have been developed. The majority of the experiments have been conducted in the oscillatory flow tunnels (OFT). Also, most of these experiments are done with sinusoidal and velocity skewed flows. In these experiments the process *boundary layer streaming,* which is induced by surface waves, does not occur. Boundary layer streaming is an onshore-directed constant current in the boundary layer. Various studies suggested that this process could be relevant for cross-shore sediment transport, since the current is present close to the bed and it is constant in one direction (Dohmen-Janssen and Hanes, 2002; O'Donoghue and Ribberink, 2007; Schretlen *et al.*,2008).

In the recent years practical wave-dominated cross-shore sand transport models have been developed that include boundary layer streaming. Nielsen (2006) developed a model for wave dominated cross-shore sand transport. He uses a Meyer-Peter and Müller type of formula to relate the sediment transport rate to the shear stress induced by near bed flow velocities and flow accelerations. To incorporate the influences of streaming in his sediment transport formula, Nielsen (2006) added a Wave Reynolds stress (a time-averaged shear stress) in the model. This model will hereafter be referred to as N06.

Van Rijn (2007) also developed a model that is suitable for wave dominated cross-shore sand transport. This model also relates the sediment transport rate to the shear stress induced by near bed flow velocities (and accelerations). Van Rijn (2007) modified his transport formula (Van Rijn, 1993) to incorporate the effects of boundary layer streaming. A time-averaged current at the edge of the boundary layer, representing the boundary layer streaming, will be added in the model. Van Rijn (2007) bases his method to include the effects of boundary layer streaming on the work of Davies and Villaret (1999). This model of Van Rijn (2007) will hereafter be referred to as VR07.

Recently the University of Twente and the University of Aberdeen developed a new practical sand transport model for coastal marine environment in the SANTOSS project. This model is based on the half-cycle approach of Dibajnia and Watanabe (1998); a wave will be divided into two half cycles. The sand transport rate is related to the representative bed shear stress for each half cycle. A major difference with the previous mentioned two models is that this model is able to account for phase-lag effects: sand that is entrained during the wave crest period but is transported during the trough crest period, and vice versa. Like the N06 model, this model also adds a Wave Reynolds stress to incorporate the influences of streaming (Ribberink *et al.*, 2010). This model will hereafter be referred to as the SANTOSS model.

1.2 PROBLEM DEFINITION

The three models are based on concepts of existing models. These existing models are developed with data from experiments conducted in OFTs and do not include the specific surface wave effect boundary layer streaming. To include the influences of the boundary layer streaming, the developers of the three discussed models modified the existing formulas by adding an additional streaming component into the models for surface wave conditions. However, not much measurements of sand transport in these conditions are available to validate these newly developed models.
Moreover, even though the three models can be used for wave dominated cross-shore sand transport predictions, most of the datasets used for the calibration and validation of the three models are not the same. It is not well understood which model is capable to give the best performance in predicting cross-shore wave dominated sand transport. The problem definition of this study is therefore:

> *It is not well understood which model generally performs better in cross-shore sand transport predictions and due to the limited amount of data of sand transport under surface wave conditions it is not well understood how the streaming components influences the performances of the models.*

1.3 RESEARCH OBJECTIVES

In the development of the SANTOSS model, transport measurements from different experimental facilities were collected and brought together in a large database. This database will hereafter be referred to as the SANTOSS database (Schretlen and Van der Werf, 2006; Van der Werf *et al.*, 2009). This database with measurements from different experimental facilities is available for this study for an intercomparison of the performances of the models.
Also, new surface wave experiments have been carried out in the Groβer WellenKanal in Germany (Schretlen, 2010). In these experiments detailed measurements have been conducted of sand transport and flow velocities in the boundary layer. These newly obtained data can be used to identify how well the three models perform under surface wave conditions. Therefore, the following objectives have been formulated:

> *The objectives of this study are identifying which model is the most suitable for predicting wave dominated cross-shore sand transport and gaining more understanding of the influences of the streaming components on the model performances under surface wave conditions.*

1.4 RESEARCH QUESTIONS

To reach the objectives, the following research questions have been formulated:

- *How do changes of flow and sand characteristics influence additional sand transport induced by streaming?* *(1)*
- *How does including streaming influences the performances of the models under surface wave conditions?* *(2)*
- *Which model is capable to give the best performance in cross-shore sand transport predictions for different wave dominated conditions?* *(3)*
- *Is it possible to achieve a better performance by adjusting a model with concepts of the other two models?* *(4)*

The following sub-question has been formulated:

- *Under which range of flow and bed conditions does each of the models perform well in predicting sand transport?* *(3.a)*

1.5 METHODOLOGY

This paragraph presents the approach to achieve the objectives. An overview of the necessary steps to answer the research questions is presented below.

- To make use of the SANTOSS database the formulas of the N06 and VR07 models are first programmed in MATLAB (a numerical computing environment and a programming language). The SANTOSS model is already programmed in MATLAB.
- Next, insight in the influences of the streaming components on the sand transport predictions under different flow and bed conditions are studied by investigating the influences of input parameters. For this, sand transport predictions of the models *with* and *without* the streaming components are compared (*question 1*).
- The third step is comparing the sand transport measured in surface wave experiments with calculations of the models *with* and *without* the streaming components. By comparing these two calculations more understanding is gained of the extent of influences of the streaming components on the performances (*question 2)*.
- Following this, the sand transport calculations of the models are compared with a large dataset of measured sand transports in wave dominated OFT experiments. Understanding is gained of the applicability and limitations of the models (sub-question 3.a).
- The performances of the three models are compared to identify which model is most suitable for sand transport predictions under general wave dominated conditions (*question 3)*.
- Finally, if the analyses indicate that the performance of a model can be improved with minor modifications, the model will be adjusted (*question 4*).

An overview of the research approach is presented in Figure 1:

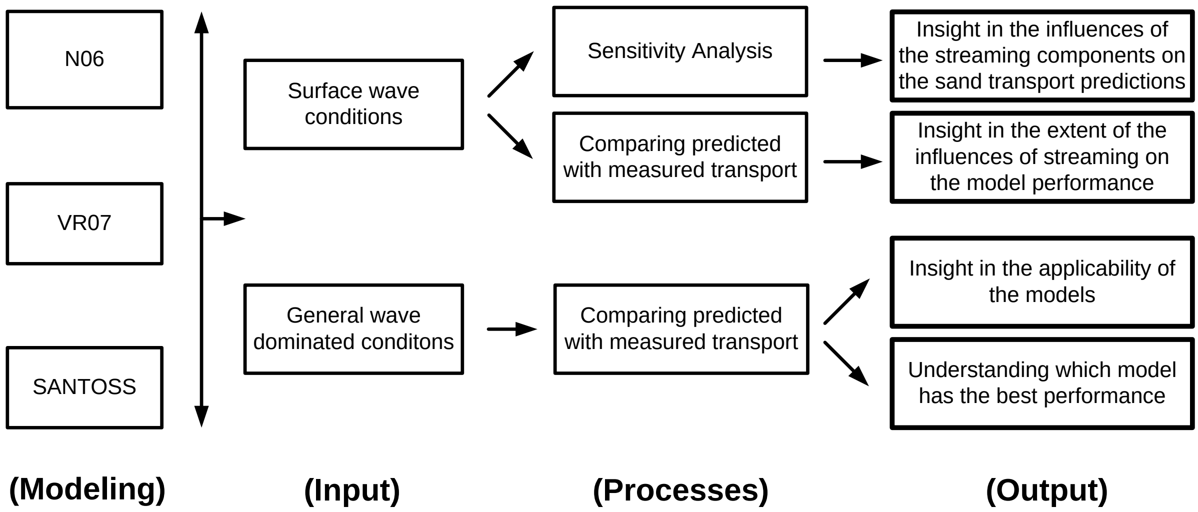

Figure 1: A research model with an overview of the approach.

1.6 FOCUS OF THE STUDY

This study is divided into two parts. The *first part* of this study focuses on getting more insight on the streaming components of the three models. These components are relevant for sand transport predictions under surface wave conditions. The streaming related sand transport can be especially large under sheet flow conditions. Due to the influence of the sea bed, the surface waves are mainly velocity skewed (chapter 2). The first part of the study therefore focuses on bed load transport in the sheet flow regime induced by non-breaking velocity skewed monochromatic surface waves. This study focuses on uniform sand.

It may be noted that streaming can be induced by surface waves and velocity skewness in oscillating flows (chapter 2). The latter type of streaming occurs under surface wave conditions *and* OFT conditions. Since the models are developed (and calibrated) with datasets obtained in OFT experiments, the influences of this type of streaming is partly indirectly included in the calibration of the models. This type of streaming is therefore not relevant in this study. This study focuses on the by surface wave induced boundary layer streaming.

The *second part* of this study focuses on the comparison of the general performances of the three models. For this, sand transport measurements under a wide range of sediment and hydrodynamic conditions from the SANTOSS database are used, i.e.:

- Non-breaking waves with different shapes (acceleration- and velocity-skewed);
- Waves combined with current;
- Large range of grain-sizes;
- Sheet flow and rippled-bed regime.

These conditions will hereafter be referred to as *general wave dominated conditions.* It may be noted that most of the sand transports are measured in OFT experiments.

1.7 OUTLINE THESIS

This study identifies how well the three sand transport models perform under wave dominated conditions. Chapter 2 starts with explaining the relevant processes for cross-shore sand transport in coastal areas. To understand how well the models perform, the sand transport predictions are compared with sand transport measurements. Chapter 3 presents an overview of the datasets with measured sand transports that are used for this comparison. Chapter 4 describes the model formulations of the three models. Using these formulas of the models, in Chapter 5 a sensitivity analysis is carried out to gain insight in the influences of the streaming components on the sand transport predictions under different flow and bed conditions (*research question 1)*. To gain more understanding of the influences of including streaming on the model performances (*research question 2*), the calculated sand transports are compared with the measured sand transport in surface wave experiments in Chapter 6. Next the model performances under general wave dominated conditions are compared in Chapter 7. More understanding will be gained about the applicability of the models. With this comparison, a conclusion is drawn about which model gives the best performance in cross-shore sand transport predictions under general wave dominated conditions (*research question 3*). Knowing the applicability and the limitations of the models, Chapter 8 proposes approaches to adjust the models for better model performances (*research question 4*). Finally, in Chapter 9 and Chapter 10 the discussion and conclusion are presented.

2 GENERAL CROSS-SHORE SAND TRANSPORT

This study focuses on wave dominated cross-shore sand transport in coastal areas. Sand transport occurs due to the interactions of the sediment lying on the sea bed and the water movements caused by waves and currents. Therefore, this chapter explains relevant processes for this interaction. First, this chapter explains how asymmetry in waves influences the near bed flow velocity. The second paragraph presents the influences of the sediment size. The relation between sand transport, flow velocity and initiation of motion expressed in the Shields parameter will be explained here. To gain more understanding of these processes, many OFT experiments have been carried out. The last paragraph discusses differences between OFT experiments and real surface waves. Explanation about the wave induced boundary layer streaming will also be given in this paragraph.

2.1 WAVE SHAPES

The influences of the roughness induced by the sea bed increases when waves travel from deep to shallow water. Due to the effects of the bed roughness the waves that are approaching a shore will shoal. In the shoaling process the wave will deform and the amplitude will increase. When the wave amplitude reaches a critical level the waves will break; large amounts of energy will be dissipated. Breaking waves transform into turbulent bores which are mostly sawtooth shaped. A wave in shallow water will not have a perfect sinusoidal shape. This paragraph describes two common type of wave asymmetry that is caused by the deformation of the waves.

When shoaling occurs in shallow water, the onshore velocity associated with the wave crest becomes stronger and of shorter duration than the offshore velocity associated with a wave trough (see Figure 2). This is known as *velocity skewness*. The degree of velocity skewness can be described as follows:

$$R = \frac{u_{\max}}{u_{\max} - u_{\min}} \tag{2.1}$$

Whereby R is the degree of velocity skewness, with u_{max} and u_{min} respectively the maximum and minimum wave induced velocity. A value of R = 0.5 means that the wave is not velocity skewed (sinusoidal).

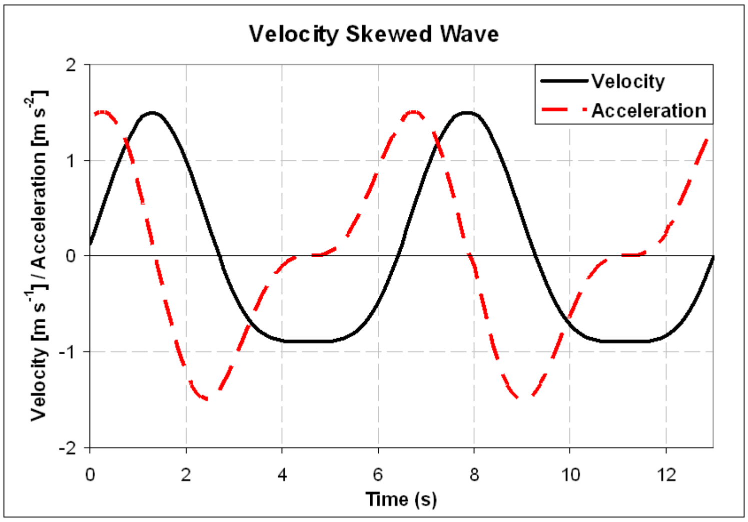

Figure 2: An example of a velocity skewed wave

During the deformation of the wave, the front of the wave can become steeper than the back; the wave become sawtooth shaped. The figure below presents the time dependent velocity and acceleration of a sawtooth shaped wave:

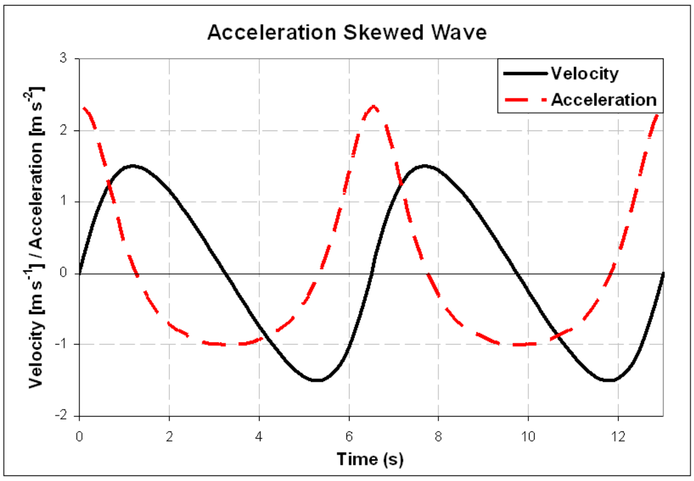

Figure 3: An example of a backward leaning acceleration skewed wave. The maximum positive acceleration is larger than the maximum negative acceleration.

As seen in the figure above, the maximum positive acceleration is larger than the maximum negative acceleration (e.g. acceleration in the negative direction). A sawtooth shaped wave is therefore also known as an acceleration skewed wave. Watanabe and Sato (2004) measured non-zero sand transport in an experiment with acceleration skewed flows that are not velocity skewed. The degree of acceleration skewness can be described as follows:

$$\beta = \frac{a_{\max}}{a_{\max} - a_{\min}} \tag{2.2}$$

Whereby β is the degree of acceleration skewness, a_{max} is the maximum positive acceleration and a_{min} is the maximum negative acceleration (acceleration in the negative direction). A value of β = 0.5 means that the wave is not acceleration skewed. The wave 'leans' forward if β < 0.5 and backward if β > 0.5. Acceleration skewness is especially important in the surf zone. It may be noted that a wave can be velocity skewed and acceleration skewed at the same time. Figure 4 presents an example of this type of wave. The wave period can be divided into the crest period T_c and trough period T_t. The T_{cu} and the T_{tu} represent the acceleration time lengths for the crest and the trough.

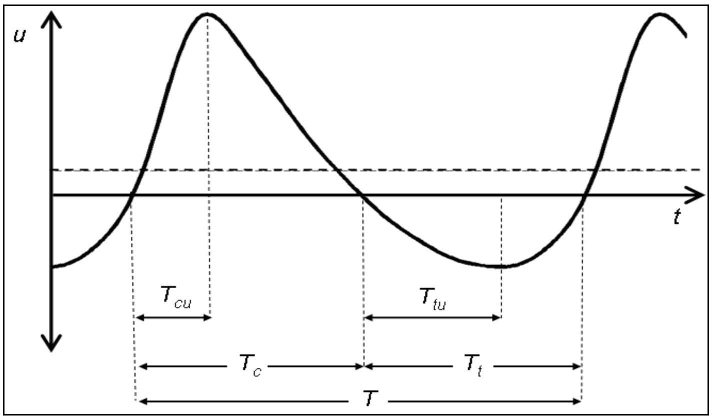

Figure 4: An example of a velocity and acceleration skewed waves as presented in Ribberink et al. (2010). T_c and T_t are the crest and trough periods, T_{cu} and T_{tu} are the crest and trough acceleration time lengths.

2.2 SAND TRANSPORT

The flow velocity caused by the waves that are described above will interact with the sand in the seabed. Sand will be brought into motion if the flow velocity is high enough. The equation below presents a way to relate the initiation of motion, the flow velocity and the sediment size. This relation can be expressed in the dimensionless stress Shields parameter:

$$\theta(t) = \frac{\frac{1}{2} f_w u_\infty^2(t)}{(s-1)gd_{50}} \tag{2.3}$$

Where s is the sediment specific gravity, d_{50} is the sediment size for which 50% of the sediment sample is finer and u_∞ is the flow velocity at the edge of the boundary layer and f_w is the wave friction factor (which is a function of the ratio between the orbital amplitude and the bed roughness). If the Shields parameter exceeds a critical value the sand particles will be brought into motion. In case of velocity skewed waves with larger velocities (onshore directed) during the positive half of the wave cycle than velocities (offshore directed) during the negative half of the wave cycle, positive onshore net sediment transport will occur.

Sand transport occurs in different regimes. O'Donoghue *et al.* (2006) characterised the regimes with the mobility number:

$$\psi_{\max} = \frac{u_{\max}^2}{(s-1)gd_{50}} \tag{2.4}$$

Whereby $u_{\max}$ the maximum velocity (velocity amplitude) represents. The ripple regime occurs for $\psi_{\max} \leq 190$ and the sheet flow regime for $\psi_{\max} \geq 300$. The transition regime has been observed for $190 < \psi_{\max} < 300$.

2.2.1 *LAG IN SAND TRANSPORT*

The instantaneous sand transport is often related to the instantaneous velocity or bed shear stress. This means that the pick-up, transport and settling down of a sand particle must take place in a much shorter time than the wave period.

Sand transport does not react instantaneously to changes in the orbital velocities. It takes time for entrained sand to settle back to the bed. When the velocity becomes zero at the end of a wave half cycle, entrained sand may be still present in the water column. The sand can therefore be transported into the opposite direction during the next half cycle. This is called the *phase-lag effect*. Under velocity skewed wave conditions, the amount of sand that is entrained in the crest period is larger than in the trough period. Furthermore, the trough period is longer than the crest period. Due to the phase-lag effects the amount of sand transport into the onshore direction will therefore decrease for velocity skewed waves. For acceleration skewed waves as presented in Figure 3 and Figure 4, the sand that is entrained due the crest peak velocity has more time to settle before the direction of the flow changes. The sand that is entrained due to the trough peak velocity has less time to settle before the direction of the flow changes. This causes an additional amount of sand transport into the onshore direction.

It has been assumed that this process is relevant for suspended sediment in the ripple-bed conditions. Experimental results from the recent years show that this effect also occurs in sheet flow conditions. It is expected to be particularly important for fine sediments, large velocities and short wave period conditions (Dohmen-Janssen *et al.* 2002). In these conditions, phase-lags between sediment concentration and near-bed velocity can become so large that they lead to a reduction or reverse of the net wave averaged transport rate.

Models that are based on the assumption that the instantaneous sand transport is related to the instantaneous flow velocity or bed shear stress are known as quasi-steady models. These models do not take the discussed phase-lag effect into account. Models that account for phase-lag effects in a parameterized way are known as semi-unsteady models.

2.3 SURFACE WAVE PROCESSES

To gain more understanding of the previously mentioned processes, detailed measurements under controlled flow and sediment conditions in large-scale laboratories have been carried out. The majority of the experiments have been conducted in oscillatory flow tunnels (OFT). Although OFTs are able to simulate surface waves well, some differences still remain. Dohmen-Janssen and Hanes (2002), Schretlen *et al.* (2008) and Ribberink *et al.* (2010) mentioned the following differences:

- For surface waves vertical orbital velocities are present while OFTs only simulate horizontal velocities. These vertical velocities influences the settling of sediments;
- Due to the vertical orbital velocities, an onshore-directed boundary layer streaming is present under surface waves. Boundary layer streaming is an onshore-directed constant current in the boundary layer.
- The flows in OFTs are uniform in the flow direction, while the orbital motions under waves have gradient in the direction of the wave propagation;
- For surface waves sediment grains near the bed move with the wave during the wave crest and against the wave during the wave trough. During this mainly horizontal motion they experience a longer crest period and a shorter trough period. This is known as the Lagrangian motion;
- Due to the uniform flow in OFTs, the pressure is in phase with the acceleration. Under surface wave the pressure is in phase with the velocity rather than with the acceleration;

Various studies suggest that of the mentioned differences between OFTs and surface waves, the boundary layer streaming is likely to be of most significance (Schretlen *et al.*,2008; Dohmen-Janssen and Hanes, 2002; O'Donoghue and Ribberink, 2007).

2.3.1 WAVE INDUCED BOUNDARY LAYER STREAMING

As discussed before, surface waves can induce a steady current known as the boundary layer streaming. There are two types of boundary layer streaming. The first one is streaming that is caused by the velocity skewness. Scandura (2007) explained that the mechanism of this streaming is due to the different characteristics of turbulence during the seaward and landward half-cycles of the wave. The difference in the generated turbulent energy results into different thickness of the boundary layer, causing the streaming. This type of streaming can be onshore directed as well as offshore directed, depending on the conditions. This study will not focus on this type of streaming since it occurs both under surface waves and in OFTs.

The second type of streaming occurs under surface waves. Under real waves, the horizontal and vertical velocities in a wave motion with a viscous bottom boundary layer are not exactly 90^{o} out of phase as they would be in a perfectly wave motion (Nielsen, 1992). This results into an onshore directed mean velocity in the boundary layer. OFTs only generate horizontal velocities; this type of streaming therefore does not occur in OFT experiments.

Under sheet flow conditions the onshore directed streaming generated under surface waves is more dominant than the offshore directed streaming induced by asymmetry in the turbulence intensity due to velocity skewness (Naqshband, 2009).

Schretlen *et al*. (2008) show the total mean velocity profile in a wave flume experiment.

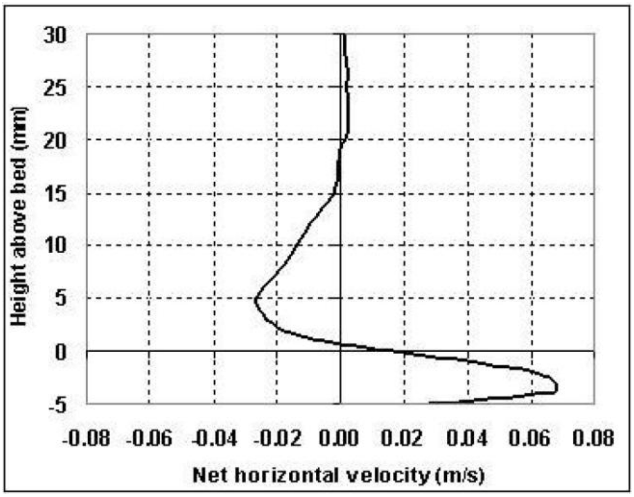

Figure 5: The velocity profile of a flume experiment as presented in Schretlen *et al*, (2008). The experimental conditions are onshore directed (positive) velocity can be seen near the bed.

Figure 5 presents a velocity profile from a flume experiment (Schretlen *et al.,* 2008). The figure shows a positive onshore directed velocity from approximately 1 mm above the original bed level downwards. Schretlen *et al.* (2008) discussed that this net onshore directed flow velocity is possibly caused by wave-asymmetry and boundary layer streaming. The magnitude of this onshore directed velocity varies between the different wave conditions in the experiments of Schretlen *et al*. (2008), but the trend is similar in all experimental runs.

The magnitude of streaming is small with respect to the orbital velocities. However, despite the small value of this streaming compared to the orbital velocities, the streaming-related sand flux can be high since it is constant in one direction and it is located in the sheet flow layer where the sand concentration is high (Schretlen *et al*.,2008; Dohmen-Janssen and Hanes, 2002; O'Donoghue and Ribberink, 2007).

3 EXPERIMENTAL DATA

To reach the objectives of this study, the sand transport predicted by the three models will be compared with sand transport measurements. For this comparison the sand transport measurements that are aggregated in the SANTOSS database will be used. The first part of this chapter presents information about this database.

The measurements in the database are mainly obtained with experiments carried out in OFTs. To extend the database with sand transport measured in surface wave conditions, new measurements were carried out in the large wave flume in Hannover. In this study more detailed analysis will be carried out for these surface wave conditions. The second part of this chapter therefore presents information about the experimental facility, the set-up of the experiments, measuring instruments and the sand transport measurements.

3.1 THE SANTOSS DATABASE

The SANTOSS model is developed in the SANTOSS project. In the SANTOSS project, cross-shore sand transport data has been collected from various experiments from the last two decades. The SANTOSS database consists of data measured in sheet-flow and ripple regimes. The measurements of the data in the database are from experiments conducted from different facilities, ranging from small scale oscillatory flow tunnels to large wave flumes (Schretlen and Van der Werf, 2006; Van der Werf *et al.*, 2009). The database contains sand transport measurements in wave dominated and current dominated experiments (this study only focuses on the wave dominated conditions). Table 1 and Table 2 present the specifications of the datasets that are used in this study. A more detailed overview of the different datasets can be seen in Appendix A.

Table 1: The different type of flow and the amount of available data

Type of flow	Amount of available data
Velocity skewed waves	94
Acceleration skewed waves	53
Wave with currents	50
Surface waves	14

Table 2: Specifications of the wave dominated data

Parameter	Range of data
Medium grain size d50 (mm)	0.13 – 0.46
Flow period T (s)	4 – 12.5
Degree of velocity skewness R (-)	0.5 – 0.75
Degree of acceleration skewness β (-)	0.5 – 0.8

3.2 Surface wave data

The database is extended with sand transports measured in flume experiments (Schretlen, 2010). First information about the experimental facility (paragraph 3.2.1) and the set-up of the experiments (paragraph 3.2.2) are given. Next an explanation about the measured velocity (paragraph 3.2.3) is presented. Finally, the sand transport measurements in flume experiments are summarized (paragraph 3.2.4).

3.2.1 *The experimental facility*

The flume data that is used in this study is obtained from experiments performed in the large wave flume the Groβer Wellenkanal (GWK) of the Coastal Research Centre in Hannover, Germany. The GWK consist of a basin with a length of 280 m, a width of 5 m and a depth of 7 m. The flume is capable of generating regular and irregular waves with heights from 0.5 to 2.5 m, with periods from 2 to 15 s. The experiments can be performed without the influences of re-reflection due to the online absorption system which is present at the wave generator (Schretlen *et al*., 2008).

3.2.2 *Measurement set-ups Grober Wellenkanal*

Figure 6 gives an overview of the set-up of the experiments. A 1 m thick horizontal sand bed is present at approximately 50 to 175 m. From approximately 175 to 280 m, a 1:12 sand beach is present. The still water level during all experiments was 4.5 m above the flumes bottom. The instruments for velocity and concentration measurements are located at approximately 110 m (represented by the dashed line in Figure 6).

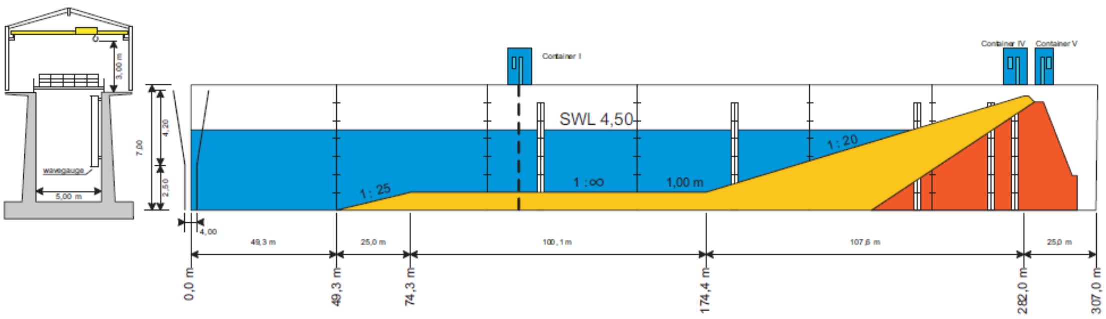

Figure 6: The experimental set-up in the Groβer Wellenkanal as presented in Schretlen *et al*. (2008)

For the detailed measurements of the near bed flow velocity and sand concentration, special rigs were designed. The measurements were performed mainly from a wall measuring frame and a measuring tank buried underneath the sand surface.

3.2.3 MEASURED VELOCITY

During the measurements in the GWK, experiments have been carried out with regular waves and (ir)regular wave groups. For this study only the single, regular waves are relevant.

In the experiments, detailed velocity profiles between approximately a depth of z = -5 mm (in the pick-up layer) and z = 60 mm have been measured. For this measurement, ultrasonic velocity profilers (UVP) have been used. The UVP based its measurements on pulsed ultrasound echography together with a detection of Doppler shift frequency. The low acoustic frequency of the UVP enables it to measure flows with high sediment concentrations (O'Donoghue and Wright, 2004). It may be noted that the models uses *free stream velocities* (i.e. velocities outside the boundary layer) as input. Only the flow velocities at a depth of 40 mm above the bed of the new flume experiments will be used in this study.

The measured velocity can be divided into two components; an oscillating, time dependent velocity and a current velocity:

$$u(t) = \langle u \rangle + \tilde{u}(t) \tag{3.1}$$

The oscillating velocity $\tilde{u}(t)$ represents the near-bed orbital velocity. The constant current velocity <u> represents the boundary layer streaming. Both the models of Nielsen (2006) and van Rijn (2007) are originally developed to calculate sand transport due to the near-bed orbital velocity $\tilde{u}(t)$. The models therefore only use the near-bed orbital velocities as input. The effects of <u> that represents the boundary layer streaming will be calculated with different methods. An overview of flow characteristics and measured velocities is given in Table 3.

3.2.4 *MEASURED NET SAND TRANSPORT*

During the GWK experiments, the bed levels over the entire length of the flume were measured before and after each test with help of echo sounders. By applying the mass conservation law to the measured bed profiles, the net sand transport is determined during each test.

The GWK experiments have been conducted with fine and medium sand. Table 3 presents the sand characteristics and the measured mean net sand transport (at the location of the instruments). It may be noted that only the experiments where sheet flow occurs are shown here.

Table 3: An overview of the surface wave data measured in the GWK.

Code	h (m)	d50 (mm)	H (m)	T (s)	Uon (m/s)	Uof (m/s)	R	β	Qs(10^{-6} m^2/s)	<u> (m/s)
Re1565_08F	3,5	0,138	1,5	6,5	1,55	0,83	0,65	0,50	51,59	0,06
Re1265_08F	3,5	0,138	1,2	6,5	1,25	0,75	0,63	0,50	37,50	0,03
Re1575_08F	3,5	0,138	1,5	7,5	1,70	0,69	0,71	0,50	69,48	0,09
Re1550_08F	3,5	0,138	1,5	5,0	1,28	1,02	0,56	0,50	40,71	0,03
Re1565_07M	3,5	0,245	1,5	6,5	1,66	0,92	0,65	0,50	64,83	0,03
Re1575_08M	3,5	0,245	1,5	7,5	1,43	0,61	0,70	0,50	42,26	0,08
Re1565_08M	3,5	0,245	1,5	6,5	1,58	0,90	0,64	0,50	48,43	0,06
Re1550_08M	3,5	0,245	1,5	5,0	1,49	1,21	0,55	0,50	32,91	0,04
MI	3,5	0,240	1,4	6,5	1,03	0,75	0,58	0,50	33,80	0,05
MH	3,5	0,240	1,6	6,5	1,13	0,68	0,62	0,46	42,90	0,04
MF	3,5	0,240	1,3	9,1	1,35	0,66	0,67	0,56	76,70	0,04
ME	3,5	0,240	1,5	9,1	1,50	0,59	0,72	0,56	107,30	0,05

H is the wave height, h is the water depth, d_{50} is the medium grain size, T is the period, U_{on} and U_{off} are the peak crest and trough orbital velocities, R and β are the degree of velocity and acceleration skewness and Q_s is the measured net sand transport rate.

As seen in the table, there are twelve sand transport measurements. The first eight conditions are newly obtained data. These are data obtained by Schretlen (2010). The last four conditions are surface wave data obtained by Dohmen-Janssen and Hanes (2002). These data are longer available and are used to validate the N06 model. The reference level of the data of Schretlen (2010) is z = 40 mm and Dohmen-Janssen and Hanes (2002) is approximately z = 100 mm.

4 MODELS

This chapter gives the descriptions of the three sand transport models. Each model description starts with describing how the model accounts for the near bed flow velocity. Next the calculation of the bed shear stress is described. Finally, the relation between the bed shear stress and the sand transport is presented. Paragraphs 4.1, 4.2 and 4.3 present the model formulations of respectively N06, VR07 and the SANTOSS model. Paragraph 4.4 presents an overview of the three practical models. It may be noted that both the N06 and the VR07 models requires time dependent near bed velocities as input. This is not available in the SANTOSS database. Therefore, to use the SANTOSS database, time dependent velocities will be generated with the peak crest orbital velocity and the peak trough orbital velocity. See Appendix C for more information.

4.1 THE N06 MODEL

The N06 model is a quasi-steady model developed for wave dominated cross-shore sand transport. This model is based on the formulas of Nielsen and Calaghan (2003). The N06 model incorporates the influence of different wave shapes (velocity- and acceleration skewness). A 'filter method' (Nielsen, 1992) is used in which the influences of the acceleration is weighted against the influences of the velocity. The N06 model incorporates the surface wave specific effect boundary layer streaming by adding a Wave Reynolds stress (which is a time-averaged shear stress) on top of the stress induced by near bed flow velocities and flow accelerations. This paragraph presents the formulas of the N06 model.

4.1.1 APPLICABILITY

The N06 model can be applied for the calculation of:

- Instantaneous wave induced cross-shore sediment transport;
- sediment transport due to waves with different shapes (velocity- and/or acceleration-skewed);
- sediment transport induced by wave boundary layer streaming.

4.1.2 THE FILTER METHOD

The N06 model uses the filter method (Nielsen, 1992) to account for both the effects of the velocity and the acceleration skewness. The effects of the acceleration skewness and velocity skewness will be weighted with the angle φ_τ ; a sediment mobilizing velocity is calculated:

$$u_\theta(t) = \sqrt{\frac{1}{2} f_{2.5}} \left(\cos\varphi_\tau u_\infty + \sin\varphi_\tau \frac{1}{\omega_p} \frac{du_{\delta,w}}{dt} \right) \tag{4.1}$$

In which:

$$u_\infty(t) = u_{\delta,w} + u_\delta \tag{4.2}$$

$$f_{2.5} = \exp\left[5.5 \left(\frac{2.5 d_{50}}{A} \right)^{0.2} - 6.3 \right] \tag{4.3}$$

$$A = \frac{\sqrt{2}}{\omega} \sqrt{\operatorname{var}\{u_\infty(t)\}} \tag{4.4}$$

Whereby $f_{2.5}$ is the grain roughness friction factor, u_∞ the instantaneous velocity due to currents and waves is at the edge of the boundary layer, $u_{\delta,w}$ is the instantaneous velocity due to waves at the edge of the boundary layer and u_δ is the current velocity at the edge of the boundary layer, ω is the angular frequency, A is the representative semi excursion, $du_{\delta,w} / dt$ is the acceleration and φ_τ is the angle that weights the effect of the sediment mobilizing forces due to drag and to acceleration. Var{u_∞(t)} represents the variance of the free stream velocity. An optimized angle of φ_τ = 47° is found (Guard and Nielsen, 2010). It may be noted that this filter method is applied to all sand transport calculations (Nielsen, 2006), even for conditions in which the wave shape is not acceleration skewed.

4.1.3 STREAMING RELATED BED SHEAR STRESS

The non-dimensional bed shear stress is calculated as the Shield parameter:

$$\theta(t) = \frac{u_\theta^2}{(s-1)gd_{50}} \tag{4.5}$$

Surface waves induce an additional steady current in the boundary layer that results into an additional shear stress. Nielsen (2006) adds an additional stress for surface wave conditions. The total Shields parameter for surface wave is described as follows:

$$\theta(t) = \left| \frac{|u_\theta| u_\theta - (\overline{\tilde{u}\tilde{w}})_\infty}{(s-1)gd_{50}} \right| \tag{4.6}$$

In which:

$$-(\overline{\tilde{u}\tilde{w}})_\infty = \frac{2}{3\pi} f_e A^3 \omega^3 / c \tag{4.7}$$

$$f_e = \exp\left[5.5 \left(\frac{170\sqrt{\hat{\theta}_{2.5} - 0.05} d_{50}}{A} \right)^{0.2} - 6.3 \right] \tag{4.8}$$

$$\omega = \frac{2\pi}{T} \tag{4.9}$$

Whereby ω is the angular frequency, T is the wave period, *s* is sediment specific gravity ($s = \rho_s / \rho$), *c* is the wave celerity, $\hat{\theta}_{2.5}$ is the peak value of the grain roughness Shields parameter corresponding to the friction equation (4.3) and f_e is the wave energy dissipation factor. The term $-(\overline{\tilde{u}\tilde{w}})_\infty / \left[(s-1)gd_{50}\right]$ represents the time averaged dimensionless shear stress caused by the fact that the horizontal and vertical velocities in a wave motion with a viscous bottom layer are not exactly 90° out of phase (Nielsen and Callaghan, 2003). It may be noted that for the calculation of the effects of streaming, the friction factor for 'mobile bed' f_e is used, instead of the grain roughness friction factor $f_{2.5}$.

4.1.4 MEYER-PETER AND MÜLLER SEDIMENT TRANSPORT

Finally, to calculate the instantaneous sediment transport rate, a Meyer-Peter Müller type of formula is used:

$$q_s(t)\begin{cases}12\left[\theta(t)-0.05\right]\sqrt{\theta(t)}\,\dfrac{u_\theta(t)}{|u_\theta(t)|}*\sqrt{(s-1)gd_{50}^3} & for \quad \theta(t)>0.05\\ 0 & for \quad \theta(t)<0.05\end{cases} \tag{4.10}$$

Whereby $q_s(t)$ is the instantaneous sediment transport rate, s is the sediment specific gravity, d_{50} is the sediment size for which 50% of the sediment sample is finer, u_θ is the sediment mobilizing velocity and $\theta(t)$ is het instantaneous Shields parameter.

4.1.5 VALIDATION N06

Nielsen (2006) used tunnel data of Watabe and Sato (2004) for the calibration of his filter method. He validates this filter method and his wave Reynolds stress with a dataset of transport measured in flume experiments of Dohmen-Janssen and Hanes (2002). This dataset contains sand transports measured in experiments with surface waves that are velocity skewed and acceleration skewed. In the experiments sand transport of sand with a d_{50} of 0.25 mm is measured at 10 cm above the bed. The flow period ranges from 6.4 to 9.2 s and the wave height from 1.3 to 1.6 m. Furthermore, Nielsen (2006) also compared his model with datasets of Ribberink and Al-Salem (1994), Dohmen-Janssen (1999) and O'Donoghue and Wright (2004). It may be noted that these datasets are also collected in the SANTOSS database (Van der Werf *et al.*, 2009).

4.1.6 LIMITATIONS N06

The N06 model has several limitations:

- N06 is not able to account for the influences of the phase-lag effects. The model is therefore not suitable for rippled-bed conditions and sheet flow conditions with fine sediments, large velocities and short wave periods;
- The value of φ_τ = 47° is an optimal overall value. The range of the optimal values of φ_τ for different conditions in the experiments of Nielsen (2006) is relatively large (between φ_τ =40° and φ_τ =62°). However, Nielsen (2006) concluded that the general shift in results due to the change of 11° in the value of φ_τ is seen to be of the same order as the general scatter;
- Lagrangian motion has not been addressed explicitly. It has been correlated with the part with boundary layer streaming in equation (4.6);
- The effects of vertical orbital velocity has not been addressed;
- The results of the model are only compared to the net transport rate $\overline{q}_s$. It may be noted that a good agreement of the model results with the $\overline{q}_s$ should not be taken as a proof of equally good general agreement with $q_s(t)$.

4.2 THE VR07 MODEL

The VR07 model is a general bed-load transport model that can be used for both steady and oscillatory flows. It is a quasi-steady model in which the local instantaneous transport rate is related to the instantaneous bed-shear stress. Van Rijn (2007) suggests using the approach of Nielsen and Callaghan (2003) to include the influences of acceleration skewness in his model.

To include the effects of boundary layer streaming, Van Rijn (2007) analysed the work of Davies and Villaret (1999) and suggests a method to add an additional current velocity at the edge of the boundary layer. This paragraph presents the formulas of the VR07 model.

4.2.1 APPLICABILITY

The VR07 model can be applied for the calculation of:

- instantaneous wave induced cross-shore sediment transport;
- sediment transport due to steady currents;
- sediment transport due to waves with different shapes (velocity- and/or acceleration-skewed);
- sediment transport induced by wave boundary layer streaming.

4.2.2 VELOCITY

The velocity in the VR07 model contains a wave-related and a current related component. The wave-related component is a time dependent oscillatory flow, while the current-related component is a steady flow. The velocity at the edge of the boundary layer can therefore be described as follows:

$$u_\infty(t) = u_{\delta,w}(t) + u_\delta \tag{4.11}$$

Whereby u_∞ the instantaneous velocity due to currents and waves is at the edge of the boundary layer, $u_{\delta,w}$ is the instantaneous velocity due to waves at the edge of the boundary layer and u_δ is the current velocity at the edge of the boundary layer. The current velocity u_δ can represents any current velocities at the edge of the boundary layer. For instance, the current velocity can be induced by wind, tide or the steady flow in a river. For this study the wave boundary layer is the most important current.

To account for the influences of boundary layer streaming, an additional steady current velocity is added at the edge of the boundary layer. Van Rijn (2007) analysed the model and experimental results of Davies and Villaret (1999) and found a relation between the relative roughness and the magnitude and direction of the streaming velocity:

$$A_w = \frac{H}{2\sinh(2kh)} \tag{4.12}$$

$$u_{\delta,s} \begin{cases} 0.75 U_W^{\,2}/c & \text{for } A_w/K_{s,w} \geq 100 \\ \left(-1 + 0.875\log\left(\dfrac{A_w}{K_{s,w}}\right)\right) U_W^{\,2}/c & \text{for } 1 < A_w/K_{s,w} < 100 \\ -U_W^{\,2}/c & \text{for } A_w/K_{s,w} \leq 1 \end{cases} \tag{4.13}$$

Whereby $u_{\delta,s}$ is the wave-induced boundary layer streaming, U_w is the peak orbital velocity at the edge of the boundary layer (added to the current velocity u_δ in equation (4.11)), c is the wave celerity, A_w is the orbital excursion at the edge of the boundary layer and $K_{s,w}$ is the wave-related bed roughness. A_w/ $K_{s,w}$ represent the relative roughness. The streaming velocity is onshore directed under conditions with a large relative roughness (i.e. sheet flow conditions) and offshore directed under conditions with a small relative roughness (i.e. rippled-bed conditions). Van Rijn (2007) proposes to calculate the wave-related bed roughness with the same equation as the current-related bed roughness:

$$k_{s,w}\begin{cases}150 f_{cs} d_{50} & for\,\psi \le 50 \\ (182.5-0.652\psi) f_{cs} d_{50} & for\,50 < \psi \le 250 \\ 20 f_{cs} d_{50} & for\,\psi > 250\end{cases} \tag{4.14}$$

In which:

$$\psi = \frac{U_{wc}^2}{(s-1)gd_{50}} \tag{4.15}$$

$$U_{wc} = \sqrt{U_w^2 + u_c^2} \tag{4.16}$$

$$U_w = \frac{\pi H_s}{T\ \sinh(2kh)} \tag{4.17}$$

$$f_{cs}\begin{cases}(0.25 d_{gravel} / d_{50})^{1.5} & d_{50} > 0.25 d_{gravel} \\ 1 & d_{50} \le 0.25 d_{gravel}\end{cases} \tag{4.18}$$

Whereby U_w is the peak orbital velocity at the edge of the boundary layer (van Rijn, 1993), u_c is the depth averaged current velocity, H_s is the significant wave height, d_{gravel} = 0.002m, s is sediment specific gravity and ψ is the mobility number.

4.2.2.1 ACCELERATION SKEWED WAVES

To weigh the effects between velocity skewness and acceleration skewness van Rijn suggests using the approach of Nielsen and Callaghan (2003). This is the earlier mentioned 'filter method'. Van Rijn (2007) indicates that he uses this method as an 'input switch'. In this study, this method will therefore only be applied to acceleration skewed waves (in contrary to the N06 model in which the filter method is applied to all conditions).

$$U_\infty(t) = \cos\varphi_\tau (u_{\delta,w}(t) + u_\delta) + \sin\varphi_\tau \frac{1}{\omega}\frac{du_{\delta,w}}{dt} \tag{4.19}$$

Van Rijn (2007) suggests to use φ_τ =40°.

4.2.3 BED SHEAR STRESS

The VR07 model uses an instantaneous grain-related bed-shear stress. The instantaneous grain-related bed-shear stress can be calculated as follows:

$$\tau'_{b,cw}(t) = 0.5\rho_w f'_{cw}\left[u_\infty(t)\right]^2 \tag{4.20}$$

In which:

$$f'_{cw} = \alpha\beta f_c' + (1-\alpha) f'_w \tag{4.21}$$

With:

$$\alpha = \frac{u_c}{u_c + U_w} \tag{4.22}$$

$$f_c' = \frac{8g}{[18\log(12h/k_{s,grain})]^2} \tag{4.23}$$

$$f'_w = \exp[-6 + 5.2(\hat{A}_\delta / k_{s,grain})^{-0.19}] \tag{4.24}$$

$$\beta = 0.25\left[\frac{-1+\ln(30h/k_{s,c})}{\ln(30\delta/k_{s,c})}\right]^2 \tag{4.25}$$

Whereby $\tau'_{b,cw}$ is the instantaneous grain-related bed-shear stress, u_c is depth-averaged current velocity, β is the coefficient related to the vertical structure of the velocity profile, $k_{s,c}$ is the current-related bed roughness that is calculated like the wave-related bed roughness (equation(4.14)), ρ_w is the water density, f_c' is the current-related grain friction coefficient based on $k_{s,grain} = d_{90}$ and f'_w is the wave-related grain friction coefficient based on $k_{s,grain} = d_{90}$.

4.2.4 THE SEDIMENT TRANSPORT

The bed-load transport in VR07 can be calculated with the following equation:

$$q_s(t) = \gamma\rho_s f_{silt} d_{50} D_*^{-0.3}(\tau'_{b,cw}(t)/\rho)^{0.5}[(\tau'_{b,cw}(t)-\tau_{b,cr})/\tau_{b,cr}]^\eta \frac{U_{\delta,cw}(t)}{\left|U_{\delta,cw}(t)\right|} \tag{4.26}$$

In which:

$$D_* = d_{50}[(s-1)g/\upsilon^2]^{1/3} \tag{4.27}$$

$$f_{silt}\begin{cases} d_{sand}/d_{50} & if\ d_{50} \le d_{sand} \\ 1 & if\ d_{50} > d_{sand} \end{cases} \tag{4.28}$$

$$\tau'_{b,cr} = \vartheta_{cr} \cdot g\left(\rho_s - \rho\right) \cdot d_{50} \tag{4.29}$$

With θ_{cr} (Whitehouse, 1998):

$$\theta_{\mathrm{cr}} = \frac{0.24}{D_*} + 0.055\left(1 - \exp\left(-0.02 D_*\right)\right) \tag{4.30}$$

Whereby $q_s(t)$ is the instantaneous sediment transport rate, γ is the a coefficient with the value 0.5, D_* is the dimensionless particle size, f_{silt} is the silt factor, $\tau'_{b,cr}$ is the critical bed-shear stress according to Shields, ρ_s is the sediment density, s is the relative density, η is equal to 1, d_{sand} is the class separation diameter for sand which is equal to 62 μm and υ is the kinematic viscosity coefficient. The coefficients γ and η were recalibrated using measured data sets (d_{50} > 0.2 mm) of the large-scale wave tunnel of Delft Hydraulics (Ribberink 1998; Van Rijn 2000). It may be noted that the calculation of the transport works well if the medium grain size is larger than 2 millimetres (Van Rijn, 2007).

4.2.5 VALIDATION

Van Rijn (2007) mentioned in his paper that he calibrated his model with datasets of Ribberink (1998) and Van Rijn (2000). A part of these datasets are obtained by Katapodi et al. (1994), Ramadan (1994) and Ribberink and Al-Salem (1994). These datasets are also collected in the SANTOSS database.
Van Rijn (2007) used field measurements of bed-form transport (sand transport in rippled-bed regime) in coastal areas to validate his model (for wave dominated situations). Field data obtained by Hoekstra *et al*. (2001) in the project COAST3D is used for the validation. In the project, bed-form dimensions, bed-form migration and bed-form transport of sand with a d_{50} of 0.3 mm is measured in shallow depth on Spratt Sand near the town of Teignmouth, United Kingdom. The tidal range was about 4-5 m, water depths were between 1 and 4 m. Wave and current conditions at about 1 m above the bed were also recorded during the tidal cycle (van Rijn, 2007). It may be noted that no information is given about the shape of the waves during the field measurements. It is therefore not clear if Van Rijn (2007) used the filter method (which he includes in his model as an *input switch* for acceleration skewed waves) for these conditions.

The filter method with φ_τ =40^{o} to account for the influences of acceleration skewness is validated for one sand transport measurement of Ribberink *et al*. (2000). It may be noted that no information is given about the degree of acceleration skewness of the waves during the experiment.

4.2.6 LIMITATIONS

The VR07 model has several limitations:

- VR07 is not able to account for the influences of the phase-lag effects. The model is therefore not suitable for rippled-bed conditions and sheet flow conditions with fine sediments, large velocities and short wave periods;
- Lagrangian mass transport of sediment has not been addressed;
- The effects of vertical orbital velocity has not been addressed;
- The results of the model are only compared to the net transport rate $\overline{q}_s$. Good agreement of the model results with the $\overline{q}_s$ should not be taken as a proof of equally good general agreement with the time dependent $q_s(t)$.

4.3 SANTOSS

SANTOSS is a model for net sand transport induced by non-breaking waves and currents. The model is based on the 'half-cycle' approach of Dibajnia and Watanabe (1998). By modifying this approach, the SANTOSS model incorporates the influences of phase-lag and different wave shapes in the sand transport calculations. The model is calibrated on a large set of data from oscillatory flow tunnel experiments covering a wide range of hydraulic conditions. Like the N06 model, this model also adds a Wave Reynolds stress to incorporate the influences of streaming

4.3.1 APPLICABILITY

The SANTOSS model can be applied for the calculation of:

- wave induced cross-shore sediment transport;
- sediment transport due to steady currents;
- sediment transport due to waves with different shapes (velocity- and/or acceleration-skewed);
- sediment transport for surface wave conditions (including the effects of lagrangian motion, vertical orbital velocities and wave boundary layer streaming);
- sediment transport for conditions in which phase-lag is important (i.e. rippled-bed conditions or in sheet flow conditions for fine sediment, large velocities and short wave periods).

4.3.2 VELOCITY

The SANTOSS model does not uses time series as input for the model. Instead of this two representative values of the velocity are used for the calculation of the sand transport. The figure presents the velocities the model uses for the calculation:

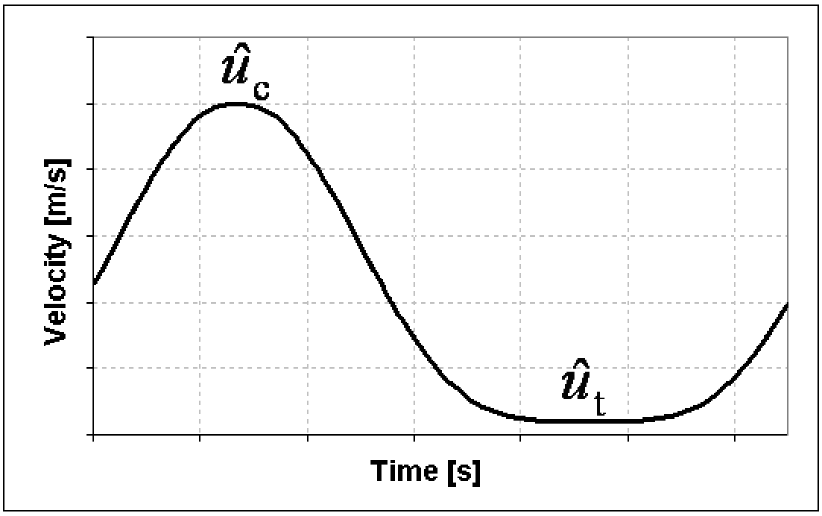

Figure 7: A velocity skewed wave with the representative velocities that the model uses.

The figure above shows the maximum onshore and offshore velocities at the edge of the boundary layer (respectively $\hat{u}_c$ and $\hat{u}_t$). On top of these two values, the model is capable to include a steady current velocity. It may be noted that boundary layer streaming is incorporated in this model as a Wave Reynolds stress and not as a current velocity. Figure 8 presents a short overview of how the velocity of a current is included in the model.

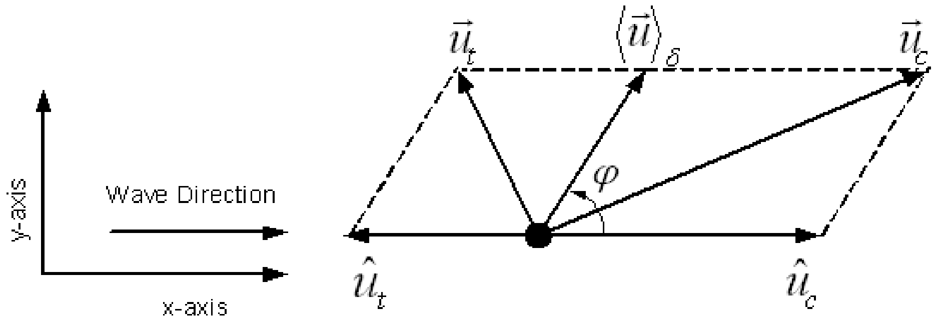

Figure 8: An overview of the waves and the currents in the SANTOSS model

The direction of the x-axis is determined by the wave direction. In the figure $\hat{u}_c$ and $\hat{u}_t$ are the peak crest and peak trough orbital velocity respectively. The $\vec{u}_\delta$ in the figure represents the current that can be induced by density gradients, tide, wind or waves. It may be noted that for this study the angle between the current and the direction of the wave propagation φ is 0^O or 180^o.

4.3.2.1 SAWTOOTH SHAPED WAVES; HALF-CYCLE APPROACH

To include the effects of acceleration skewness, the SANTOSS model divide a wave period as follows:

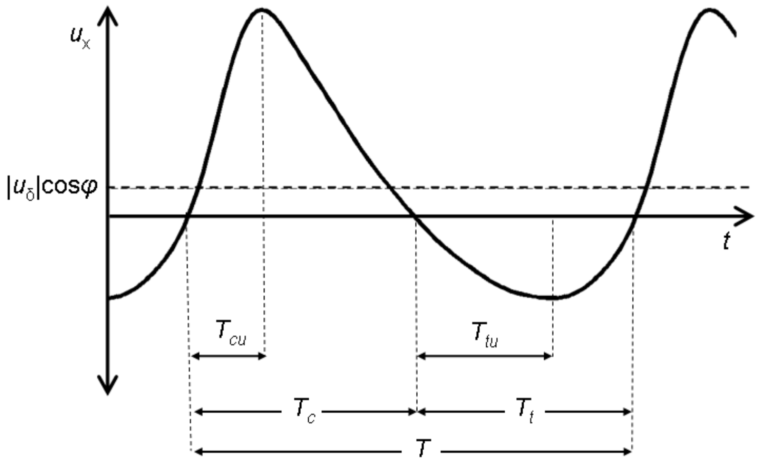

Figure 9: Velocity time series in wave direction. T_c and T_t are the crest and trough periods, T_{cu} and T_{tu} are the crest and trough acceleration time lengths.

In the figure above, T_c and T_t are the crest and trough periods, T_{cu} and T_{tu} are the crest and trough acceleration time lengths. For acceleration-skewed waves the acceleration time length of the crest T_{cu} is generally shorter than the acceleration time length for the trough T_{tu}. The parameters T_{cu} and T_{tu} will be used for the calculation of the friction factors and the calculation of the transport rate. The formulas will be presented later on in this chapter. The characteristic orbital velocity amplitude $\hat{u}$ and the characteristic orbital excursion amplitude $\hat{a}$ can be calculated as follows:

$$\hat{u} = \sqrt{\frac{1}{2}\hat{u}_c^2 + \frac{1}{2}\hat{u}_t^2} \tag{4.31}$$

$$\hat{a} = \frac{\hat{u}T}{2\pi} \tag{4.32}$$

In order to enhance the wave friction factor (which will be presented later on) for acceleration skewness, the excursion amplitudes for the crest and trough half cycles are determined as follows (see Figure 9):

$$\hat{a}_{\mathrm{c}} = \frac{2T_{\mathrm{cu}}}{T_{\mathrm{c}}}\hat{a} \tag{4.33}$$

$$\hat{a}_{\mathrm{t}} = \frac{2T_{\mathrm{tu}}}{T_{\mathrm{t}}}\hat{a} \tag{4.34}$$

4.3.3 BED SHEAR STRESS

The magnitudes of the non-dimensional bed shear stresses under the wave crest and trough are defined as follows:

$$|\theta_{\mathrm{c}}| = \frac{\frac{1}{2} f_{\mathrm{w\delta c}} |u_{\mathrm{c}}|^2}{(s-1)gd_{50}} \tag{4.35}$$

$$|\theta_{\mathrm{t}}| = \frac{\frac{1}{2} f_{\mathrm{w\delta t}} |u_{\mathrm{t}}|^2}{(s-1)gd_{50}} \tag{4.36}$$

The friction factors include both the friction due to the oscillating flow and the friction due to a constant current. The friction factors are calculated as follows:

$$f_{\mathrm{w\delta c}} = \alpha f_{\delta} + (1-\alpha) f_{\mathrm{wc}} \tag{4.37}$$

$$f_{\mathrm{w\delta t}} = \alpha f_{\delta} + (1-\alpha) f_{\mathrm{wt}} \tag{4.38}$$

In which:

$$\alpha = \frac{\sigma |u_{\delta}|}{\sigma |u_{\delta}| + \hat{u}} \tag{4.39}$$

Factor σ is a calibration factor for wave + current conditions. In the final calibration σ = 3.

The formulas to calculate the friction factors are presented below. The wave friction factor at the wave crest can be calculated as follows:

$$f_{\mathrm{wc}} = 0.00251 \exp\left[5.21\left(\frac{\left(\frac{2T_{\mathrm{cu}}}{T_{\mathrm{c}}}\right)^2 \hat{a}}{k_{\mathrm{sw}}}\right)^{-0.19}\right] \quad \text{for} \quad \frac{\hat{a}}{k_{\mathrm{sw}}} > 1.587$$

$$f_{\mathrm{wc}} = 0.3 \quad \text{for} \quad \frac{\hat{a}}{k_{\mathrm{sw}}} \leq 1.587 \tag{4.40}$$

The wave friction factor at the trough can be calculated as follows:

$$f_{\mathrm{wt}} = 0.00251\exp\left[5.21\left(\frac{\left(\frac{2T_{\mathrm{tu}}}{T_{\mathrm{t}}}\right)^2 \hat{a}}{k_{\mathrm{sw}}}\right)^{-0.19}\right] \qquad \text{for} \qquad \frac{\hat{a}}{k_{\mathrm{sw}}} > 1.587$$

$$f_{\mathrm{wt}} = 0.3 \qquad \text{for} \qquad \frac{\hat{a}}{k_{\mathrm{sw}}} \leq 1.587 \qquad (4.41)$$

The current-related friction factor is calculated assuming a logarithmic velocity profile:

$$f_{\delta} = 2\left[\frac{0.4}{\ln\left(30\delta/k_{s\delta}\right)}\right]^2 \qquad (4.42)$$

The current roughness height and wave roughness height include additional roughness related to the sheet flow layer in the following way:

$$k_{\mathrm{sw}} = \max\{d_{50}, d_{50}[\mu + 6(\langle|\theta|\rangle - 1)]\} + 0.4\eta^2/\lambda \qquad (4.43)$$

$$k_{s\delta} = \max\{3d_{90}, d_{50}[\mu + 6(\langle|\theta|\rangle - 1)]\} + 0.4\eta^2/\lambda \qquad (4.44)$$

With:

$$\langle|\theta|\rangle = \frac{\frac{1}{2} f_{\delta} |u_{\delta}|^2}{(s-1)gd_{50}} + \frac{\frac{1}{4} f_{\mathrm{w}} \hat{u}^2}{(s-1)gd_{50}} \qquad (4.45)$$

$$\mu = \begin{cases} 6 & \text{if } d_{50} \leq 0.15\ 10^{-3}\ \mathrm{m} \\ \left[6 + \left(10^3 d_{50} - 0.15\right)\frac{(1-6)}{(0.20-0.15)}\right] & \text{if } 0.15\ 10^{-3}\mathrm{m} < d_{50} < 0.20\ 10^{-3}\mathrm{m} \\ 1 & \text{if } d_{50} \geq 0.20\ 10^{-3}\ \mathrm{m} \end{cases} \qquad (4.46)$$

Whereby η and λ respectively the ripple height and ripple length represent. These values are based on the approach of O'Donoghue *et al*. (2006) (See Ribberink *et al.* (2010) for more details).

In case no waves are present (α = 0) and a mean current is the only driving mechanism for sand transport the expressions above automatically lead to a Shields parameter for current alone:

$$|\theta_c| = |\theta_t| = \frac{\frac{1}{2} f_{\delta} u_{\delta}^2}{(s-1)gd_{50}} \qquad (4.47)$$

4.3.4 *SANTOSS'* RELEVANT SURFACE WAVE PROCESSES

While the other two models only consider wave induced boundary layer streaming as the only relevant surface wave process, the SANTOSS model incorporates three surface wave effects in the calculation of the sand transport;

- The influence of Lagrangian grain motion on the crest and trough period ;
- The influence of the vertical orbital velocity on the grain settling velocity;
- The influence of the wave-Reynolds stress.

4.3.4.1 LAGRANGIAN MOTION

For surface waves sediment grains move with the wave during the wave crest and against the wave during the wave trough (Lagrangian motion). In this way they experience a longer crest period and a shorter trough period.

$$T_{c,sw} = T_c + \Delta T_c \tag{4.48}$$

$$T_{t,,sw} = T_t - \Delta T_t \tag{4.49}$$

In which:

$$\Delta T_c = \left\{ \frac{c}{\zeta \hat{u}} \pi - 2 \right\}^{-1} T \tag{4.50}$$

$$\Delta T_t = \left\{ \frac{c}{\zeta \hat{u}} \pi + 2 \right\}^{-1} T \tag{4.51}$$

Whereby ΔT_c and ΔT_t represent respectively the longer crest period and the shorter trough period. Herein ζ is the ratio of the horizontal grain-velocity amplitude and free-stream velocity amplitude. Based on measurements in a large wave flume (GWK, Hannover) under sheet flow conditions, Schretlen (2010) showed that this factor is constant for a range of conditions. The reduction factor is approximately $\zeta = 0.55$.

4.3.4.2 VERTICAL ORBITAL VELOCITY

For surface waves a vertical orbital velocity is present which affects the settling (velocity) of grains. The following expression for the vertical orbital velocity amplitude has been used at elevation *z* near the bed $\hat{w}(z)$, based on non-linear (2nd-order Stokes) wave theory:

$$\hat{w}_1(z) = \frac{\pi H}{T} \frac{z}{h} \quad \text{(first order)} \tag{4.52}$$

$$\hat{w}_2(z) = \hat{w}_1 2(2R-1) \quad \text{(second order)} \tag{4.53}$$

The maximum amplitude (for $R \neq 0.5$) can be calculated with:

$$\hat{w}(z) = \frac{1}{8}\hat{w}_1 \sqrt{64 - \frac{\left(-\hat{w}_1 + \sqrt{\hat{w}_1^2 + 32\hat{w}_2^2}\right)^2}{\hat{w}_2^2}} + \hat{w}_2 \sin\left(2\arccos\left(\frac{1}{8}\frac{-\hat{w}_1 + \sqrt{\hat{w}_1^2 + 32\hat{w}_2^2}}{\hat{w}_2}\right)\right) \tag{4.54}$$

This vertical velocity amplitude influences the phase-lag effects, which will be discussed later on in this chapter. During the settling of the of the crest-load the vertical orbital velocity is downward and enhance the settling. During the settling of the trough-load the vertical orbital velocity is upward and reduces the settling. The vertical orbital velocity therefore contributes to additional onshore directed sand transport (Ribberink *et al.* , 2010).

4.3.4.3 WAVE REYNOLDS STRESS

The SANTOSS model includes the effects of boundary layer streaming with the same method as the model of Nielsen (2006). An extra Reynolds stress (in the direction of the wave propagation) will be added to the shear stress that is calculated as described above.

$$\theta_{c,sw} = \theta_c + \theta_{wRe} \tag{4.55}$$

$$\theta_{t,sw} = \theta_t - \theta_{w_{Re}} \tag{4.56}$$

It may be noted that for the calculation of the mean absolute Shields parameter, the Reynolds stress is not included. The wave Reynolds Shields parameter θ_{wRe} can be calculated as follows:

$$\theta_{\mathrm{w\,Re}} = \frac{\tau_{\mathrm{wRe}}}{\rho(s-1)gd_{50}} \tag{4.57}$$

Whereby

$$\tau_{\mathrm{w\,Re}} = \rho \frac{4 f_{\mathrm{w}\delta}}{6\pi c} \hat{u}^3 \tag{4.58}$$

It may be noted that the friction factor used here is not the same as the *friction factor for mobile bed* that is used by Nielsen (2006). The Wave Reynolds stress is therefore not the same as the one in the N06 model.The wave propagation speed *c* can be calculated using the (implicit) dispersion relation:

$$c = \frac{L}{T} \tag{4.59}$$

$$L = \frac{gT^2}{2\pi} \tanh\left(\frac{2\pi h}{L}\right) \tag{4.60}$$

4.3.5 SEDIMENT TRANSPORT

In the SANTOSS model the net sand transport $\vec{q}_s$ is computed as follows:

$$\vec{q}_{\mathrm{s}} = \frac{\sqrt{|\theta_{\mathrm{c}}|} T_{\mathrm{c}} \left(\Omega_{\mathrm{cc}} + \frac{T_{\mathrm{c}}}{2T_{\mathrm{cu}}} \Omega_{\mathrm{tc}}\right) \frac{\vec{\theta}_{\mathrm{c}}}{|\theta_{\mathrm{c}}|} + \sqrt{|\theta_{\mathrm{t}}|} T_{\mathrm{t}} \left(\Omega_{\mathrm{tt}} + \frac{T_{\mathrm{t}}}{2T_{\mathrm{tu}}} \Omega_{\mathrm{ct}}\right) \frac{\vec{\theta}_{\mathrm{t}}}{|\theta_{\mathrm{t}}|}}{T} \sqrt{(s-1)gd_{50}^3} \tag{4.61}$$

Note that for surface wave transport: $\vec{\theta}_c = \vec{\theta}_{c,sw}$, $\vec{\theta}_t = \vec{\theta}_{t,sw}$, $T_c = T_{c,sw}$ and $T_t = T_{t,sw}$. The transport is divided into four contributions (distinguished by when sand is entrained and when sand is transported). The table below presents an overview of these contributions:

Table 4: The four contributions of the sand transport

Transported / Entrained	Crest	Trough
Crest	Ω_{cc}	Ω_{ct}
Trough	Ω_{tc}	Ω_{tt}

The transport contributions are calculated in the following manner:

$$\Omega_{\mathrm{cc}} = \begin{cases} \Omega_{\mathrm{c}} & \text{if} \quad P_c \le 1 \\ \frac{1}{P_{\mathrm{c}}} \Omega_{\mathrm{c}} & \text{if} \quad P_c > 1 \end{cases} \tag{4.62}$$

$$\Omega_{\mathrm{ct}} = \begin{cases} 0 & \text{if} \quad P_{\mathrm{c}} \le 1 \\ \frac{(P_{\mathrm{c}} - 1)}{P_{\mathrm{c}}} \Omega_{\mathrm{c}} & \text{if} \quad P_c > 1 \end{cases} \tag{4.63}$$

$$\Omega_{tt} = \begin{cases} \Omega_t & \text{if} \quad P_t \le 1 \\ \dfrac{1}{P_t}\Omega_t & \text{if} \quad P_t > 1 \end{cases} \tag{4.64}$$

$$\Omega_{tc} = \begin{cases} 0 & \text{if} \quad P_t \le 1 \\ \dfrac{(P_t - 1)}{P_t}\Omega_t & \text{if} \quad P_t > 1 \end{cases} \tag{4.65}$$

Where the sand loads are described as:

$$\Omega_c = \begin{cases} 0 & \text{if} \quad |\theta_c| \le \theta_{cr} \\ m\left(|\theta_c| - \theta_{cr}\right)^n & \text{if} \quad |\theta_c| > \theta_{cr} \end{cases} \tag{4.66}$$

$$\Omega_t = \begin{cases} 0 & \text{if} \quad |\theta_t| \le \theta_{cr} \\ m\left(|\theta_t| - \theta_{cr}\right)^n & \text{if} \quad |\theta_t| > \theta_{cr} \end{cases} \tag{4.67}$$

where m=9.41 and n=1.2 (both calibration coefficients). The critical shields number is determined as follows:

$$\theta_{cr} = \frac{0.3}{\left(1 + 1.2D^*\right)} + 0.055\left(1 - \exp\left(-0.02D^*\right)\right) \tag{4.68}$$

In which

$$D^* = \left(\frac{(s-1)g}{\nu^2}\right)^{1/3} d_{50} \tag{4.69}$$

Whereby ν the kinematic viscosity of water represents. The phase-lag parameters can be calculated with the following equations.

$$P_c \begin{cases} \alpha_r \dfrac{\eta}{2\left(T_c - T_{cu}\right) w_s} & \text{if} \quad \eta > 0 \\ \alpha_s \dfrac{\delta_{sc}}{2\left(T_c - T_{cu}\right) w_s} & \text{if} \quad \eta = 0 \end{cases} \tag{4.70}$$

$$P_t \begin{cases} \alpha_r \dfrac{\eta}{2\left(T_t - T_{tu}\right) w_s} & \text{if} \quad \eta > 0 \\ \alpha_s \dfrac{\delta_{st}}{2\left(T_t - T_{tu}\right) w_s} & \text{if} \quad \eta = 0 \end{cases} \tag{4.71}$$

In the equations above, α_s =8 and α_r = 9.3 (both are calibration coefficients). δ_{st} represents the sheet flow layer thickness (see Ribberink *et al*. 2010 for more details). W_s represents the fall velocity and can be calculated as follows:

$$w_s = \frac{\nu}{0.8 d_{50}}\left(\sqrt{10.36^2 + 1.049 D_s^{*3}} - 10.36\right) \quad (4.72)$$

In which:

$$D_s^* = \left(\frac{(s-1)g}{\nu^2}\right)^{1/3} 0.8 d_{50} \quad (4.73)$$

For surface waves, the settlings velocities are corrected with the vertical orbital velocity at level $z = r$ above the bed as follows:

$$\begin{aligned} w_{s,c} &= w_s + \hat{w}(r_c) \\ w_{s,t} &= w_s - \hat{w}(r_t) \ \ (\geq\ 0) \end{aligned} \quad (4.74)$$

With:

$$r_c = \begin{cases} 3\eta & \text{if } \eta > 0 \text{ (ripple regime)} \\ 3\delta_{sc} & \text{if } \eta = 0 \text{ (sheet flow regime)} \end{cases} \quad (4.75)$$

$$r_t = \begin{cases} 3\eta & \text{if } \eta > 0 \text{ (ripple regime)} \\ 3\delta_{st} & \text{if } \eta = 0 \text{ (sheet flow regime)} \end{cases} \quad (4.76)$$

4.3.6 VALIDATION

The SANTOSS model is calibrated using a wide range of data. The following specifications can be given of the calibration data (Ribberink *et al*. 2010):

- Number of wave-alone (velocity-skewed) experiments : 92
- Number of wave-alone (acceleration-skewed) experiments : 53
- Number of wave+current experiments: 50
- Number of experiments with progressive surface waves: 11
- Total number of experiments : 206

It may be noted that even though a lot of data is used for the calibration, the model has not been validated for the wave-dominated situations. The model is only validated for a set of 137 bed-load transport measurements in steady currents (Guy *et al*., 1966; Nnadi and Wilson, 1992).

4.3.7 LIMITATIONS

The only limitation of the SANTOSS model is that it is not able to calculate time dependent sand transport $q_s(t)$.

4.4 OVERVIEW OF THE MODELS

As seen in the previous paragraphs, the three models use different approaches to account for processes that are relevant for wave dominated sand transport. This paragraph presents an overview of the models and a comparison of the approaches of the three models.

Table 19 summarizes how the models account for different processes. As seen in the table, both N06 and VR07 are quasi-steady models. The two models relate the instantaneous sand transport to the instantaneous flow velocity; the models do not account for the influences of the phase-lag effects. Among the three models, SANTOSS is the only semi-unsteady model. The model accounts for the phase-lag effects in a parameterized way. A phase-lag parameter is calculated as the ratio of stirring height and settling distance during each half cycle. Due to this approach to account for the influences of the phase-lag effects, the SANTOSS model can be applied to rippled-bed conditions and sheet flow conditions with fine sediment, large velocities and short wave periods. However, in contrary to the other two models, the SANTOSS model is not able to calculate time dependent sand transports.

Table 19 shows that all three models account for the influences of boundary layer streaming under surface wave conditions. Both N06 and the SANTOSS model use the wave Reynolds stress to do this. The wave Reynolds stress is a constant stress that induces additional onshore directed sand transport. The difference between the wave Reynolds stress of N06 and the SANTOSS model is that N06 uses the *friction factor for mobile bed* while the SANTOSS model uses the *wave friction factor* (or the *combined wave-current friction factor* for the 'waves combined with current' conditions). The friction factor used by N06 is larger than the one used by the SANTOSS model, which means that the wave Reynolds stress of N06 induces more additional sand transport. The approach of VR07 to account for the influences of boundary layer streaming is totally different compared to the other two models. Instead of a constant wave Reynolds stress, a steady current velocity is added to the orbital velocity. This current is onshore directed under sheet flow conditions and offshore directed under rippled-bed conditions. Among the streaming components of the three models, only the streaming component of VR07 can be offshore directed.

While N06 and VR07 consider boundary layer streaming as the only relevant surface wave effect, the SANTOSS model accounts for three surface wave effects; the boundary layer streaming, Lagrangian motion and vertical orbital velocity. All three processes contribute to additional onshore directed sand transport.

As seen in Table 19, all three models are able to account for the influences of acceleration skewness. N06 and VR07 both use the filter method in which the influences of velocity skewness and acceleration skewness are weighted with the angle φ_τ. N06 uses the angle φ_τ = 47^o and VR07 the angle φ_τ = 40^o. The SANTOSS model uses a different approach to account for the influences of acceleration skewness. The friction factor, amount of bed load and phase-lag parameter of each half-cycle are adjusted based on the degree of acceleration skewness.

The short comparison in this paragraph shows that all three models are able to account for the surface wave effects and the influences of acceleration skewness. A difference is that the surface wave effects are described more extensively by the SANTOSS model. Furthermore, compared to the other two models the SANTOSS model can be applied to a wider range of conditions due to its approach to accounts for the influences of the phase-lag effects. However, only N06 and VR07 can be used for time dependent sand transport calculations.

Table 5 An overview of the three practical sand transport models

	N06	VR07	SANTOSS
Type of model	Quasi-steady	Quasi-steady	Semi-unsteady
Applicability	Wave dominated conditions	Wave and current dominated conditions	Wave and current dominated conditions
Phase-lag effects	None	None	A phase-lag parameter is calculated as the ratio of stirring height and settling distance during each half cycle.
Boundary layer streaming	Adding a positive wave Reynolds stress. The friction factor for mobile bed f_e is used.	Adding a steady current at the edge of the boundary layer. Current can be onshore or offshore directed.	Adding a positive wave Reynolds stress. The wave friction factor is used. If a current is present, a combined wave-current friction factor is used.
Other surface wave effects	None	None	Vertical orbital velocity and Lagrangian motion.
Acceleration skewness	Weighing the influences of acceleration skewness and velocity skewness with the angle $\varphi_\tau = 47^o$.	Weighing the influences of acceleration skewness and velocity skewness with the angle $\varphi_\tau = 40^o$.	Influences of acceleration skewness are accounted in the calculation of the friction factors, the sediment loads and the phase-lag parameter.

5 SENSITIVITY ANALYSIS

This chapter presents a sensitivity analysis to gain insight in the influences of the streaming components on the sand transport predictions under different flow and bed conditions. This is done by changing the input conditions and analyzing the variations in the output. To identify the specific influences of the streaming components on the computed sand transports, the behaviours of the models have been analysed i) without the streaming component and ii) with the streaming components.

First paragraph 5.1 presents the conditions that are used for the sensitivity analysis. The choice of these conditions will be explained. Paragraph 5.2 until paragraph 5.4 present the results of the sensitivity analysis. Finally, in paragraph 5.5 the results of the sensitivity analysis are summarized.

5.1 RANGE OF CONDITIONS

In the sensitivity analysis the variation in the output due to changes in the input will be analyzed. For this, a random realistic starting condition has been chosen. The table below presents this starting condition.

Table 6: The starting condition of the sensitivity analyses

h (m)	d50	Hw (m)	T (s)	Uon (m/s)	Uoff (m/s)	R	B
3	0,25	1	5	1,3	0,87	0,6	0,5

One parameter will be varied to see the corresponding effect on the sand transport. It may be noted that flat beds are assumed to be present. The parameters that will be varied are parameters that are used in all three of the models for the sand transport calculation. The following parameters will be varied:

- *The flow period T*: The flow period characterize the duration of a wave. This parameter influences the wave propagation speed that is relevant for the streaming component of all three models (see chapter 4). The flow period also influences processes like the phase-lag effect (since a short flow period means that a sand particle has less time to settle before the direction of the flow changes);
- *The grain size d_{50}*: The grain size is an important parameter for the amount of sand being brought into motion. It influences the shear stress at the bed. Also, as discussed earlier, fine sand is more sensitive to the phase-lag effects due to the smaller fall velocity and the lower critical velocity for entrainment. Furthermore, the grain size influences the friction factors and bed roughness, both parameters are used in the three models for computing the effects of streaming on the sand transport;
- *The onshore peak orbital velocity U_{on} (and U_{off})*: The onshore peak orbital velocity influences the amount of entrained sand. Furthermore, high flow velocities cause sand particles to be stirred up high. This influences the phase-lag effects as well.

The range in which the parameters will be varied is based on data from the SANTOSS database. This database contains real experimental conditions and therefore represents a realistic range of variation of the parameters. For each parameter, maximum and minimum values have been found in the database. These values are presented in Table 7:

Table 7: The minimum and maximum values of the parameters

Parameter	Minimum value	Maximum value
d50 (mm)	0.128	0.460
T (s)	4	12
Uon (m/s)	0.77	1.72

It may be noted that the degree of velocity skewness is remained constant on R = 0.6 during the sensitivity analysis of the peak orbital velocities by varying the U_{on} and U_{off} simultaneously. Furthermore, the changes of the flow period T and the peak orbital velocities U_{on} and U_{off} influences the wave height H_w. The non-linear wave theory has been used to account for the changes of the wave height:

$$H_w = 2\frac{\sinh kh}{\omega}u_1 \tag{5.1}$$

$$u_1 = \frac{U_{on} + |U_{off}|}{2} \tag{5.2}$$

5.2 BEHAVIOUR MODELS ON GRAIN SIZE VARIATION

In this paragraph the behaviour of the models are studied by investigating the influence of the medium grain size. Figure 10 presents the calculated net transport rates as function of the medium grain size. In this paragraph, first the behaviours of the models are investigated without the streaming components. After that, the influences of the streaming components on the predicted sand transport are investigated.

The dotted lines represent the calculations of the sand transport without including the streaming components. As seen in the figure, the behaviours of the three models are comparable to each other. The amount of calculated sand transport increases for the increasing sediment size. For the conditions d_{50} < 0.2 mm, the SANTOSS model behaves differently compared to the other two models; the amount of calculated sand transport decreases faster for a decreasing sediment size. This is due to the phase-lag effects (equation (4.70) and equation (4.71)); the amount of transport in the onshore direction decreases. A 'change in trend' can be observed in the sand transport calculation by the SANTOSS model at d_{50} = 0.16 mm. This is caused by the method used for the calculation of the wave roughness height (equation (4.43) and equation (4.46)). Three different formulas are given for the conditions $d_{50} \leq 0.15$ mm, 0.15 mm < d_{50} < 0.20 mm and $d_{50} \geq 0.20$ mm. As seen in the figure, if the effects of streaming are not included, the N06 model predicts the largest amount of sand transport compared to the other models. VR07 calculates the smallest amount of sand transport.

In Figure 10 the solid lines in the figure represent the calculations of the sand transport including the streaming components. The difference between a solid line and a dotted line represents the additional sand transport induced by the streaming component of a model. The behaviours of the three models are no longer comparable to each other. The amount of sand transport predicted by the N06 model nearly tripled after streaming is included into the calculation of the sand transport. Even though the SANTOSS model also uses the Wave Reynolds stress to account for the influences of streaming, the same amount of additional sand transport due to streaming cannot be observed. This is due to the different friction factor that is used for the N06 model. For the calculation of the wave Reynolds stress, Nielsen (2006) uses a friction factor for mobile bed f_e that is considerably larger than the grain roughness friction factor $f_{2.5}$ (equation (4.8)). This results into a larger Wave Reynolds stress.

After including the streaming component, the VR07 model behaves differently compared to the N06 model. The N06 model shows a steady increase in sand transport predictions for an increasing sediment size. The VR07 only shows a steady increase in sand transport predictions for an increasing sediment size between d_{50} = 0.13 mm and d_{50} = 0.31 mm. Further increase in sediment size after d_{50} = 0.31 mm results into a decrease of the amount of predicted sand transport. This is caused by the method that is used for the calculation of the streaming velocity (equation (4.13)). The streaming velocity is onshore directed for a large relative roughness ($A_w/k_{s,w} \geq 100$) and offshore directed for a small relative roughness ($A_w/k_{s,w} \leq 1$). In Figure 10, after the grain size became larger than 0.31 mm, the relative roughness became smaller than 100. The amount of additional transport induced by the streaming velocity therefore gradually decreases for the increasing sediment size. It may be noted that among the three models, VR07 is the only model that is able to generate offshore directed streaming.

As seen in Figure 10, the additional sand transport caused by the streaming component of the SANTOSS model is the smallest among the three models. As discussed before, the wave Reynolds stress of the SANTOSS model is smaller compared to the one of the N06 model due to the different friction factors. Furthermore, while the other models consider streaming as the only surface wave effect, the SANTOSS model accounts for more surface wave effects. The model splits the surface wave effects up in i) boundary layer streaming, ii) Lagrangian motion and iii) vertical orbital velocities. All three processes contribute to additional onshore directed sand transport.

For the SANTOSS model with streaming, the change in trend still can be observed at d_{50} = 0.20 mm and d_{50} = 0.16 mm (not as clear as before). As explained before, this is due to the fact that different formulas are used for the calculation of the wave roughness height for the conditions $d_{50} \leq$ 0.15 mm, 0.15 mm < d_{50} < 0.2 mm and $d_{50} \geq$ 0.2 mm. It may be noted that the 'the change of trend' looks different compared to before. The reason for this is that for the calculation of the wave Reynolds stress the wave roughness height is used. The wave Reynold stress use different wave roughness heights at d_{50} = 0.13 mm, d_{50} = 0.16 mm and d_{50} = 0.20 mm.

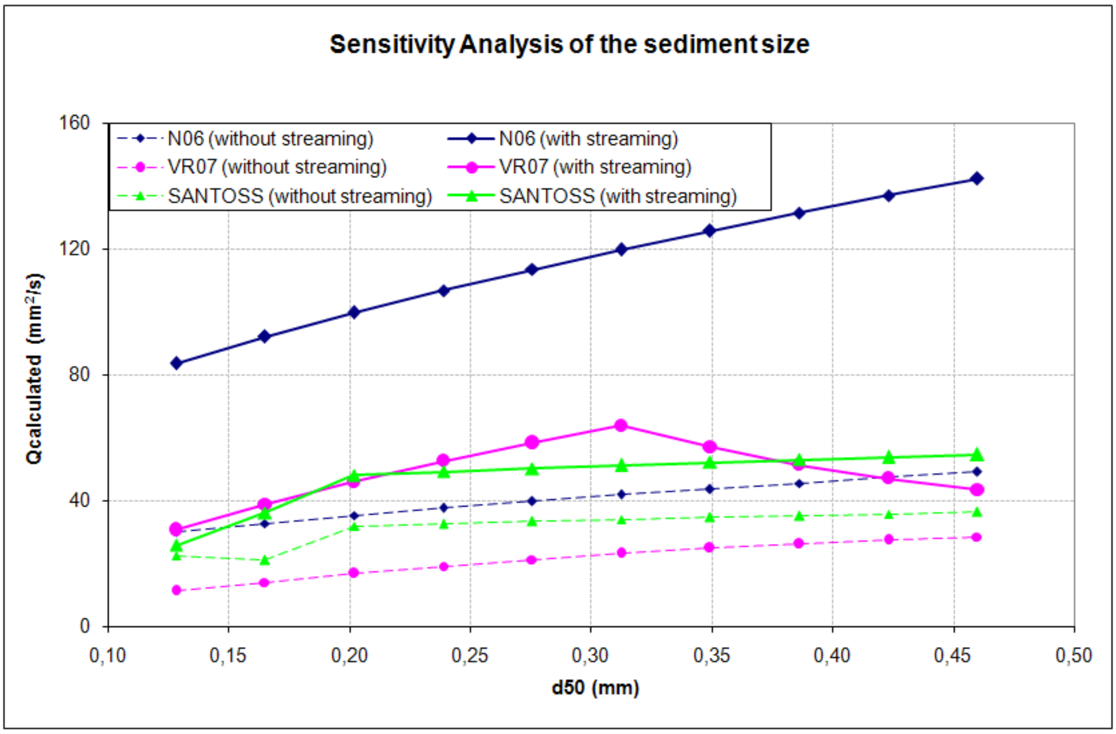

Figure 10: The calculated net transport rates as function of the medium grain size. The dotted lines and the solid lines represent the sand transport calculations respectively with and without the inclusion of streaming

5.3 Behaviour models on flow period variation

Figure 11 presents the calculated net transport rates as function of the flow period. The dotted lines represent the calculations of the sand transport without including the streaming components. As seen in the figure, the behaviours of the models without streaming are similar to each other. The amount of computed sand transport slightly decreases for the increasing wave period. The three models are not sensitive to the changes in the flow period. Just like before, the N06 model predicts the largest amounts of sand transports while the VR07 model predicts the smallest amounts of sand transports.

The solid lines in Figure 11 represent the calculations of the sand transport including the effects of boundary layer streaming. Both the VR07 model and the SANTOSS model behave nearly the same as in the situation without including streaming. The amount of sand transport predicted in the onshore (positive) direction slightly increased. Just like before, the amount of additional transport caused by the streaming component of the N06 model is considerably larger than the additional transport caused by the streaming components of the other two models. The additional transports caused by the streaming components of the three models show a similar behaviour; the amount of additional sand transports decrease when the flow period increases.

At T = 4 s the amount of predicted transport of N06 with streaming is 126 mm²/s. At T = 12 s the amount of predicted transport of N06 with streaming nearly halved to 67 mm²/s. Similar magnitude of sensitivity can also be observed in the previous paragraph for the analysis with the grain size d_{50}.

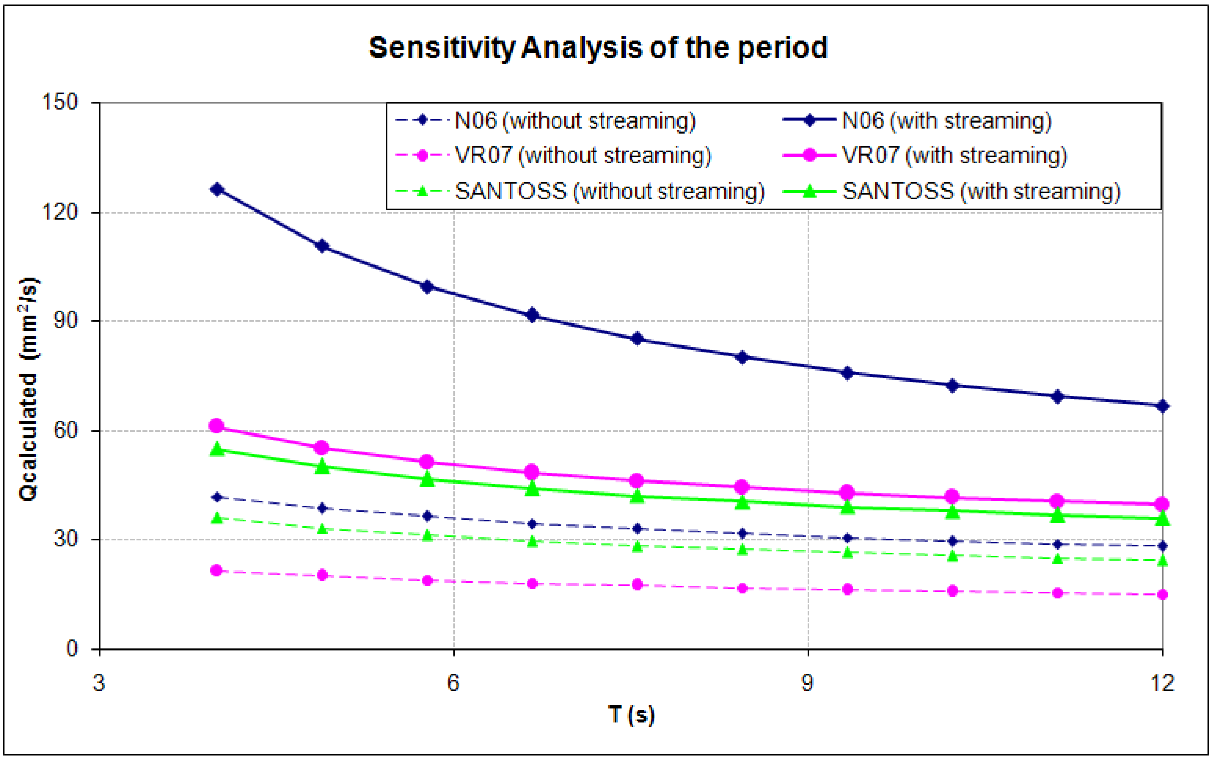

Figure 11: The calculated net transport rates as function of the flow period. The dotted lines represent the sand transport calculations of the models without including the effects of boundary layer streaming. The solid lines represent the calculations including the effects of boundary layer streaming.

5.4 Behaviour models on peak orbital velocity variation

Figure 12 presents the calculated net transport rates as function of the peak orbital velocity. The U_{on} and U_{off} have been varied simultaneously to keep the degree of velocity skewness constant on R = 0.6. The dotted lines represent the calculations of the sand transport without including the streaming components. If streaming is not included, the amounts of predicted sand transports of N06 and the SANTOSS model are nearly the same. The VR07 model predicts smaller amounts of sand transports, but the behaviour is comparable to the other two models. As seen in the figure, the computed sand transports of the three models are sensitive to changes of the peak orbital velocities.

The solid lines in Figure 12 represent the calculations of the sand transport including the effects of boundary layer streaming. If streaming is included, the VR07 model and the SANTOSS model predict nearly the same amounts of sand transport while the N06 model predicts a much larger amount of sand transport. The figure shows that the streaming components of the three models are sensitive to changes of the peak orbital velocity. While the amount of additional transports of the three models are small at U_{on} = 0.77 m/s (nearly 0 mm^2/s for VR07 and the SANTOSS model and 10 mm^2/s for N06) the amount of additional transports are large at U_{on} = 1.72 m/s (53 mm^2/s for the SANTOSS model, 99 mm^2/s for VR07 and 178 mm^2/s for N06). The amount of additional sand transport induced by the streaming component of the N06 model is the largest among the three models. As explained before this is due to the use of the friction factor for mobile bed f_e. Among the three models N06 is the most sensitive to changes of the peak orbital velocity; small changes in the peak orbital velocity may have large influences on the amount of additional sand transport due to the streaming component.

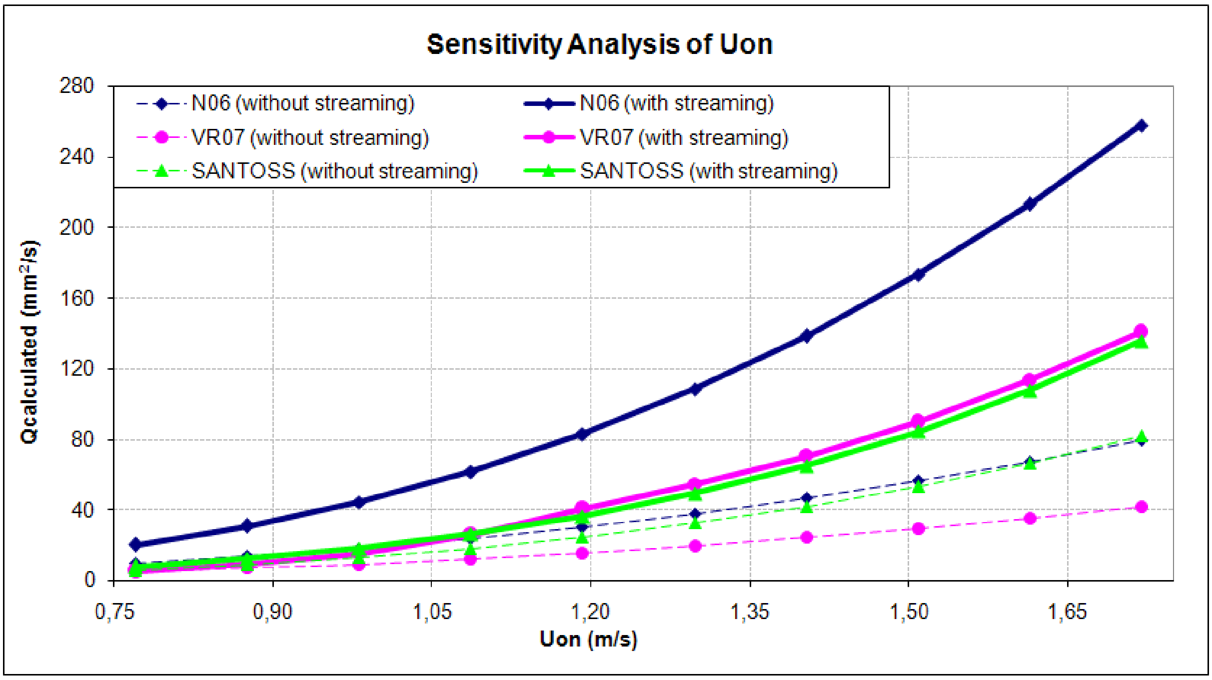

Figure 12: The calculated net transport rates as function of the peak orbital velocity. The dotted lines represent the sand transport calculations without streaming and the solid lines with streaming. The degree of velocity skewness has been remained on R = 0.6.

This paragraph shows that if streaming is included, the amount of sand transport predicted by VR07 and the SANTOSS model are nearly the same. This similarity can also be observed in the previous paragraph in the analysis with the period T. This is interesting, since the approaches of VR07 and the SANTOSS model to account for the influences of the surface wave effects are entirely different. Therefore, to gain more understanding of this similarity a comparison is made between the influences on the sand transport prediction due to i) the streaming component of the VR07 model and ii) the *three* surface wave effects of the SANTOSS model. The results are shown in Appendix B. The appendix shows that under non-fine sand sheet flow conditions, the amounts of additional sand transports induced by the streaming component of VR07 and by the three surface wave effects of SANTOSS are nearly the same. This may indicate that even though VR07 does not describe the surface wave effects as extensively as the SANTOSS model and only accounts for the influences of streaming, the influences of other surface wave processes are implicitly included. Van Rijn (2007) used model and experimental results of Davies and Villaret (1999) to calibrate his streaming velocity. A possibility is that the influences of other surface wave effects are indirectly included in the streaming velocity during the calibration.

5.5 SUMMARY OF THE BEHAVIOUR

In this chapter insight in the influences of the streaming components on the sand transport predictions are gained by investigating the influences of input parameters (*research question 1*). The following has been observed:

- *If streaming is not included, N06 computes the largest amounts of sand transport under all conditions. Among the three models, the method to include streaming of N06 results into the largest amount of additional transport under all conditions. This is due to the use of the friction factor for mobile bed f_e for the calculation of the wave Reynolds stress.*

- *If streaming is not included, VR07 computes the smallest amounts of sand transport under all conditions.*

- *For VR07, the influences of grain size variation on the additional sand transport due to streaming changes under different ranges relative roughness ($A_w/k_{s,w}$). For $A_w/k_{s,w} \geq 100$, an increase in the sediment size results into an increase of the additional onshore directed sand transport. For $A_w/k_{s,w} < 100$, an increase in sediment size results into a decrease of additional sand transport. The same cannot be observed for the other two models; an increase in the sediment size will only results into an increase of the onshore directed additional sand transport due to streaming.*

- *The amount of additional transport caused by the streaming component of SANTOSS is the smallest among the three models. A possible explanation for this is that the SANTOSS model splits the surface wave effects up in the boundary layer streaming, vertical orbital velocities and Lagrangian motion. The other two models consider boundary layer streaming as the only relevant surface wave process. Furthermore, compared to the N06 model, the SANTOSS model uses a smaller friction factor.*

- *The amount of sand transport predictions of the SANTOSS model strongly reduces if the grain size becomes smaller than 0.2 mm. This is due to the influences of the phase-lag effects. SANTOSS is the only model that accounts for the phase-lag effects.*

- *After the inclusion of streaming, the amount of predicted transport by VR07 and the SANTOSS model are very similar to each other. This similarity cannot be observed for fine sand conditions due to the phase-lag effects of the SANTOSS model. Also, the streaming velocity of VR07 is offshore directed for conditions with a small relative roughness of* $A_w/k_{s,w} \leq 1$ *(rippled-bed conditions) while the streaming of SANTOSS remains onshore directed under all conditions. This indicates that this similarity in sand transport prediction will not occur under rippled-bed conditions. Note that the sand transport predictions of N06 are not similar to VR07 and the SANTOSS model. N06 predicts much larger amounts of sand transports.*

- *To gain more understanding of the similar transport predictions of VR07 and the SANTOSS model a comparison is made between the influences of i) the streaming velocity of VR07 and ii) the three surface wave effects of the SANTOSS model. This comparison shows that under non-fine sand sheet flow conditions the amounts of additional sand transports induced by the streaming velocity of VR07 and the three surface wave effects of SANTOSS are nearly the same. Van Rijn (2007) used model and experimental results of Davies and Villaret (1999) to calibrate his streaming velocity. A possible explanation for the similar sand transport predictions is that the influences of other surface wave effects are indirectly included in the streaming velocity during the calibration.*

- *The amounts of additional sand transport caused by the three streaming components are very sensitive to the changes of the peak orbital velocities. The amounts of additional transports due to the streaming components rapidly increase for the increasing peak orbital velocity. Among the three models, the additional transports due to the streaming component of N06 are the most sensitive to the changes of the peak orbital velocities.*

6 ANALYSIS OF IMPORTANCE OF STREAMING

In this chapter cross-shore sand transport under surface wave conditions will be calculated with the three models. The formulas of the three models described in chapter 4 are used. For each model, two runs are carried out; one including the effects of streaming and one without the effects of streaming. The computed sand transports are compared with the measured sand transports in surface wave experiments (see Table 3). This way, understanding will be gained of how the inclusion of streaming influences the performances of the models under surface wave conditions (research question 2).

Figure 13 to Figure 18 illustrate the comparison between the calculated sand transport and measured sand transport. A distinction is made between the sediment sizes in the plots. This is done because experiments are conducted under comparable flow conditions with two different sediment sizes. The results are summarized in the last paragraph. It may be noted that the performance of a model is defined as the measured transport ($Q_{s,meas}$) divided by the calculated transport ($Q_{s,calc}$). The models are considered to perform well if the computed transport rates correspond with the measured data within a factor two ($0.5 < Q_{s,meas}/ Q_{s,calc} < 2$).

6.1 TRANSPORT PREDICTION N06 FOR FLUME EXPERIMENTS

In this paragraph the importance of the streaming component of the N06 model is studied by comparing the computed sand transports with the measured sand transports. Figure 13 presents the results of the runs with the N06 model without the streaming component. The model without streaming performs well. Nearly all of the predicted sand transports lie within a factor two of differences compared to the measured transports. For surface wave conditions, Nielsen (2006) suggests that a positive wave Reynolds stress is required for good sand transport predictions. Without the wave Reynolds stress the model should underestimates the amount of sand transports in the onshore direction for surface wave conditions. However, only small underestimations can be observed in Figure 13 (even though they still lie within or around a factor two of differences compared to the measured transport).

Figure 14 presents the results of N06 with the streaming component. The performance of the model decreases after including the wave Reynolds stress; major overestimations can be observed. If streaming is not included, 83% of the computed transport rates correspond with the measured data within a factor two. By including the wave Reynolds stress, this value decreases to 42%. As seen before in Chapter 5, the amount of additional sand transport caused by the wave Reynolds stress is large. Since the model already performs well without the streaming component, including the streaming component will naturally cause overestimations. The overestimations may be due to the use of the friction factor for mobile bed, which is considerably larger than the grain friction factor.

Figure 14 shows noticeable results for four medium sand conditions. Nearly perfect agreement with the measured sand transport can be observed for these conditions. It may be noted that these four sand transports are measured in the surface wave experiments conducted by Dohmen-Janssen and Hanes (2002) (see Table 3). Nielsen (2006) used these four measurements to validate his wave Reynolds stress. Figure 14 shows that his wave Reynolds stress improves the performances of the sand transport predictions for these four conditions, but decrease the performances for the sand transport predictions for the remaining eight conditions.

As seen in Table 3, the conditions of the experiments of Dohmen-Janssen and Hanes (2002) and the conditions of the new surface wave experiments of Schretlen (2010) are comparable to each other. The major differences between these experiments are the larger peak orbital velocities of the new surface wave experiments. As seen in the sensitivity analysis in Chapter 5, the amount of additional sand transport due to the streaming component of N06 considerably increases for high peak orbital velocities (paragraph 5.4).

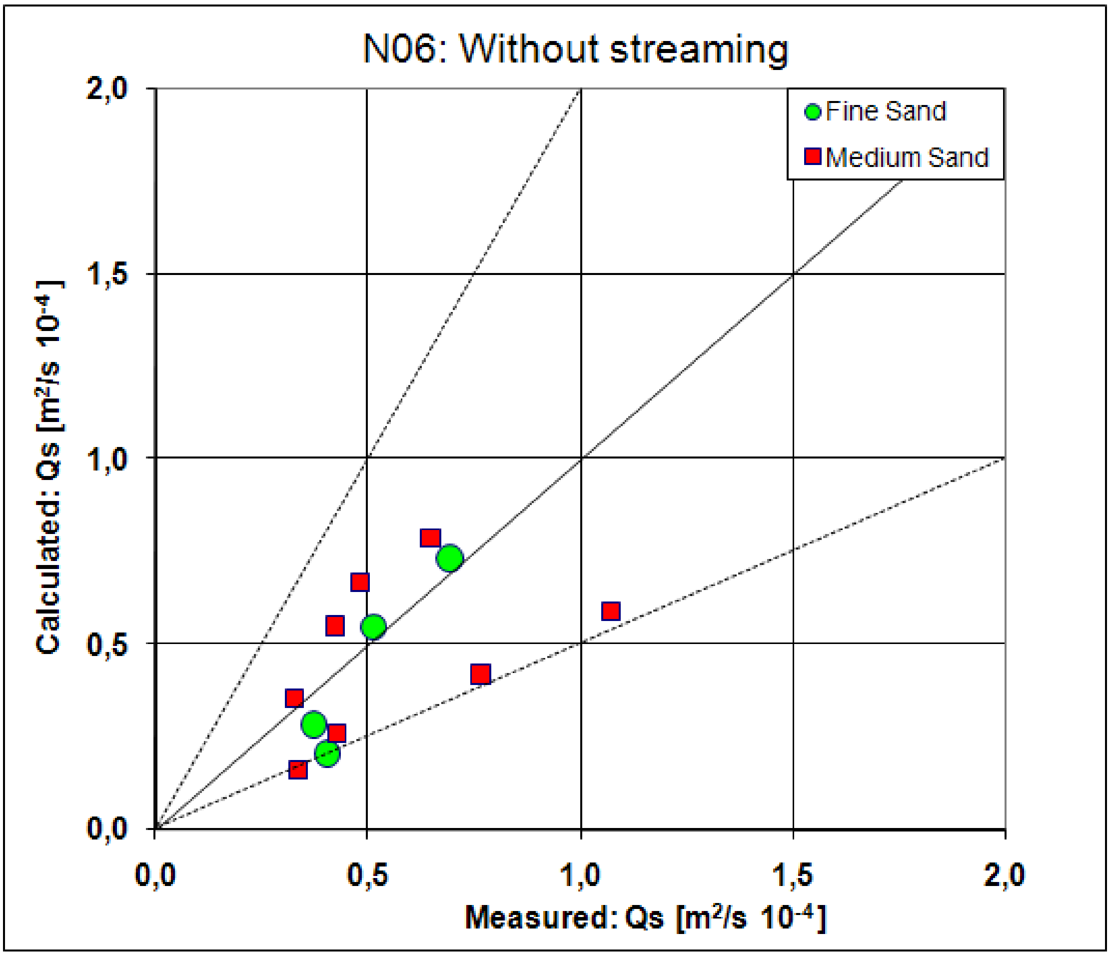

Figure 13: The model performance of N06 without including the boundary layer streaming. A distinction between fine sand (d50≤0.2mm) and medium sand (d50>0.2mm) can be seen. The solid line indicates perfect agreement; the dashed lines a factor 2 difference.

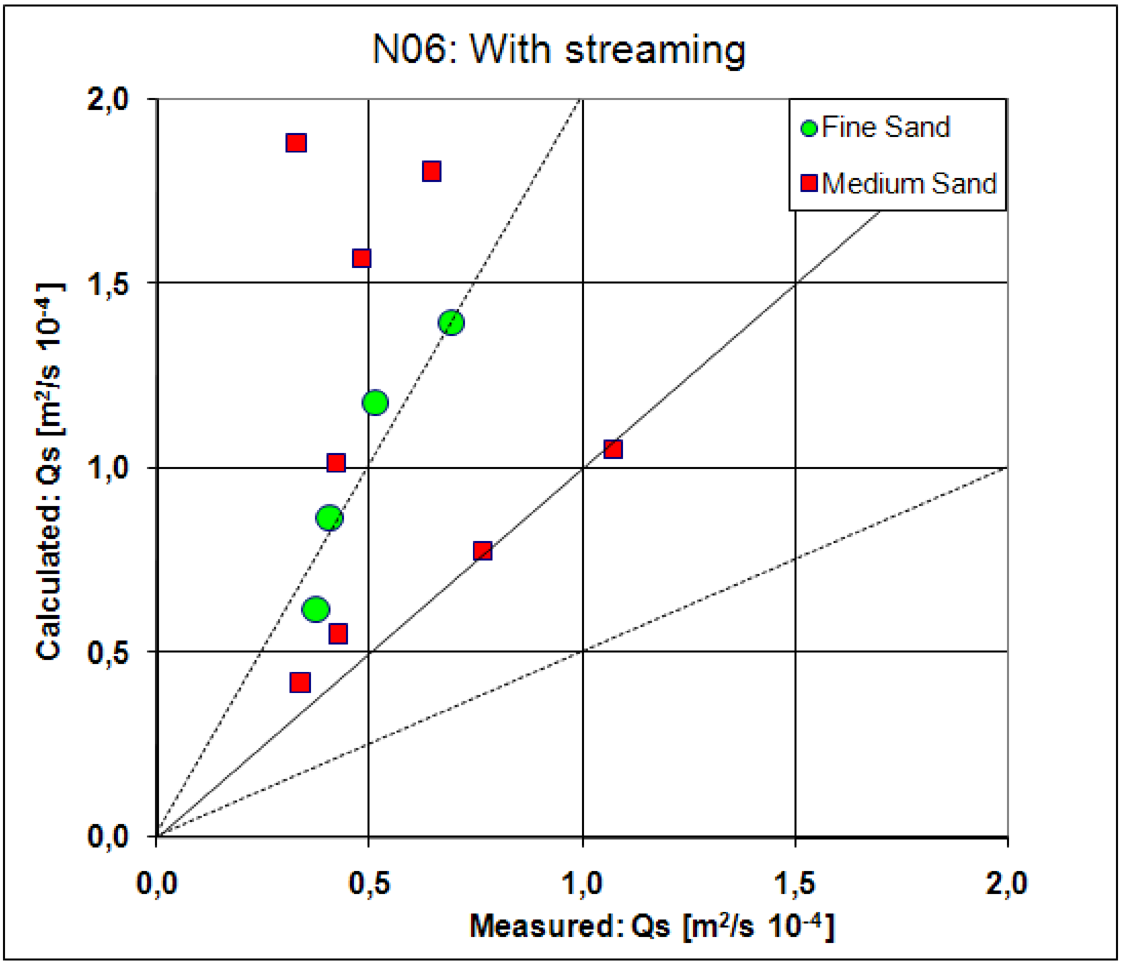

Figure 14: The model performance of N06 including the boundary layer streaming. A distinction between fine sand (d50≤0.2mm) and medium sand (d50>0.2mm) can be seen. The solid line indicates perfect agreement; the dashed lines a factor 2 difference.

6.2 Transport prediction VR07 for flume experiments

Figure 15 presents the results of VR07 without the streaming component. Underestimations can be observed. Since wave induced boundary layer streaming should increase the amount of onshore directed sand transport, underestimations are expected. Furthermore, the sensitivity analysis in the previous chapter shows that among the three models, the VR07 model predicts the smallest amount of sand transport for all conditions. Figure 15 shows that only 33% of the sand predictions lay within a factor two of differences compared to the measured sand transport.

Figure 16 presents the results of VR07 with the streaming component. The percentage of the computed transport rates corresponding with the measured data within a factor two increases to 92%. The streaming component of the VR07 considerably improves the performances of the model by adding a positive onshore directed near bed current velocity. The underestimations can no longer be observed. Note that including streaming results into an increased scatter for the medium sand. The method seems to be more suitable for the fine sand conditions.

It may be noted that Van Rijn (2007) only validated his approach to include streaming with field measurements of bed-form transport of sand with a medium grain size of 0.3 mm (see paragraph 4.2.5). Figure 16 shows that the approach of Van Rijn (2007) to include the effects of boundary layer streaming is also suitable for sand transport in sheet-flow conditions.

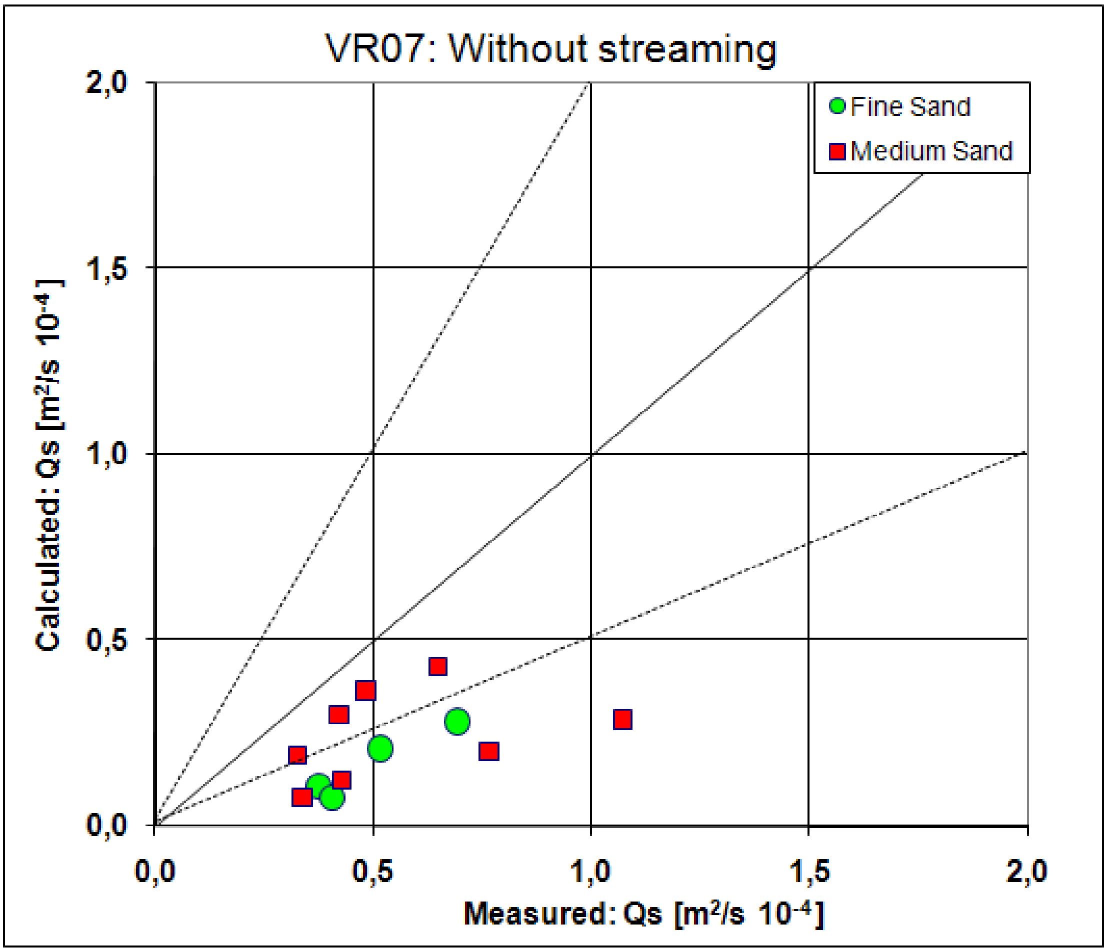

Figure 15: The model performance of VR07 without the boundary layer streaming. A distinction between fine sand (d50≤0.2mm) and medium sand (d50>0.2mm) can be seen. The solid line indicates perfect agreement; the dashed lines a factor 2 difference.

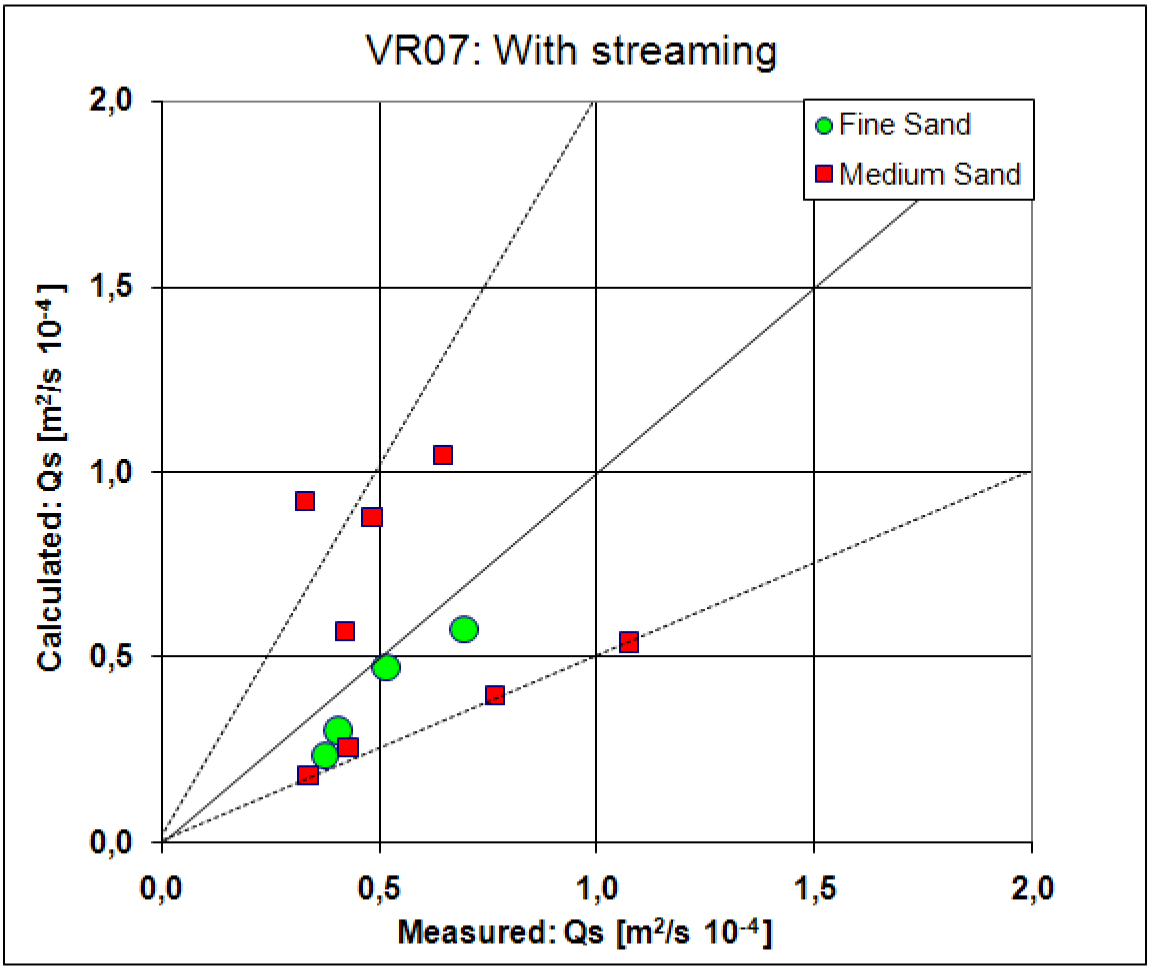

Figure 16: The model performance of VR07 including the boundary layer streaming. A distinction between fine sand (d50≤0.2mm) and medium sand (d50>0.2mm) can be seen. The solid line indicates perfect agreement; the dashed lines a factor 2 difference.

6.3 TRANSPORT PREDICTION SANTOSS FOR FLUME EXPERIMENTS

Figure 17 presents the results of the runs with the SANTOSS model without the streaming component. As seen in the figure, 58% of the computed transport rates correspond with the measured data within a factor two. Even though it is only 58%, the model performance is not bad. As illustrated in Figure 17, the remaining 42% are just minor underestimations. The figure shows that by adding a small amount of additional transport into the onshore direction, the model performance will considerably increase. A possible explanation for this reasonably well performance is that the SANTOSS model does not consider boundary layer streaming as the only relevant surface wave effect. Even though boundary layer streaming is not included in the calculations of Figure 17, other surface wave effects (Lagrangian motion and vertical orbital velocity) are still included.

Figure 18 presents the results of the runs with the SANTOSS model with the streaming component. As seen in the figure, the streaming component improves the performance of the model. The percentage of the computed transport rates corresponding with the measured data within a factor two increases to 92%. The small amount of additional onshore directed transport corrected the minor underestimations; the predictions now lay within a factor two of differences compared to the measured transport. It may be noted that some transport predictions that previously lay near the solid line, which represents a perfect agreement between the measured and the computed sand transport, now became overestimations (even though most of them still lay within a factor two of differences compared to the measured transport).

As seen in Figure 18, the performance of the SANTOSS model and the VR07 model are comparable to each other if streaming is included. Both models are able to compute 92% of the transport within a factor two of differences compared to the measured sand transport. The similarity in sand transport predictions under surface wave conditions has already been observed in Chapter 5. As explained before, this may be due to the fact that under non-fine sand sheet flow conditions, the additional transports induced by the streaming velocity of VR07 and the three surface wave effects of the SANTOSS model are nearly the same. It may be noted that the SANTOSS model is calibrated on the surface wave datasets that is used in this chapter. The good performance is therefore partly due to the calibration.

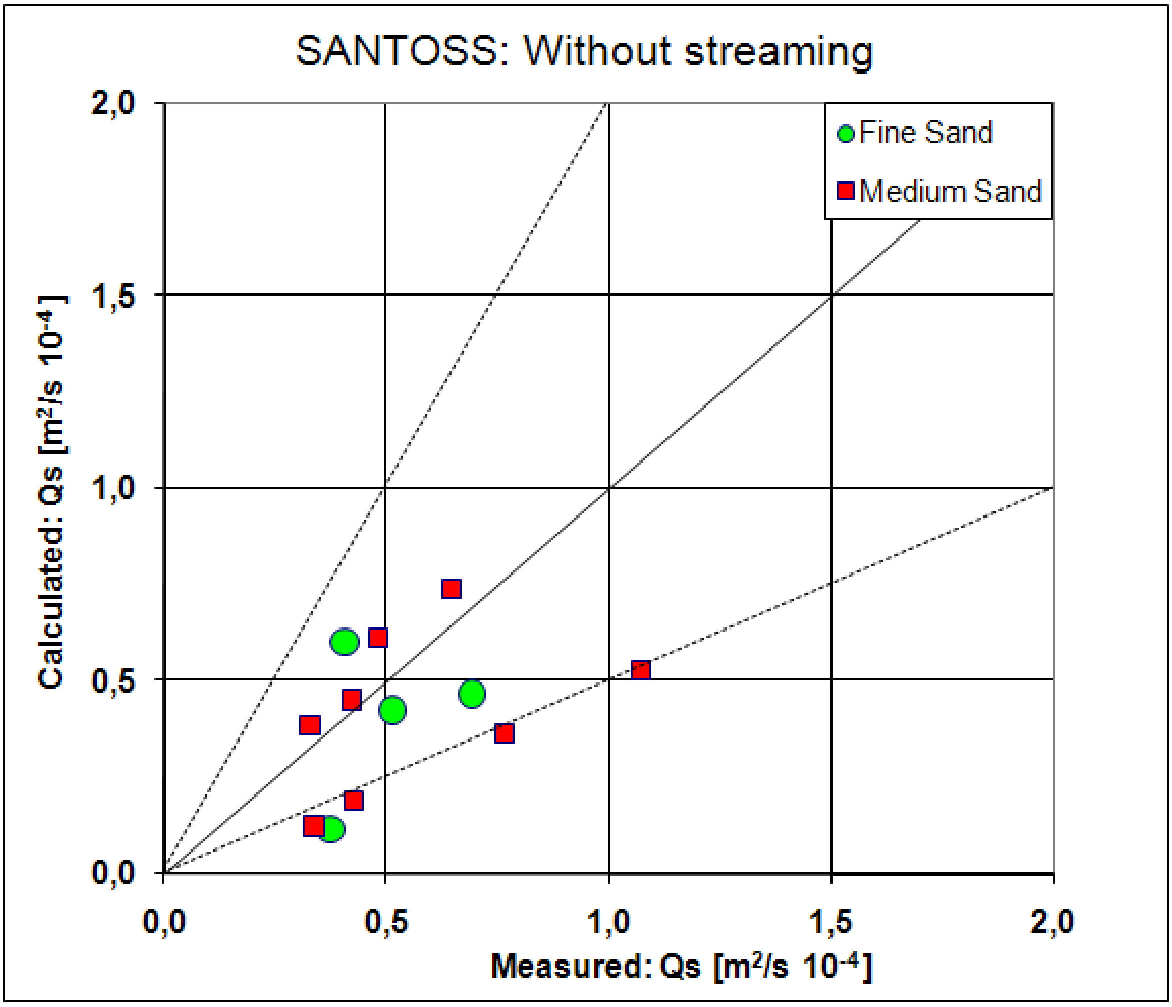

Figure 17: The model performance of SANTOSS without including the boundary layer streaming. A distinction between fine sand (d50≤0.2mm) and medium sand (d50>0.2mm) can be seen. The solid line indicates perfect agreement; the dashed lines a factor 2 difference.

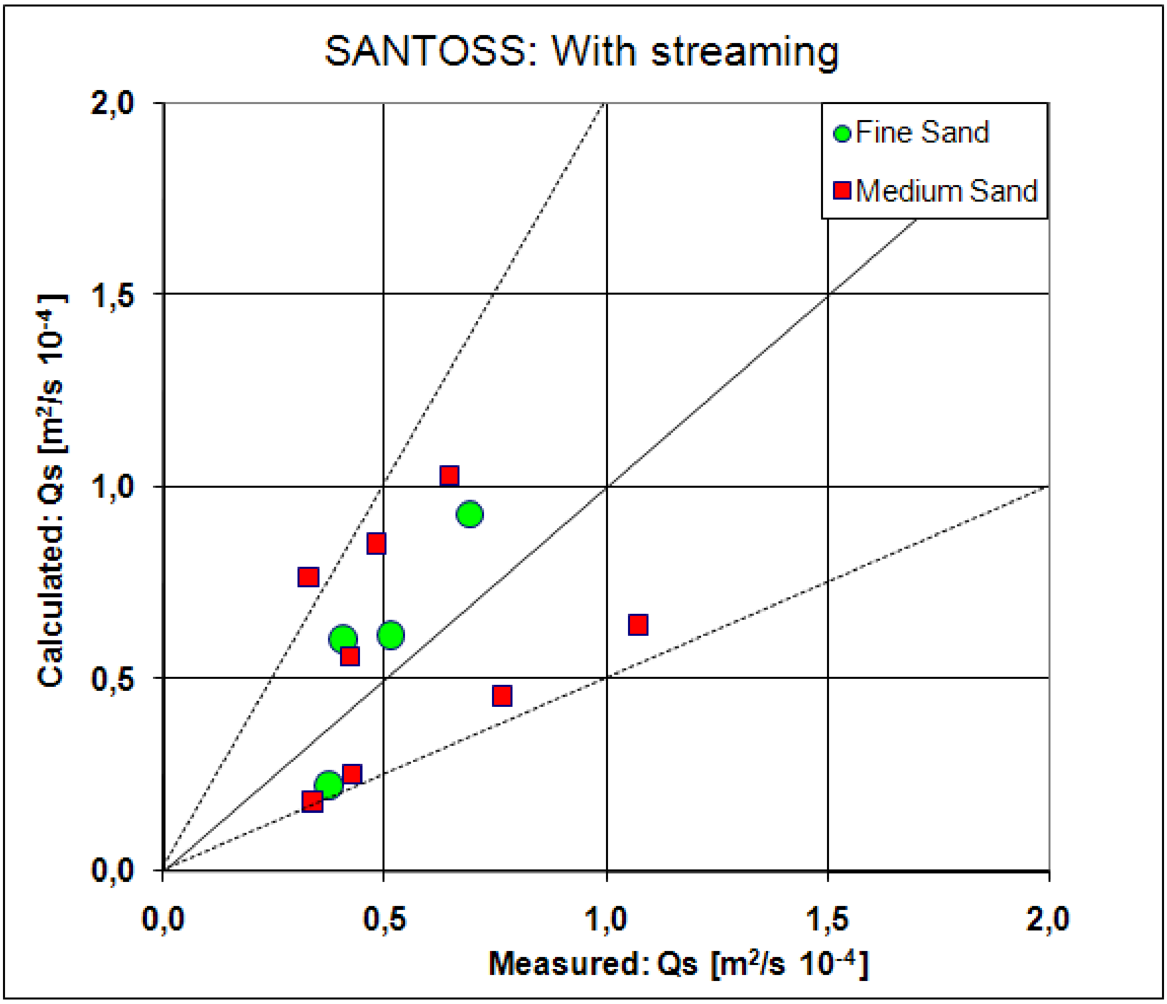

Figure 18: The model performance of SANTOSS including the boundary layer streaming. A distinction between fine sand (d50≤0.2mm) and medium sand (d50>0.2mm) can be seen. The solid line indicates perfect agreement; the dashed lines a factor 2 difference.

6.4 Overview of the model performances with streaming

In this chapter the calculated sand transports are compared with the measured sand transport in surface wave experiments. This way, understanding will be gained of how the inclusion of streaming influences the performances of the models under surface wave conditions (*research question 2*).

A comparison of the performances of the three models under surface wave conditions is illustrated in Figure 19. Table 8 presents quantitatively an overview of the performance of the models in terms of percentage of the computed transport rates corresponding with the measured data within a factor two, factor five and factor ten. The streaming components of the three models are included in these sand transport calculations. The following can be concluded from the analysis of the importance of the streaming components for sand transport predictions under surface wave conditions:

- *N06 performs well if the streaming component is not included; the sand transport predictions of N06 without the inclusion of streaming lay within or around a factor two of differences compared to the measured transports.*

- *For N06, including the streaming component causes i) an improved performance for the dataset that Nielsen (2006) used for the verification of his approach to include boundary layer streaming and ii) a decrease of the performance for the newly obtained surface wave data set. Since only four of the twelve conditions are used for the verification, the overall performance of N06 for surface wave conditions considerably decreases due to the inclusion of streaming.*

- *The VR07 model underestimates the sand transports under surface wave conditions if the streaming component is not included. The additional onshore directed sand transports due to streaming correct these underestimations and considerably improve the performance of the model under surface wave conditions.*

- *The SANTOSS model shows minor underestimations if the streaming component is not included. Small amounts of additional sand transports induced by the streaming component considerably improve the performance if the streaming component is included.*

- *If streaming is included, the performance of VR07 and the SANTOSS are comparable to each other. These two models give the best performances under surface wave conditions even though the approaches to account for the surface wave effects are different. The similar sand transport predictions have been observed earlier in the sensitivity analysis.*

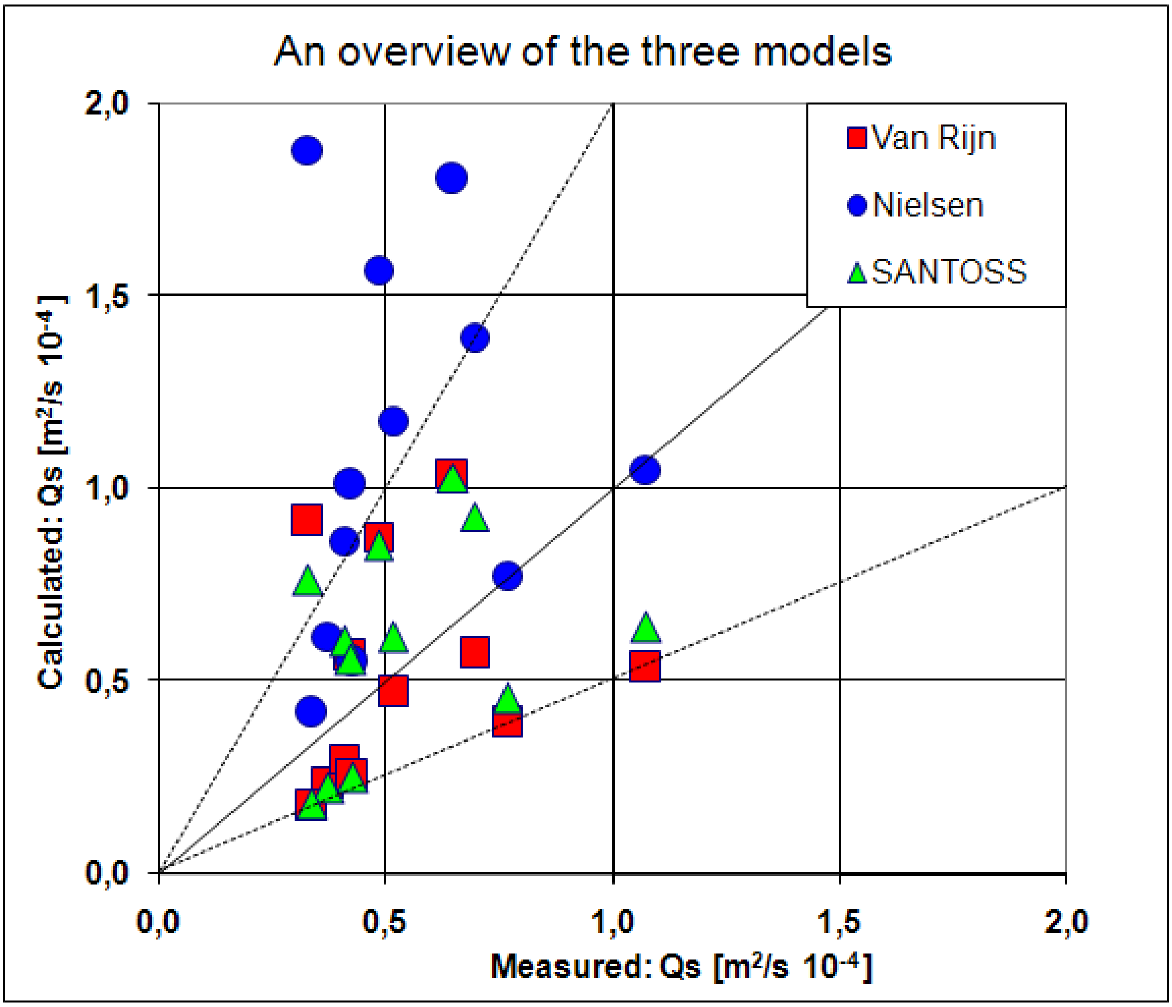

Figure 19: A comparison of the results of the three models including their streaming components. The solid line denotes perfect agreement, the dotted lines a factor 2 of differences.

Table 8: An overview of the performances of the three models in terms of percentage of the computed transport rates corresponding with the measured data within a factor 2, factor 5 and factor 10.

	Factor 2	Factor 5	Factor 10
van Rijn with streaming	92%	100%	100%
van Rijn without streaming	33%	92%	100%
Nielsen with streaming	42%	92%	100%
Nielsen without streaming	83%	100%	100%
SANTOSS with streaming	92%	100%	100%
SANTOSS without streaming	58%	100%	100%

7 COMPARISON OF THE GENERAL PERFORMANCES

Even though the three models can be used for wave dominated cross-shore sand transport predictions, most of the datasets used for the calibration and validation of the three models are not the same. Therefore, it is not well understood which model gives the best performance in wave dominated cross-shore sand transport predictions. The previous chapter focused on the performances of the models under surface wave conditions. This chapter focuses on the performances of the three models for a wide range of wave dominated datasets. For this comparison, datasets from the SANTOSS database (see chapter 3.1) are used. The SANTOSS model used the SANTOSS database for calibration. Some of the datasets in the SANTOSS database are also used for the calibration and validation of N06 and VR07. Appendix A presents an overview of which datasets are used for calibration and validation of the models.

The performances of the three models will first be analysed individually in the first three paragraphs. The last paragraph presents an overview of the performance and a conclusion will be drawn of which model is the most suitable for sand transport calculations in wave dominated conditions. The performances of the three models are presented in figures and summarized in tables. The performances are once again expressed in terms of the percentage of the computed transport rates that correspond with the measured transport rates within a factor two and factor five.

7.1 GENERAL PERFORMANCE N06

In this paragraph the performance of the N06 model is shown. The calculated sand transports are compared with 211 sand transports measured in wave dominated experiments. The datasets used in the previous chapter are all obtained from surface wave experiments. In this chapter datasets obtained from OFT experiments will also be used for a more general assessment of the performances of the models. The overall performance of the N06 model is illustrated in Figure 20. A quantitative overview of the performance is presented in Table 9. In the table a distinction is made between the various data subsets. The differences in performances of predicting sand transport are shown in the table for i) the different type of waves and ii) the different type of bed forms. It may be noted that the streaming component is only applied to the sand transport predictions under surface wave conditions.

As seen in Figure 20 and Table 9, the model performs reasonably for sand transport predictions under acceleration skewed wave conditions. For the 53 predictions of sand transports under acceleration skewed conditions, 53% of the computed transport rates correspond with the measured data within a factor two and 94% within a factor five. It may be noted that the database contains twelve measurements from experiments with acceleration skewed waves conducted by Watanabe and Sato (2004). This is a part of the data used by Nielsen (2006) to calibrate his filter method (see paragraph 4.1). Eight of the twelve sand transport predictions for these conditions deviates less than a factor two from the measurements.

On the left of Figure 20 sand transport predictions into the wrong direction can be observed. These sand transports are measured under i) rippled-bed conditions or under ii) fine sand sheet conditions (d_{50} < 0.2 mm). N06 is a quasi-steady model. The assumption of quasi-steadiness does not hold for fine sand conditions and in rippled-bed conditions. The phase-lag can become so large that the net transport is against the direction of the wave propagation. This can also be seen in Table 9; 79% of the predicted sand transports in the rippled-bed regime are predicted into the wrong direction. Table 9 shows that the model perform well for the 155 sand transport predictions under sheet flow conditions; 70% of the computed transport rates correspond with the measured data within a factor two and 92% within factor five.

It may be noted that some of the surface wave experiments are conducted with fine sands with d_{50} = 0.14 mm (see Table 3). In OFT experiments with comparable fine sands offshore directed transports (due to the phase-lag effects) have been measured. In the flume experiments, positive sand transports have been observed under the fine sand conditions. This may indicate that the surface wave effects reduce or cancel out the influences of the phase-lag effects.

N06 is able to perform well for sand transport under non-fine sand sheet flow conditions. The general performance of the model for the 211 conditions is reasonable. The model is not able to account for i) surface wave effects and ii) the influences of the phase-lag effects. Only 52% of the computed transport rates correspond with the measured data within a factor two and 72% within factor five.

Table 9 the quantitative performance results of N06 in terms of percentage of the predictions that deviate less than a factor 2 and 5 from the measurements. 'Wrong direction' represents the in transport that is predicted into the wrong. A distinction is made between the various sub sets.

Total	**N**	**Factor 2**	**Factor 5**	**Wrong direction**
All wave dominated datasets	211	52%	72%	25%
Data subset: type of flow				
Velocity-skewed waves (without currents)	94	35%	43%	53%
Acceleration-skewed waves (without currents)	53	53%	94%	2%
Waves with a superimposed current	50	86%	96%	4%
Surface waves	14	36%	93%	0%
Data subset: type of bed form				
Flat bed (Sheet flow)	155	70%	92%	6%
Rippled-bed	56	2%	14%	79%

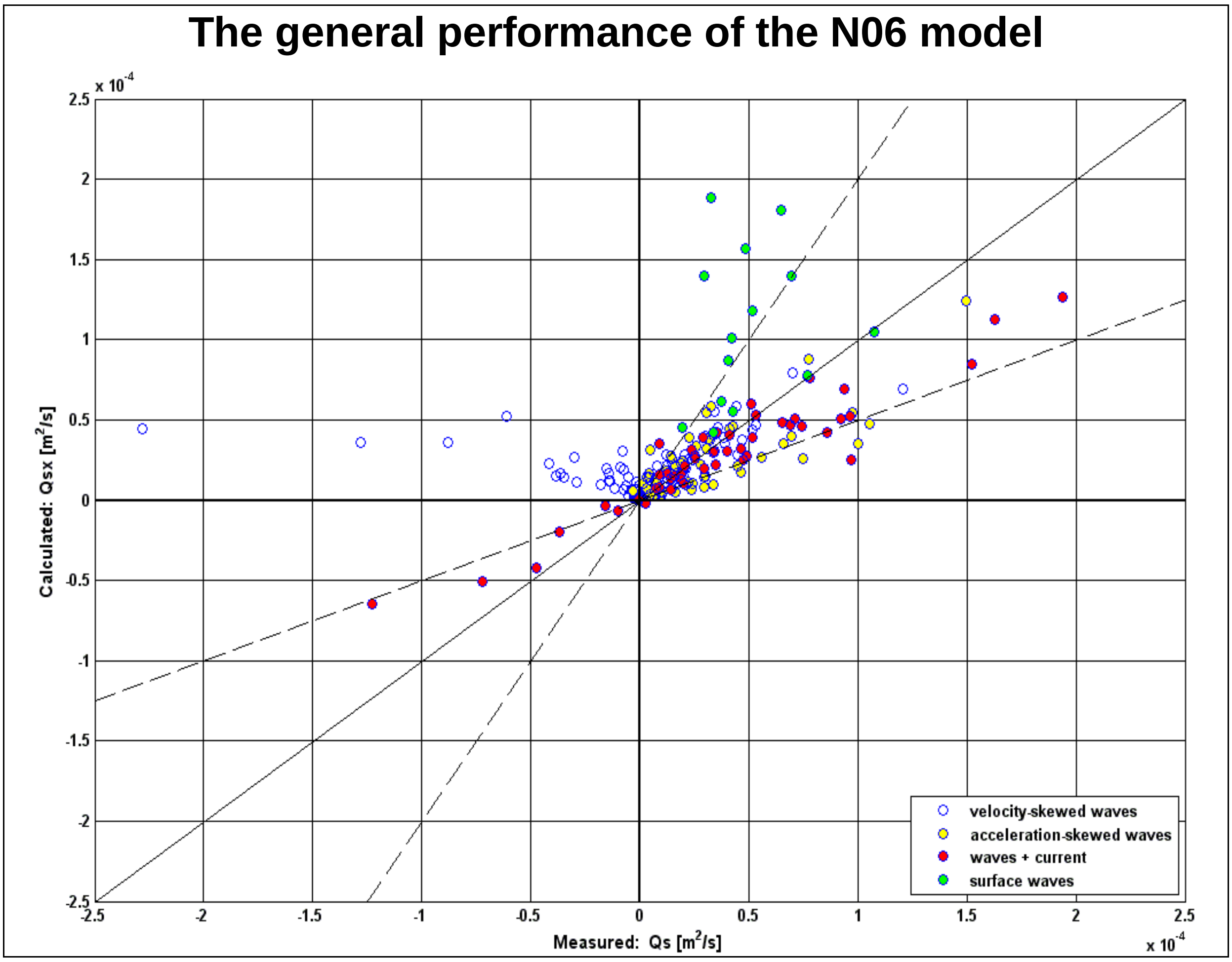

Figure 20: The transport calculated with the N06 model. The solid line indicates perfect agreement; the dashed lines a factor 2 difference.

7.2 GENERAL PERFORMANCE VR07

In this paragraph the performance of the VR07 model is shown. It may be noted that the VR07 model requires a depth averaged velocity to account for the influences of currents (see paragraph 4.2). The SANTOSS database only provides a current velocity at a specific reference level. This current velocity at a reference level will be used to calculate a depth averaged velocity. More details of this calculation can be seen in Appendix D.

As seen in Figure 21 and Table 10, the VR07 model does not perform well for sand transport predictions under acceleration skewed wave conditions. For the 53 predictions of sand transports under acceleration skewed conditions, only 38% of the computed transport rates correspond with the measured data within a factor two and 60% within a factor five. The filter method with $\varphi_\tau = 40^o$ (see paragraph 4.2), which is only validated for one sand transport conditions, does not seem to be suitable for the sawtooth shaped wave conditions; a lot of underestimations can be observed under these conditions.

Figure 21 shows that the model performs well under surface wave conditions (see the previous chapter for more information about this). Furthermore, the VR07 performs reasonably well for the 'wave with current' conditions. For the 50 predictions of sand transports in wave with current conditions, 66% of the computed transport rates correspond with the measured data within a factor two and 90% within a factor five. The figure shows that the VR07 model does not perform well under velocity skewed wave conditions. Many offshore directed transports have been observed under these conditions while the model predicts onshore directed transports. As discussed in the previous paragraph this is not due to the wave shape. The wrong predictions are due to the fine sands and the rippled-bed. Just like N06, VR07 predicts sand transports into the wrong direction under conditions in which the influences of the phase-lag effects are important. The VR07 model does perform well for the velocity skewed waves in the non-fine sand sheet flow conditions.

The general performance of the VR07 model is reasonable. The model perform well for velocity skewed waves under non-fine sand sheet flow conditions and reasonable under the 'wave with current' conditions. Good performance can be seen for surface wave conditions. The model is not able to account for i) the influences of the shape of acceleration skewed waves and ii) the influences of the phase-lag effects. For the 211 predictions of sand transports in wave with current conditions, only 43% of the computed transport rates correspond with the measured data within a factor two and 64% within a factor five.

Table 10: the quantitative performance results of VR07 in terms of percentage of the predictions that deviate less than a factor 2 and 5 from the measurements. 'Wrong direction' represents the in transport that is predicted into the wrong. A distinction is made between the various sub sets.

Total	**N**	**Factor 2**	**Factor 5**	**Wrong direction**
All wave dominated datasets	211	43%	64%	25%
Data subset: type of flow				
Velocity-skewed waves (without currents)	94	27%	46%	53%
Acceleration-skewed waves (without currents)	53	38%	60%	2%
Waves with a superimposed current	50	66%	90%	4%
Surface waves	14	86%	100%	0%
Data subset: type of bed form				
Flat bed (Sheet flow)	155	54%	79%	6%
Rippled-bed	56	13%	20%	79%

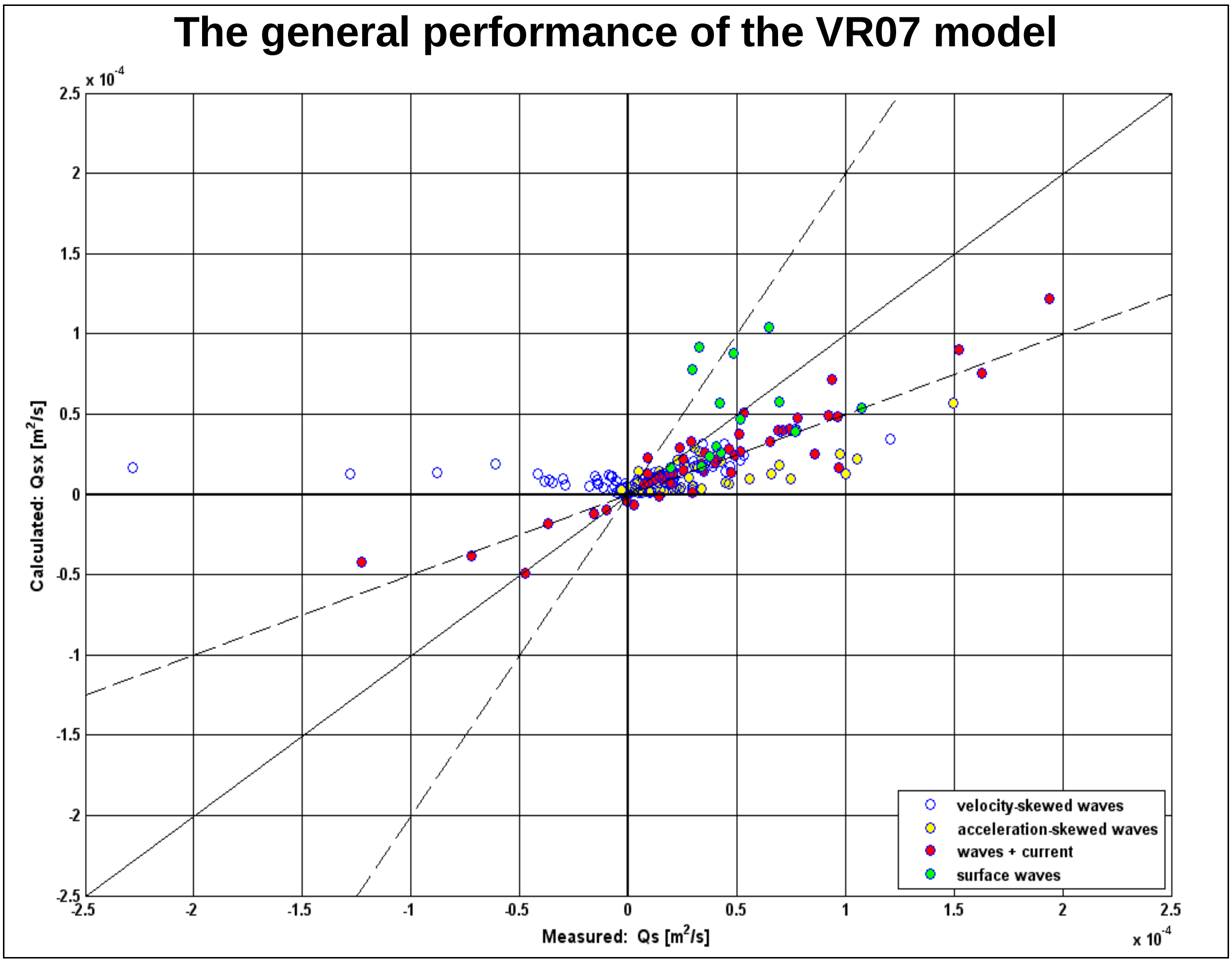

Figure 21: The transport calculated with the VR07 model. The solid line indicates perfect agreement; the dashed lines a factor 2 difference.

7.3 GENERAL PERFORMANCE SANTOSS

In this paragraph the performance of the SANTOSS model is shown. The calculated transport will be compared with the 211 sand transport measurements. Note that the datasets in the SANTOSS database are used for the calibration of the different formulas in the SANTOSS model.

As seen in Figure 22 and Table 11, the model performs well for sand transport predictions under acceleration skewed wave conditions. For the 53 predictions of sand transports in acceleration skewed conditions, 79% of the computed transport rates correspond with the measured data within a factor two and 98% within a factor five. The approach of the SANTOSS model to account for the influences of the wave shapes is suitable for these datasets with acceleration skewed waves.

Table 11 shows that the SANTOSS model performs reasonably well for sand transport predictions under rippled-bed conditions. The approach of the SANTOSS model to account for the influences of the phase-lag effects in a parameterized way is suitable for these conditions. As seen in Table 11, under rippled-bed conditions 61% of the computed transport rates correspond with the measured data within a factor two and 84% within factor five.

Under fine sand velocity skewed conditions, the SANTOSS model correctly predicts offshore directed sand transport for the conditions measured in OFT experiments and onshore directed sand transport for conditions measured in surface wave experiments. The offshore directed sand transport predictions for the OFT experiments are due to the approach of SANTOSS to account for the phase-lag effects. The SANTOSS model predicts onshore directed sand transport under comparable conditions measured in surface wave experiments due to the surface wave effects of the SANTOSS model. The boundary layer streaming induces additional onshore directed sand transport. The vertical orbital velocity and the Lagrangian motion influence the settling of a sand particle, resulting into smaller phase-lags in the crest half-cycle and larger phase-lags in the trough half cycle. This contributes to additional onshore directed sand transport. The correct predictions indicate that the SANTOSS model correctly describes the phase-lag effects and the interaction between the phase-lag effects and the surface wave effects. Under sheet flow conditions 83% of the computed transport rates correspond with the measured data within a factor two and 96% within factor five.

As seen in Table 11, the general performance of the SANTOSS model is good; 77% of the calculated transport lay within a factor two of differences compared to the measured transport.

Table 11 the quantitative performance results of SANTOSS in terms of percentage of the predictions that deviate less than a factor 2 and 5 from the measurements. 'Wrong direction' represents the in transport that is predicted into the wrong. A distinction is made between the various sub sets.

Total	N	Factor 2	Factor 5	Wrong direction
All wave dominated datasets	211	77%	93%	5%
Data subset: type of flow				
Velocity-skewed waves (without currents)	94	69%	89%	9%
Acceleration-skewed waves (without currents)	53	79%	98%	2%
Waves with a superimposed current	50	86%	92%	2%
Surface waves	14	86%	100%	0%
Data subset: type of bed form				
Flat bed (Sheet flow)	155	83%	96%	2%
Rippled-bed	56	61%	84%	13%

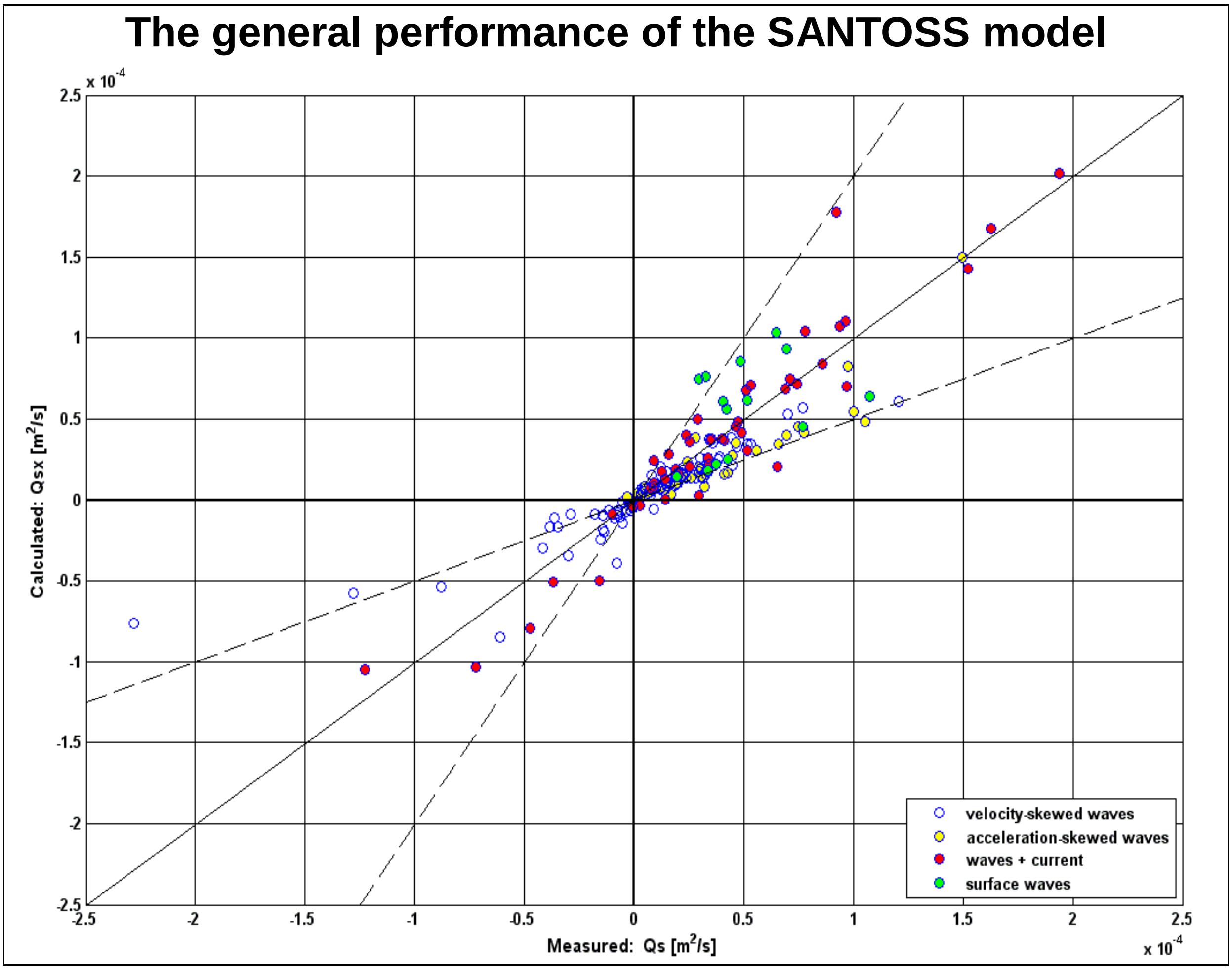

Figure 22: The transport calculated with the SANTOSS model. The solid line indicates perfect agreement; the dashed lines a factor 2 difference.

7.4 COMPARISON OF THE GENERAL PERFORMANCES

In this chapter the sand transport calculations of the models are compared with a large dataset of measured sand transport; understanding is gained of the applicability and limitations of the models (sub-question 3.a). This paragraph presents an overview of the performances of the three models. Table 12 presents qualitative the performance of the models under different conditions. Table 13 shows quantitatively an overview of the general performances of the three models. The performances of the models are compared to identify which model is most suitable for sand transport predictions under general wave dominated conditions (*question 3)*. The following can be concluded:

- *The measurements show that under fine sand (d_{50} < 0.2 mm) velocity skewed conditions the sand transports are offshore directed in OFT experiments and onshore directed in surface wave experiments. The difference in the direction of the sand transports is caused by the phase-lag effect and the surface wave effects. The offshore-directed sand transports in OFT experiments are due to the phase-lag effects. Under surface wave conditions, the surface wave effects induce additional onshore directed transport and reduce the influences of the phase-lag effects. Among the three models, only the SANTOSS model correctly predicts the magnitude and the direction of the sand transports in the OFT and the surface wave experiments. This indicates that the model correctly describes the influences of the phase-lag effects and the interaction between the phase-lag effects and the surface wave effects. N06 and VR07 do not account for the influences of the phase-lag effects and therefore only predict onshore directed sand transport.*

- *The sand transports under rippled-bed conditions are also offshore directed due to the phase-lag effects. Only the SANTOSS model accounts for the phase-lag effects and performs reasonably well under rippled-bed conditions. N06 and VR07 predict onshore directed transport under these conditions.*

- *The filter method to account for the acceleration skewness performs reasonable for N06 but poor for VR07. This may be partly caused by the different values of φ_τ .*

- *The SANTOSS model performs well under acceleration skewed wave conditions.*

- *The overall performances of N06 and VR07 are comparable. Both models generally perform well under non-fine sand sheet flow conditions.*

- *The overall best performance is obtained by the SANTOSS model. The better overall performance of the SANTOSS model is caused by i) the approach to account for the influences of surface wave processes, ii) the approach to account for the influences of acceleration skewed waves and iii) the approach to account for the influences of the phase-lag effects.*

- *The better performance of the SANTOSS model is also partly caused by the fact that the model is calibrated with the datasets in the SANTOSS database. However, as shown in Appendix A, a small amount of the datasets in the SANTOSS database are also used for calibration and validation of N06 and VR07.*

Table 12: An overview of the performances of the three models.

	N06	VR07	SANTOSS
Performance velocity skewed waves	Poor	Poor	Good
Performance acceleration skewed waves	Reasonable	Poor	Good
Performance waves with currents	Good	Reasonable/Good	Good
Performance surface waves	Poor	Good	Good
Performance sheet flow regime	Good	Reasonable	Good
Performance rippled-bed regime	Poor	Poor	Reasonable/good
Overall performance	Reasonable	Reasonable	Good

Table 13: A quantitative overview of the performances of the three models.

	Factor 2	Factor 5	Wrong direction
N06	52%	72%	25%
VR07	43%	64%	25%
SANTOSS	77%	93%	5%

8 ADJUSTMENTS OF THE MODELS

In the previous chapter the applicability of the models are analysed and a comparison is made between the performances of the three models. The results of the previous chapter show that the N06 and the VR07 models do not perform well for certain conditions. This chapter focuses on adjusting the models to enhance the model performances under these conditions. First an approach to adjust N06 is proposed in paragraph 8.1. The performance of the adjusted N06 model is presented in Figure 24 and Table 14. Next an approach to adjust the VR07 model is proposed in paragraph 8.2. The results of these adjustments are presented in Figure 26 and Table 15. Finally, an overview of the performances of the adjusted models is presented in the last paragraph. It may be noted that the previous chapter shows that for the different conditions the SANTOSS model performs better or as good as the other two models. The SANTOSS model is therefore not adjusted in this chapter.

8.1 ADJUSTMENT OF N06

This paragraph proposes possible adjustments of N06. As seen in the previous chapters, the N06 model does not perform well under surface wave conditions. N06 overestimates the sand transport under surface wave conditions. These overestimations can especially be seen for conditions with high peak orbital velocity. The influences of boundary layer streaming are included with the wave Reynolds stress. This stress can be calculated as follows (see Chapter 4):

$$-\rho(\overline{\tilde{u}\tilde{w}})_{\infty} = \rho \frac{2}{3\pi} f_e A^3 \omega^3 / c \qquad (8.1)$$

As seen in the formula, the friction factor for mobile bed f_e is used instead of the grain roughness friction factor $f_{2.5}$. The friction factor for mobile bed is much larger than the grain roughness friction factor and is therefore causing the overestimations for the majority of the surface wave data. The first adjustment is to replace the f_e with the $f_{2.5}$. Replacing the f_e with the $f_{2.5}$ reduces the additional transport due to streaming and thus reduces the overestimations. It may be noted that this adjustment also influences the surface wave conditions with low peak orbital velocity; the additional transport due to streaming under these conditions will also decrease. However, it is expected that the model still performs well under these conditions since the underestimations are small even without the inclusion of streaming (as showed in Chapter 6).

With this adjustment the N06 model now consistently uses the friction factor $f_{2.5}$. The wave Reynolds stress is now calculated as follows:

$$-\rho(\overline{\tilde{u}\tilde{w}})_{\infty} = \rho \frac{2}{3\pi} f_{2.5} A^3 \omega^3 / c \qquad (8.2)$$

The previous chapter also shows that the N06 model is not able to perform well under conditions in which the phase-lag effects are important. The model predicts sand transports into the wrong direction under these conditions. Appendix E shows the performance of the SANTOSS model without its phase-lag component (described with equation (4.62) until equation (4.71)). As seen in the appendix, the SANTOSS model without its phase-lag component and N06 predicts sand transport into the wrong direction for the same conditions. This indicates that the phase-lag component of the SANTOSS model is potentially capable to correct the sand transports that are predicted into the wrong direction by the N06 model. To improve the performance of N06 under conditions in which the phase-lag effects are important, the approach of the SANTOSS model to account for the influences of the phase-lag effects will be implemented into the N06 model.

The approach of the SANTOSS model to account for the phase-lag effects can be summarized as follows (Ribberink *et al.*, 2010):

- Sediment loads stirred up during the wave crest and wave trough are calculated separately;
- The magnitude of the phase-lag parameter determines the proportions of these loads that are transported during i) the same half-cycle as they were generated, and ii) during the next half cycle.

It may be noted that the SANTOSS model calculates representative loads for the onshore and offshore half-cycles while the N06 model calculates instantaneous transport rates. To make use of the phase-lag parameter of the SANTOSS model, the instantaneous transport rates of the N06 model are divided into two representative transport rates; Q_c and Q_t. Q_c is the sum of the sand transport during the onshore half-cycle of a wave and Q_t is the sum of the sand transport during the offshore half-cycle of a wave. The figure below illustrates Q_c and Q_t:

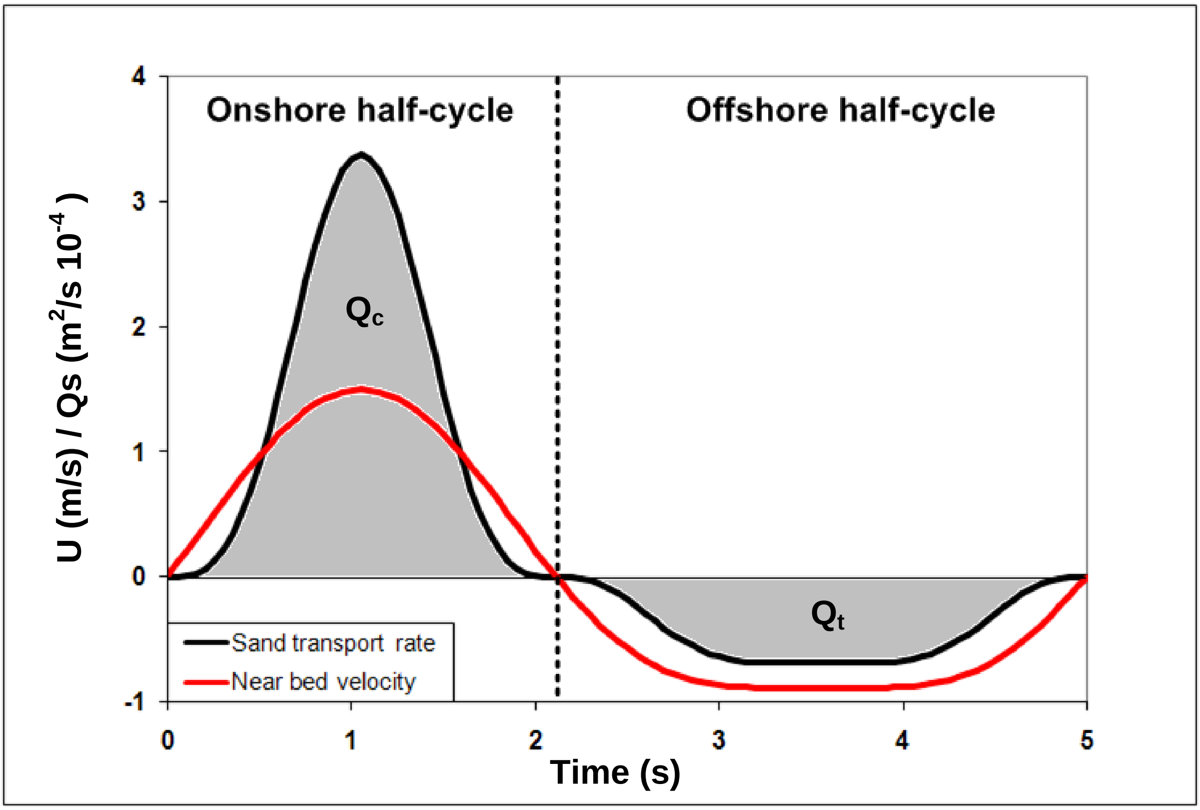

Figure 23: The sand transport is divided into sand that is transported during the onshore half-cycle of a wave (Q_c) and the offshore half-cycle of the wave (Q_t).

The magnitude of the phase-lag parameter now determines the proportion of i) sand that is transported during the same half-cycle as they were generated and ii) sand that is transported in the next half-cycle due to the phase-lag effects.

The equations below present how the phase-lag parameter is included into the N06 model. The equations are applied to equation (4.10) as follows:

$$Q_s = Q_{cc} + Q_{tc} - (Q_{tt} + Q_{ct}) \tag{8.3}$$

In which

$$Q_{cc} = \begin{cases} Q_c & \text{if} \quad P_c \le 1 \\ \dfrac{1}{P_c} Q_c & \text{if} \quad P_c > 1 \end{cases} \tag{8.4}$$

$$Q_{ct} = \begin{cases} 0 & \text{if} \quad P_c \le 1 \\ \dfrac{(P_c - 1)}{P_c} Q_c & \text{if} \quad P_c > 1 \end{cases} \tag{8.5}$$

$$Q_{tt} = \begin{cases} Q_t & \text{if} \quad P_t \le 1 \\ \dfrac{1}{P_t} Q_t & \text{if} \quad P_t > 1 \end{cases} \tag{8.6}$$

$$Q_{tc} = \begin{cases} 0 & \text{if} \quad P_t \le 1 \\ \dfrac{(P_t - 1)}{P_t} Q_t & \text{if} \quad P_t > 1 \end{cases} \tag{8.7}$$

With the phase-lag parameters:

$$P_c \begin{cases} \alpha_r \dfrac{\eta}{2(T_c - T_{cu}) w_s} & \text{if} \quad \eta > 0 \\ \alpha_s \dfrac{\delta_{sc}}{2(T_c - T_{cu}) w_s} & \text{if} \quad \eta = 0 \end{cases} \tag{8.8}$$

$$P_t \begin{cases} \alpha_r \dfrac{\eta}{2(T_t - T_{tu}) w_s} & \text{if} \quad \eta > 0 \\ \alpha_s \dfrac{\delta_{st}}{2(T_t - T_{tu}) w_s} & \text{if} \quad \eta = 0 \end{cases} \tag{8.9}$$

In the formulas above, α_s and α_r are both calibration coefficients. They determine the extent of influences of the phase-lag parameter in respectively the sheet flow regime and the rippled-bed regime. These two values have been recalibrated to α_s =0 and α_r = 13.94. Figure 24 and Table 14 presents the performances of the N06 model with the adjustments for the wave Reynolds stress and the phase-lag effects. The percentage of the computed transport rates corresponding with the measured data within a factor two increased from 52% to 67%. The improvement is mainly caused by the better sand transport predictions in the rippled-bed regime. Most of the sand transport predictions in the wrong direction under rippled-bed conditions are now corrected. For the rippled-bed conditions only 11% of the sand transports are predicted into the wrong direction (previously 79% were predicted into the wrong direction). The adjustment of the wave Reynolds stress improved the performance under surface wave conditions. For the surface wave conditions 86% of the sand transports are predicted within a factor two of differences compared to the measurements (previously only 36% was predicted within a factor two of differences).

As discussed in the previous chapter, under fine sand sheet flow conditions with velocity skewed waves the sand transports are offshore directed in OFT experiments and onshore directed in surface wave experiments. N06 does not account for the influences of the phase-lag effects. Therefore, the model predicts onshore directed sand transport under both conditions. An attempt is made to correct this with the phase-lag parameter of the SANTOSS model (an example of this is shown in Appendix F). After the inclusion of the phase-lag parameter, N06 correctly predicts the transport under fine sand OFT conditions into the offshore direction. However, the direction of the transport predictions under fine sand surface wave conditions also changed; the sand transports are now incorrectly predicted into the offshore direction. These wrong predictions under surface wave conditions are due to the fact that the N06 model considers boundary layer streaming as the only relevant surface wave process. The SANTOSS model also accounts for other surface wave effects; the vertical orbital velocity and Lagrangian motion. The Lagrangian motion and the vertical orbital velocity reduce the influences of the phase-lag effects under surface wave conditions. The phase-lag parameter is therefore suitable for the SANTOSS model. Since the vertical orbital velocity and the Lagrangian motion are not included into N06, the phase-lag parameter for sheet flow conditions is not suitable for N06. Therefore, the phase-lag parameter for sheet flow conditions is not included in this adjustment (α_s = 0). Only the phase-lag parameter for rippled-bed conditions is included.

Table 14 the quantitative performance results of the adjusted N06 in terms of percentage of the predictions that deviate less than a factor 2 and 5 from the measurements.

Total	**N**	**Factor 2**	**Factor 5**	**Wrong direction**
All wave dominated datasets	211	67%	91%	7%
Data subset: type of flow				
Velocity-skewed waves (without currents)	94	63%	84%	13%
Acceleration-skewed waves (without currents)	53	53%	94%	2%
Waves with a superimposed current	50	86%	96%	4%
Surface waves	14	86%	100%	0%
Data subset: type of bed form				
Flat bed	155	74%	93%	6%
Rippled-bed	56	50%	84%	11%

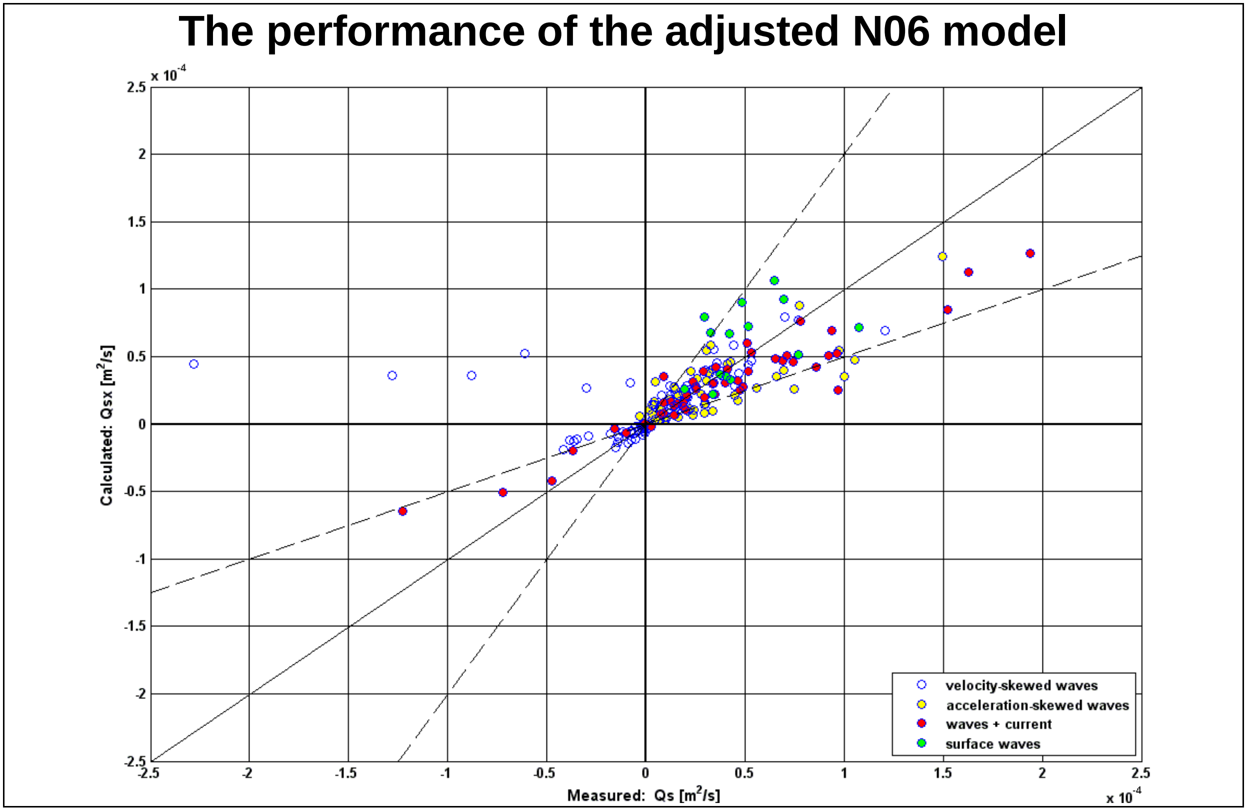

Figure 24: The transport calculated with the adjusted N06 model. The solid line indicates perfect agreement; the dashed lines a factor 2 difference. A distinction is made between the various types of flows

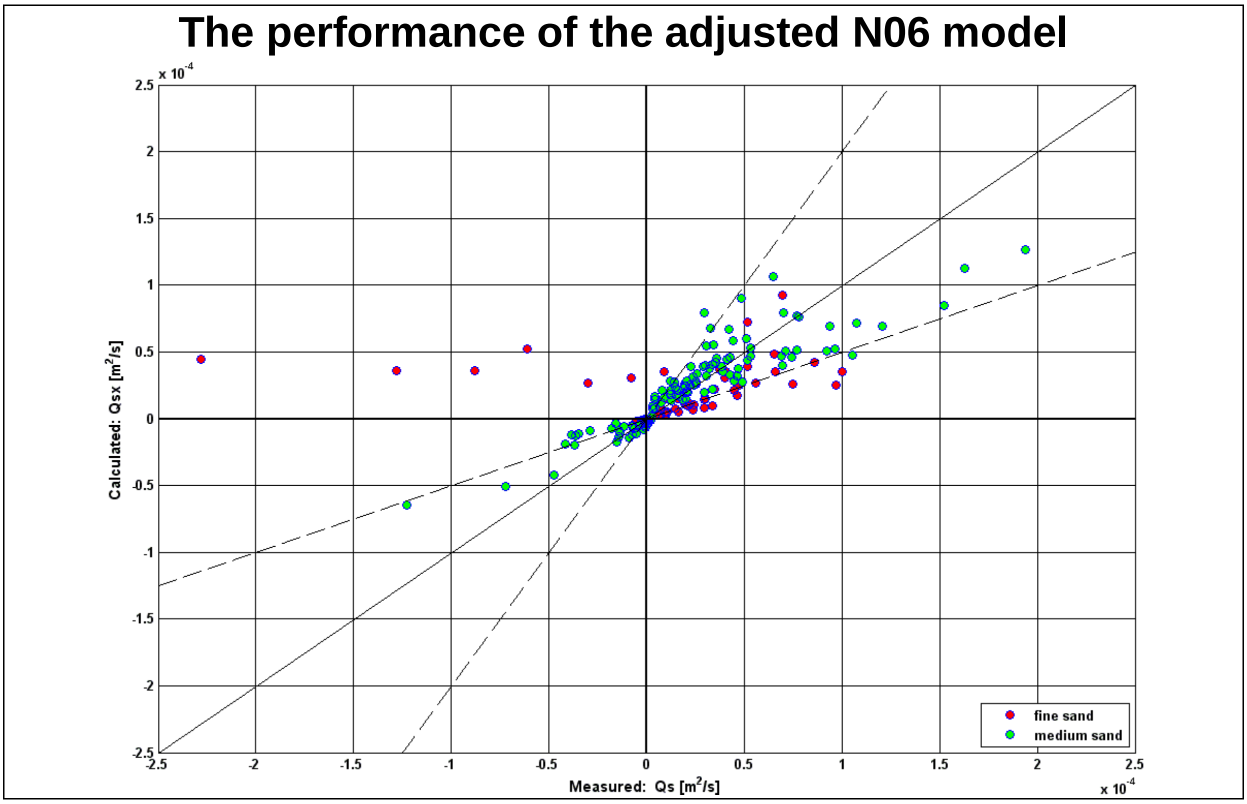

Figure 25: The transport calculated with the adjusted N06 model. The solid line indicates perfect agreement; the dashed lines a factor 2 difference. A distinction is made between fine sand d50 ≤ 0.2mm and medium sand d50 > 0.2 mm

8.2 ADJUSTMENT OF VR07

This paragraph proposes possible adjustments of the VR07 model. As seen in the previous chapters, the VR07 model is not able to account for the phase-lag effects and the influences of acceleration skewed waves. As seen in Figure 21, underestimations occur for the acceleration skewed waves conditions. To correct this, a higher value will be used for φ_τ (which means that the influences of the acceleration increases during the calculation of the sand transport (see paragraph 4.2). Guard and Nielsen (2010) found an optimal value of $\varphi_\tau = 47^o$ for the N06 model. To improve the performance of the VR07 model for acceleration skewed wave conditions, this higher value of $\varphi_\tau = 47^o$ will now be used for the VR07 model.

Furthermore, just like the N06 model, the VR07 model does not perform well under conditions in which the phase-lag effects are important. To account for the influences of the phase-lag effects, the approach of the SANTOSS model is used as proposed in the previous paragraph (equation (8.3) until equation (8.9)). The calibration coefficient α_r is recalibrated to $\alpha_r = 16.8$. Just like in the N06 model, including the phase-lag effects for the sheet flow regime will worsen the model performance for fine sand surface wave conditions. Therefore, the calibration coefficient α_s is remained as $\alpha_s = 0$. Figure 26 and Table 15 presents the performance of the adjusted VR07 model.

Due to the adjustments the performance of the VR07 model improved. The percentage of the computed transport rates corresponding with the measured data within a factor two increased from 43% to 49%. The improvement is mainly caused by the better sand transport predictions in the rippled-bed regime. The percentage of sand transport predictions into the wrong direction in rippled-bed regime is reduced from 79% to 13%. Just like in the N06 model, the sand transport predictions into the wrong direction due to the fine sediments in the sheet flow regime are not corrected.

The performance of VR07 for acceleration skewed waves slightly improves due to the adjustment of φ_τ. For the acceleration skewed wave conditions, the percentage of the computed transport rates corresponding with the measured data within a factor two of differences increases from 38% to 43%. However, this performance is still considered as poor.

Table 15 the quantitative performance results of the adjusted VR07 in terms of percentage of the predictions that deviate less than a factor 2 and 5 from the measurements.

Total	N	Factor 2	Factor 5	Wrong direction
All wave dominated datasets	211	49%	82%	8%
Data subset: type of flow				
Velocity-skewed waves (without currents)	94	40%	77%	14%
Acceleration-skewed waves (without currents)	53	43%	83%	2%
Waves with a superimposed current	50	62%	88%	4%
Surface waves	14	86%	100%	0%
Data subset: type of bed form				
Flat bed	155	54%	86%	6%
Rippled-bed	56	36%	71%	13%

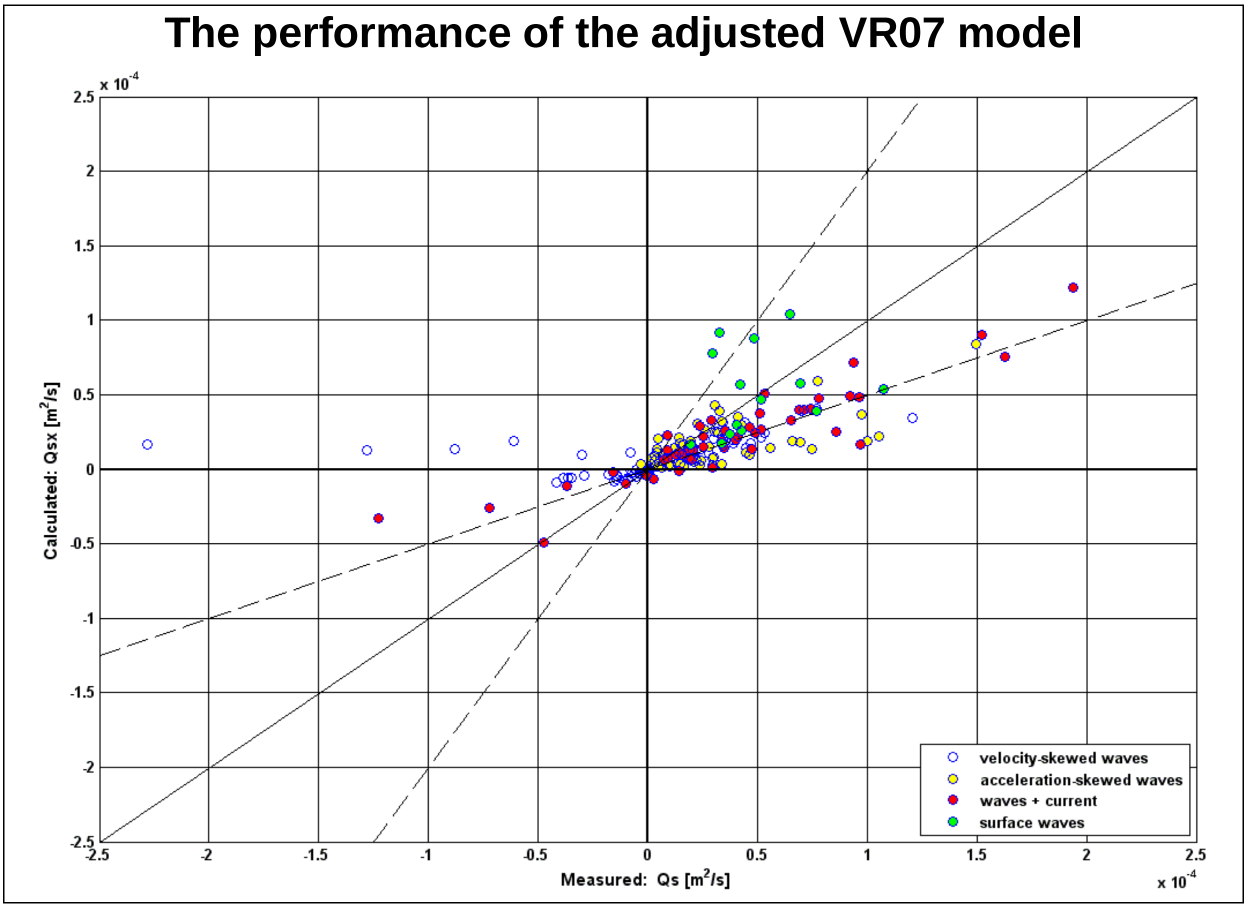

Figure 26: The transport calculated with the adjusted VR07 model. The solid line indicates perfect agreement; the dashed lines a factor 2 difference. A distinction is made between the various types of flows

8.3 OVERVIEW ADJUSTMENTS

In this chapter an attempt is made to achieve better performances by adjusting N06 and VR07 (*research question 4*). This paragraph compares the performances of the modified models. Table 16 presents a quantitative overview of the performances of the SANTOSS model and the adjusted N06 and VR07. The following can be concluded:

- *N06 overestimates the sand transport under surface wave conditions. To reduce these overestimations, the friction factor for mobile bed, which is used for the calculation of the wave Reynolds stress, is replaced with the grain friction factor. After the adjustment the performance of N06 under surface wave conditions improved and is comparable to the other two models.*

- *The performance of the VR07 model under acceleration skewed wave conditions improves by adjusting the* φ_τ *to 47°. It may be noted that the performance under these conditions is still considered as poor.*

- *Including the approach of the SANTOSS model to account for the influences of phase-lag under rippled-bed conditions considerably enhance the performances of N06 and VR07.*

- *The approach of the SANTOSS model to include the phase-lag effects in the sheet flow regime is not suitable for N06 and VR07. Due to the inclusion of the phase-lag parameter for sheet flow conditions, the performances of the models reduces under fine sand surface wave conditions; offshore directed transports are predicted while onshore directed transports are measured under these conditions. This is due to the fact that N06 and VR07 do not account for the vertical orbital velocity and Lagrangian motion; both processes reduce the influences of the phase-lag effects under surface wave conditions. Therefore, the approach of the SANTOSS model to account for the phase-lag effects under sheet flow conditions is not included N06 and VR07.*

- *VR07 obtained less improvement than N06.*

- *After adjusting N06 and VR07, the best performance is still obtained by the SANTOSS model.*

Table 16: A quantitative overview of the performances of the three models.

	Factor 2	Factor 5	Wrong direction
Adjusted N06	68%	91%	6%
Adjusted VR07	49%	82%	8%
SANTOSS	77%	93%	5%

9 DISCUSSION

In this study the datasets in the SANTOSS database are used as input for the models. N06 and VR07 both require time series as input. These time dependent data are not available and are therefore generated with data in the database. It is assumed that velocity skewed waves have the shape of second-order Stokes waves. Furthermore, a wave is assumed to be velocity skewed *or* acceleration skewed. This is not the case for the three surface wave conditions of Dohmen-Janssen and Hanes (2002) and three conditions measured in the TRANSKEW experiment (Silva *et al.,* 2010). These waves are velocity skewed and acceleration skewed, but are assumed to be only velocity skewed. Also, for the calculation of a depth average velocity that is required for the VR07 model as input for the 'wave with current' conditions, a logarithmic profile is assumed. The extent of influences on the performances of these assumptions is unknown. However, the models do not seem to have problems with the six acceleration and velocity skewed wave conditions; most the predicted transport lie within or around a factor two of differences compared to the measured transport. Furthermore, VR07 does not especially perform worse under 'wave with current' conditions.

Another discussion point is the value of φ_τ that is used in this study. In the paper of Nielsen (2006) an optimal angle of $\varphi_\tau = 51^o$ has been found. Guard and Nielsen (2010) discussed that due to an error in the calculations, the optimal angle should be $\varphi_\tau = 47^o$. This value is used for this study. However, no official papers have been released yet for this value. This value is based on personal communication with Guard and Nielsen.

During the assessment of the performances of the three models, the contribution of physical correctness against the contribution of calibration has been neglected. Physical correctness means focusing on correctly describing different physical processes while the main focus of calibration is tuning the model parameters so desired output can be obtained with the input. The SANTOSS model is calibrated on all the datasets of the SANTOSS database. It is therefore not surprising that this model performs well for this database. The other two models are only calibrated with a small amount of datasets that are collected in the SANTOSS database. The question is therefore if the SANTOSS model performs well due to physical correctness or due to calibration. As seen earlier, the SANTOSS model is not a black box model that is only based on calibration. The formulas are based on physical processes. It is therefore expected that calibration and correctly describing the different processes both contribute to the good performance. Furthermore, an attempt is made to implement the approach of the SANTOSS model to account for the phase-lag effects in N06 and VR07. The calibration coefficients of this approach have been recalibrated for these two models. However, due to the fact that N06 and VR07 does not describe surface wave processes as extensively as the SANTOSS model, the good performance of the SANTOSS model still cannot be obtained, even with the recalibration. This indicates that it is hard to obtain good performances for such a large dataset with calibration only if the relevant processes are not described correctly.

The measurements in OFT experiments show that under fine sand sheet flow conditions, the sand transport is offshore directed. N06 and VR07 are quasi-steady models and do not account for the influences of the phase-lag effects; the models predict onshore directed transport under these conditions. Based on these results a conclusion can be drawn that the models are not suitable for fine sand sheet flow conditions. However, under comparable fine sand sheet flow conditions, onshore directed sand transport has been measured in a surface wave experiment. This can be due to the surface wave effects that reduce or cancel out the influences of the phase-lag effects. Sand transports in coastal areas are due to surface waves; the influences of the surface wave effects are therefore always present under field conditions. This may indicate that even though N06 and VR07 are not able to account for the influences of the phase-lag effects under fine sand sheet flow conditions, the models are still suitable for practical use under these conditions, since the surface wave effects reduce or cancel out the influences of the phase-lag effects under field conditions.

It may be noted that there are only four measurements available of sand transport under fine sand sheet flow conditions in surface wave experiments. It is therefore unknown if the surface wave effects always reduce or cancel out the influences of the phase-lag effects. Furthermore, since there are no measurements available of sand transport under rippled-bed conditions in surface wave experiments, it is unknown if the surface wave effects have similar influences on the phase-lag effects in the rippled-bed regime. Therefore, it might be interesting to investigate how the surface wave effects influences the phase-lag effects to understand the practical applicability of the quasi-steady models under field conditions. For this, new measurements can be carried out in surface wave experiments under conditions in which the phase-lag effects are important.

10 CONCLUSION

In this study the sand transport predictions of the models of Nielsen (2006), Van Rijn (2007) and the recently developed SANTOSS model are compared with a large dataset of measured sand transports in OFT experiments and surface wave experiments to

i) identify which model is the most suitable for predicting wave dominated cross-shore sand transport;
ii) gain more understanding of the influences of the streaming components on the model performances under surface wave conditions.

In this study first a sensitivity analysis have been carried out for the models of Nielsen (N06), Van Rijn (VR07) and the SANTOSS model to gain understanding of how changes in flow and sand characteristics influence the additional sand transport induced by streaming. Then the sand transport rates predicted by the three models are compared with sand transport measured in surface wave experiments. This is for understanding to what extent including streaming in the models influences the model performances under surface wave conditions. Next the sand transport predictions of the three models are compared with 211 sand transport rates measured in various wave dominated flume and oscillatory flow tunnel experiments to gain understanding of the applicability of the models and to identify which model is the most suitable for sand transport predictions in wave dominated conditions. Finally the models of Nielsen (2006) and Van Rijn (2007) are adjusted to improve the model performances.

In this chapter conclusions are drawn with respect to the four research questions:
1) How do changes of flow and sand characteristics influence additional sand transport induced by streaming?
2) How does including streaming influences the performances of the models under surface wave conditions?
3) Which model is capable to give the best performance in cross-shore sand transport predictions for different wave dominated conditions?
4) Is it possible to achieve a better performance by adjusting a model with concepts of the other two models?

The following conclusions are drawn with respect to the first research question:

- Among the three models, N06 predicts the largest amount of additional sand transport due to streaming. SANTOSS predicts the smallest amount of additional sand transport. This may be due to the fact that the SANTOSS model does not consider the boundary layer streaming as the only relevant surface wave effect; the model splits the surface wave effects up in the boundary layer streaming, vertical orbital velocities and Lagrangian motion.
- The amount of additional transport induced by streaming is the most sensitive to changes in the peak orbital velocities.
- After including streaming, the amount of predicted transport by VR07 and the SANTOSS model are very similar to each other. To gain more understanding of this similarity, a comparison is made between the influences of i) the streaming velocity of VR07 and ii) the three surface wave effects of the SANTOSS model. This comparison shows that under non-fine sand sheet flow conditions (d_{50} > 0.2 mm), the additional transports due to the streaming velocity of VR07 and the three surface wave effects of the SANTOSS model are nearly the same. Van Rijn (2007) used model and experimental results to calibrate his streaming velocity. He may have indirectly included different surface wave processes in his streaming velocity during the calibration.

The following conclusions are drawn with respect to the second research question:

- The comparison between the sand transport predictions with datasets of measured sand transport in surface wave experiments shows that including a streaming component in the formula does not necessarily improve the model performances under surface wave conditions.
- The N06 model performs better if the streaming component is not included. The model overestimates the sand transport under surface wave conditions if streaming is included. The streaming component is only suitable for the dataset that Nielsen (2006) used for the verification of his approach to include boundary layer streaming. The major difference between this dataset and the newly obtained dataset is the peak orbital velocity; the new dataset of sand transport is measured in surface wave experiments with higher peak orbital velocity. The additional transport due to streaming is large under conditions with high peak orbital velocity. This caused the overestimations under surface wave conditions.
- The streaming components of the VR07 and the SANTOSS models do improve the model performance under surface wave conditions. Even though the approaches are different, both the VR07 and the SANTOSS model perform well under these conditions.

The following conclusions are drawn with respect to the third research question:

- To gain more understanding of the applicability of the models, comparisons have been made between the predicted sand transport rates and 211 measured sand transport rates. This comparison shows that N06 and VR07 do not perform well under rippled-bed conditions and fine sand sheet flow conditions; the models predict the sand transports into the wrong direction under these conditions. This is due to the fact that the models do not account for the influences of the phase-lag effects.
- Due to its approach to account for the influences of the phase-lag effects, the SANTOSS model is able to perform well under fine sand sheet flow conditions and rippled-bed conditions.
- Under acceleration skewed wave conditions, the SANTOSS model is able to give the best performance. The N06 model performs reasonable and the VR07 performs poor. The N06 and VR07 models use the same filter method to account for the influences of acceleration skewness. The differences in performances of the N06 and the VR07 are partly caused by the different values of φ_τ (N06 use $\varphi_\tau = 47^o$ and VR07 use $\varphi_\tau = 40^o$).
- The general best performance is obtained by the SANTOSS model due to i) the approach to account the influences of surface wave processes, ii) the approach to account for the influences of sawtooth shaped waves and iii) the approach to account for the phase-lag effects. The better performance is also partly caused by the fact that the model is calibrated with the datasets of the SANTOSS database. It may be noted that a small amount of the datasets in the SANTOSS database are also used for calibration and validation of N06 and VR07
- The overall performances of the N06 and VR07 models are comparable.

The following conclusions are drawn with respect the fourth research question:

- An attempt is made to improve the performances of N06 and VR07 under rippled-bed conditions and under fine sand sheet flow conditions. To do this, the approach of the SANTOSS model to include the phase-lag effects is implemented into the two models. The SANTOSS model uses two phase-lag parameters to account for the influences of the phase-lag effects; one parameter for under rippled-bed conditions and one parameter for under sheet flow conditions. Including the phase-lag parameter for rippled-bed conditions considerably enhance the performances of N06 and VR07 under these conditions.
- The approach of the SANTOSS model to account for the influences of the phase-lag effects under sheet flow conditions is not suitable for N06 and VR07. After including the phase-lag parameter for sheet flow conditions, offshore directed transports are predicted while onshore directed transports are measured under fine sand surface wave conditions. This is due to the fact that N06 and VR07 do not account for the vertical orbital velocity and the Lagrangian motion. Both processes reduce the influences of the phase-lag effects under surface wave conditions.
- N06 overestimates the sand transport under surface wave conditions. To reduce the overestimations, the friction factor for mobile bed, which is used for the calculation of the wave Reynolds stress, is replaced with the grain friction factor. After the adjustment the performance of N06 under surface wave conditions improved and is comparable to the other two models.
- VR07 underestimates the sand transport under acceleration skewed wave conditions. To improve the performance of the model under these conditions, the angle $\varphi_\tau = 40^o$ is adjusted to $\varphi_\tau = 47^o$. The performance of VR07 under acceleration skewed wave conditions slightly improved due to this adjustment. However, this performance is still considered as poor.
- Even though the performances of N06 and VR07 improve due to the adjustments, the good performance of SANTOSS still cannot be obtained.

11 REFERENCE

Davies A. G. and Villaret C. (1999). Eulerian drift induced by progressive waves above rippled and very rough beds, *Journal of Geophysical Research vol.* **104**, pp. 1465-1488

Dibajnia M. and Watanabe A. (1998). Transport rate under irregular sheet flow conditions. *Coastal Engineering* **53**, pp. 167-183.

Dohmen-Janssen C.M., Kroekenstoel D.F., Hassan W.N. and Ribberink J.S. (2002). Phase-lags in oscillatory sheet flow: experiments and bed load modeling, *Coast. Eng. 53,* pp. 61–87

Dohmen-Janssen C.M. and Hanes D.M. (2002). Sheet flow dynamics under monochromatic nonbreaking waves, *Journal of Geophysical Research vol.* **107**

Guard P. and Nielsen P. (2010). Personal communication.

Naqshband S. (2009). Wave boundary layer streaming: Analysis on wave boundary layer streaming and its effect on bed shear stress. University of Twente, The Netherlands.

Nielsen P. (1992). *Coastal* bottom boundary layers and sediment transport. *World Scientific Publishing*, Singapore: JBW Printers & Binders.

Nielsen P. (2006). Sheet flow sediment transport under waves with acceleration skewness and boundary layer streaming, *Coastal Engineering* **53**, pp. 749–758

O'Donoghue T., Doucette J.S., van der Werf J.J. and Ribberink J.S. (2006). The dimensions of sand ripples in full-scale oscillatory flows, *Coastal Engineering* **53**, pp. 997 – 1012

O'Donoghue T. and Ribberink J.S. (2007). Laboratory Experiments and the Development of Wave-Driven Sand Transport Models, *Publs. Inst. Geophys. Pol. Acad. Sc.* **E-7 (401)**, pp. 177-194

O'Donoghue T. and Wright S. (2004). Flow tunnel measurements of velocities and sand flux in oscillatory sheet flow for well-sorted and graded sands. *Coastal Engineering* **51**, pp. 1163-1184

Ribberink J. S. (1998). Bed-load transport for steady flows and unsteady oscillatory flows. *Coastal Engineering* ***34***, pp. 59-82.

Ribberink J.S., Dohmen-Janssen C.M., Hanes D.M., McLean S.R. and Vincent C. (2000). Near bed sand transport mechanisms under waves. *Proceedings 29th International Conference on Coastal Engineering*, pp. 3263–3276.

Ribberink J.S., Van der A, D. A. And Buijsrogge R.H. (2010). SANTOSS transport model: A new formula for sand transport under waves and currents. University of Twente, The Netherlands

Scandura P. (2007). Steady streaming in a turbulent oscillating boundary layer. *J. Fluid Mech. Vol.* **571**, pp. 265 - 280

Silva P., Abreu T., Ruessink G., Michallet H., Sancho F., Van der A D., Van der Werf J., Ribberink J., O'Donoghue T. and Temperville A. (2010). A laboratory experiment in acceleration-skewed oscillatory sheet flow. *Proceedings of the HYDRALAB III Joint User Meeting,* Hannover, Germany

Schretlen J.J.L.M. (2010). Ph.D thesis. University of Twente, The Netherlands.

Schretlen J.J.L.M., van der Werf J.J. (2006). SANTOSS Database: Existing data from experiments in oscillatory flow tunnels and large wave flumes. University of Twente, The Netherlands

Schretlen J.J.L.M., van der Werf J.J., Ribberink J.S., Kleinhans M., Zuijderwijk W.M. and O'Donoghue T. (2008). New high-resolution measurements of wave boundary layer flow under full-scale surface waves. *International conference on coastal engineering 2008*

Van der Werf J.J., Schretlen J.J.J.L.M., Ribberink J.S. and O'Donoghue T. (2009). Database of full-scale laboratory experiments on wave-driven sand transport processes, *Coastal Engineering* **56**, pp. 726 – 732

Van der A D. A. (2008). SANTOSS data report: AOFT–Santoss-Series-C Experiments. University of Aberdeen, United Kingdom

Van Rijn L.C. (1993). Principles of sediment transport in Rivers, estuaries and coastal seas. Aqua publications, The Netherlands: Bariet

Van Rijn L.C. (2007). Unified view of sediment transport by currents and waves. I: Initiation of motion, bed roughness, and bed-load transport. *Journal of hydraulic engineering*, pp. 649-667

Watanabe A. and Sato S. (2004). A sheet-flow transport rate formula for asymmetric, forward-leaning waves and currents. *Proceedings 29th International Conference on Coastal Engineering*, pp. 1703-1714

Whitehouse R. (1998). Scour at Marine Structures. Thomas Telford Publications, London

APPENDIX

Appendix A : Overview of the used datasets

For the comparison of the model performances the datasets from the SANTOSS database are used. Table 13 presents an overview of these datasets (based on Schretlen and Van der Werf, 2006). For each dataset the table present the facility in which the experiments were carried out, the type of flow, the type of bed form and the number of used conditions. The table also shows which datasets are used for calibration of validation of the models.

Table 17 The used datasets from the SANTOSS. 'C' and 'V' mean that the dataset is (partly) used for respectively the calibration and validation of a model.

Reference	Code	Facility	Flow	Type of bed form	Number of used conditions	N06	VR07	SANTOSS
Clubb (2001)	CLU2001	aoft	rs + ra	2d	4			C
Dibajnia and Watanabe (1992)	DIB1992	toft	rs + ra	fb	17			C
Dohmen-Janssen (1999)	DOH1999	lowt	rs	fb	23			C
Dohmen-Janssen and Hanes (2002)	DOH2002	gwk	ra	fb	4	V		C
Hassan (2003)	HAS2003	lowt	rs + ra	fb	5			C
Katopodi et al. (1994)	KAT1994	lowt	rs	fb	4		C	C
O'Donoghue and Wright (2004)	ODO2004	aoft	rs + ra	fb	6	V		C
Ramadan (1994)	RAM1994	lowt	rs + ra	fb + 2d	5		C	C
Ribberink and Chen (1993)	RIB1993	lowt	ra	fb	4			C
Ribberink and Al-Salem (1995)	RIB1994	lowt	rs + ra + ia	fb + 2d + 3d	20		C	C
Ribberink (1995)	RIB1995	lowt	ra	fb	5			C
Sato (1987)	SAT1987	toft	ra + ia	2d + 3d	21			C
Schretlen (2010)	SCH2010	gwk	ra	fb + bm	10			C
Silva et al. (2008)	TRS2007	lowt	rss + ras + ra	fb	11			C
Van der Werf et al. (2006)	VAN2006	aoft	ra + ia + is	2d + 3d	20			C
Van der Werf et al. (2007)	VAN2007	aoft	ra + rs	2d	3			C
Van der A et al. (2009)	VDA2008	aoft	rss + ras	fb	35			C
Watanabe and Sato (2004)	WAT2004	toft	rss	fb	12	C		C
Wright and O'Donoghue (2002)	WRI2002	aoft	rs + ra	fb	2			C

The abbreviations in the table have the following meaning:

Experimental facility:

aoft *Aberdeen oscillatory flow tunnel*
coft *Cambridge oscillatory flow tunnel*
delta *Delta flume at WL|Delft Hydraulics*
gwk *Groβer Wellenkanal at Forschungszentrum Küste Hannover*
lowt *Large oscillating water tunnel at WL|Delft Hydraulics*
pwt *Pulsating water tunnel at HR Wallingford*
toft *Tokyo oscillatory flow tunnel*

Bedform regime:

2d *Two-dimensional ripples*
3d *Three-dimensional ripples*
bm *Bi-modal bed*
fb *Flat-bed*

Type of oscillatory flow:

ia *Irregular, velocity skewed*
ias *Irregular, velocity skewed, acceleration skewed*
is *Irregular, symmetric (not velocity skewed)*
ra *Regular, velocity skewed*
ras *Regular, velocity skewed, acceleration skewed*
rs *Regular, symmetric (not velocity skewed)*
rss *Regular, acceleration skewed*

The last three columns of the table show which datasets are used for the development of a model. The characters ‘C’ and ‘V’ indicate that a dataset is (partly) used for respectively the calibration and validation of a model.

Appendix B : A comparison of surface wave effects of VR07 and the SANTOSS model

The sensitivity analysis in Chapter 5 shows a noticeable result. If streaming is included, the amount of sand transport predicted by VR07 and the SANTOSS model under surface wave conditions are comparable to each other. This is surprising since the approaches of the two models to account for surface wave effects are entirely different.

VR07 considers boundary layer streaming as the only surface wave effect. Under surface wave conditions, an additional steady current velocity is added to the orbital velocity. Based on the model and experimental results of Davis and Villaret (1999), Van Rijn (2007) found a relation between the relative roughness and the magnitude and direction of the streaming velocity.

On contrary to the VR07 model, the SANTOSS model does not consider boundary layer streaming as the only surface wave effect. Ribberink *et al.* (2010) separate the surface wave effects up in three processes; the vertical orbital velocity, the Lagrangian motion and the boundary layer streaming. In the SANTOSS model, a positive wave Reynolds stress is used to account for the influences of the boundary layer streaming instead of a steady current. Compared to the VR07 model, the processes that are relevant under surface wave conditions are described more extensively in the SANTOSS model. However, the results of the sensitivity analysis in Chapter 5 show that under surface wave conditions, the predicted transports by the two models are comparable to each other.

To gain more understanding of the similarities in the transport predictions of VR07 and the SANTOSS model, a comparison is made in this chapter between the sand transport calculated by the models with and without the surface wave effects. It may be noted that this is nearly the same as the sensitivity analysis in Chapter 5. The only difference is that the influences of all three surface wave effects of the SANTOSS model are analysed, instead of only analysing the influences of boundary layer streaming. For VR07 the only surface wave effect is still the boundary layer streaming. For the calculations a random realistic surface wave condition (Table 6) is used. One parameter will be varied to see the corresponding effect on the sand transport. Figure 27, Figure 28 and Figure 29 presents the results of the sand transport calculations of VR07 and the SANTOSS model.

Figure 27 presents the calculated net transport rates as function of the grain size. The dotted and the solid lines represent respectively the calculations without and with the surface wave effects. The difference between the dotted and the solid line can be seen as the additional transport due to the surface wave effects. As seen in the figure, under fine sand conditions (d_{50} < 0.2 mm) the additional transport due to the surface wave effects of the two models are different. This is due to the fact that the SANTOSS model accounts for the phase-lag effects. Furthermore, the Lagrangian motion and the vertical orbital velocity of the SANTOSS model influence the phase-lag effects. This causes the large difference in additional transport due to surface wave effects under fine sand conditions. As seen in the figure the amount of additional transport due to the surface wave effects of the two models are comparable to each other under medium sand conditions (d_{50} > 0.2 mm). It may be noted that further increase of the grain size after d_{50} = 0.31 mm results into a decrease of additional transport due to the streaming velocity of VR07 but an increase of additional transport due to the surface wave effects of SANTOSS. This indicates that under coarser sand conditions the additional transport due to the surface wave effects of the two models are not comparable.

Figure 28 and Figure 29 present the calculated net transport rates as function of respectively the period and the peak orbital velocity. As seen in the figure, the amount of additional transport induced by the surface wave effects of the SANTOSS model is in the same order of magnitude as the additional transport induced by the boundary layer streaming of VR07. Also, the variations in the additional transports due to the variations in the period and peak orbital velocity are also comparable to each other.

This appendix shows that the influences of the surface wave effects of the two models are nearly similar to each other (except for the fine sand conditions). The by surface wave effects induced additional transports of the two models are in the same order of magnitude. This may indicate that even though the VR07 model does not describe the surface wave effects as extensively as the SANTOSS model, the influences of the surface wave processes are still similar to each other. Van Rijn (2007) used model and experimental results of Davis and Villaret (1999) for the calibration of the streaming velocity. A possible explanation is that the influences of other surface wave effects (vertical orbital velocity and Lagrangian motion) are implicitly included in the streaming velocity through the calibration.

It may be noted that it is expected that these similarities cannot be observed for coarser sand since the amount of the additional sand transport due to streaming decreases for an increasing sediment size for d_{50} > 0.31 mm. It's also expected that this similarity cannot be observed under rippled-bed conditions, since the streaming of VR07 will be offshore directed under these conditions.

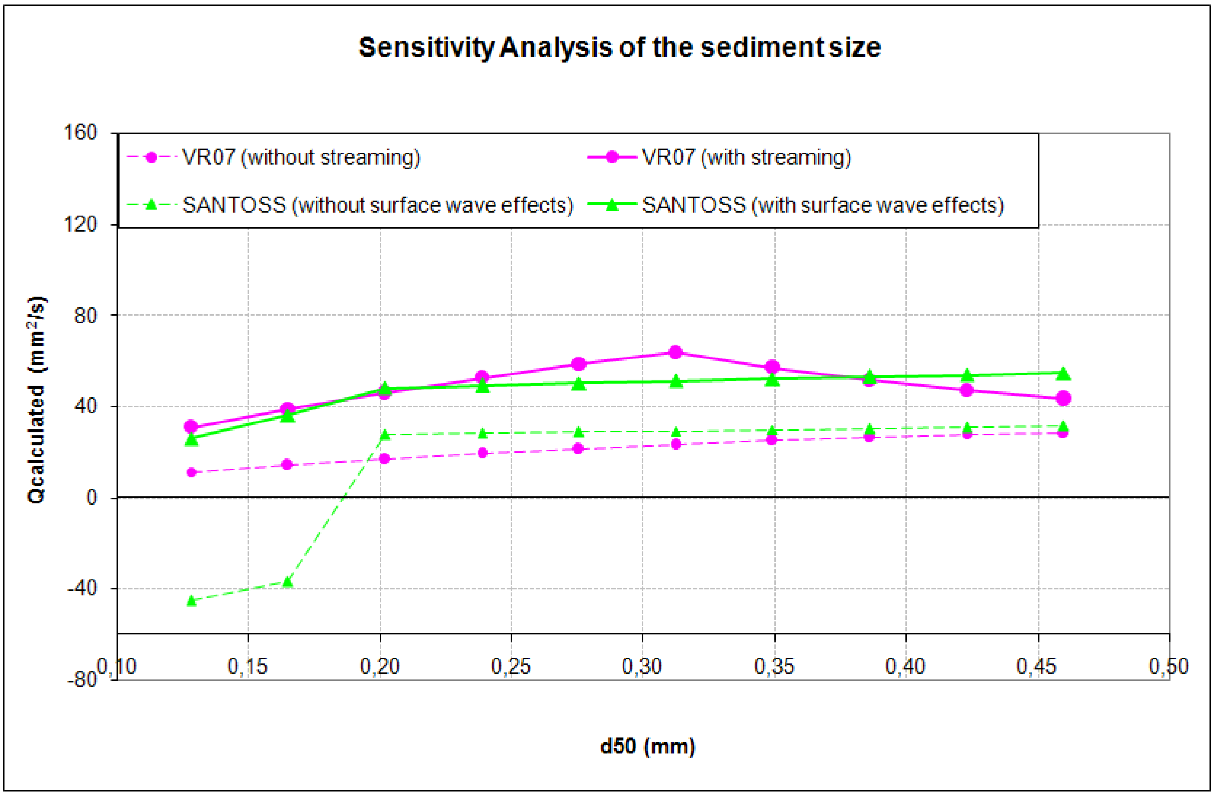

Figure 27: The calculated net transport rates as function of the grain size. The dotted lines represent the sand transport calculations of the models without including the surface wave effects. The solid lines represent the calculations including the surface wave effects.

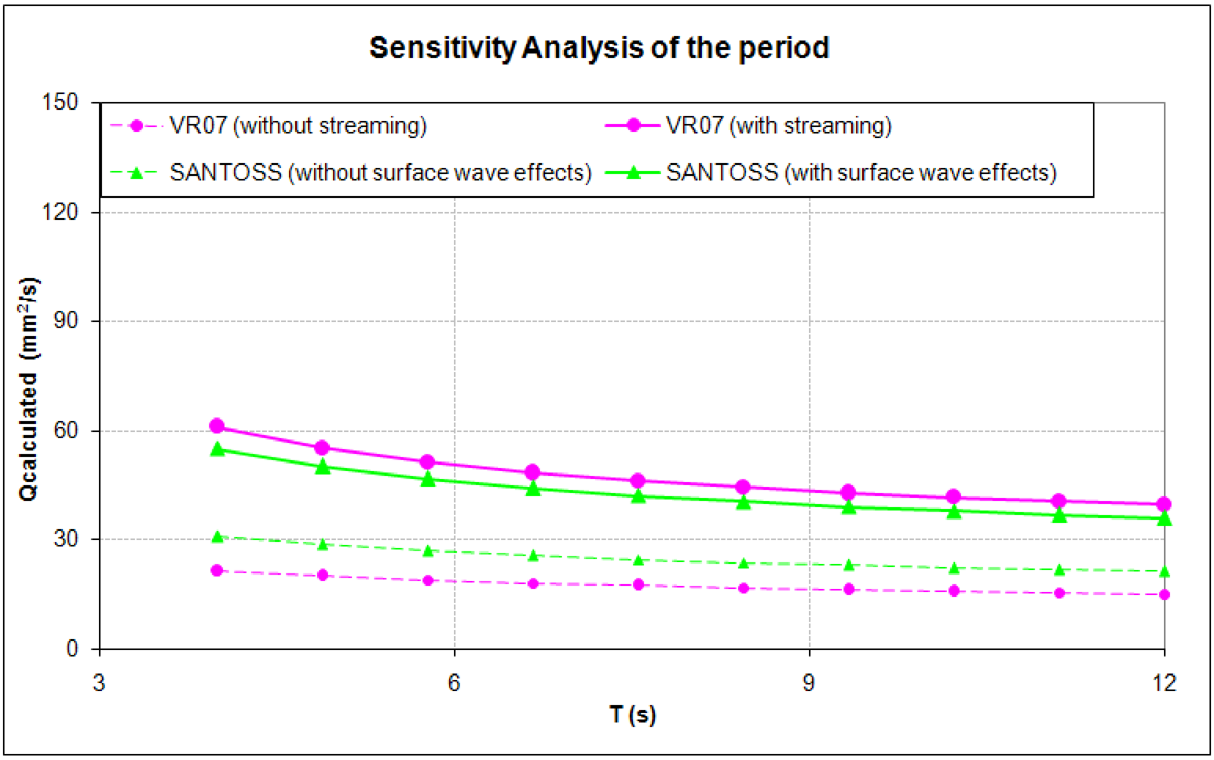

Figure 28: The calculated net transport rates as function of the flow period. The dotted lines represent the sand transport calculations of the models without including the surface wave effects. The solid lines represent the calculations including the surface wave effects.

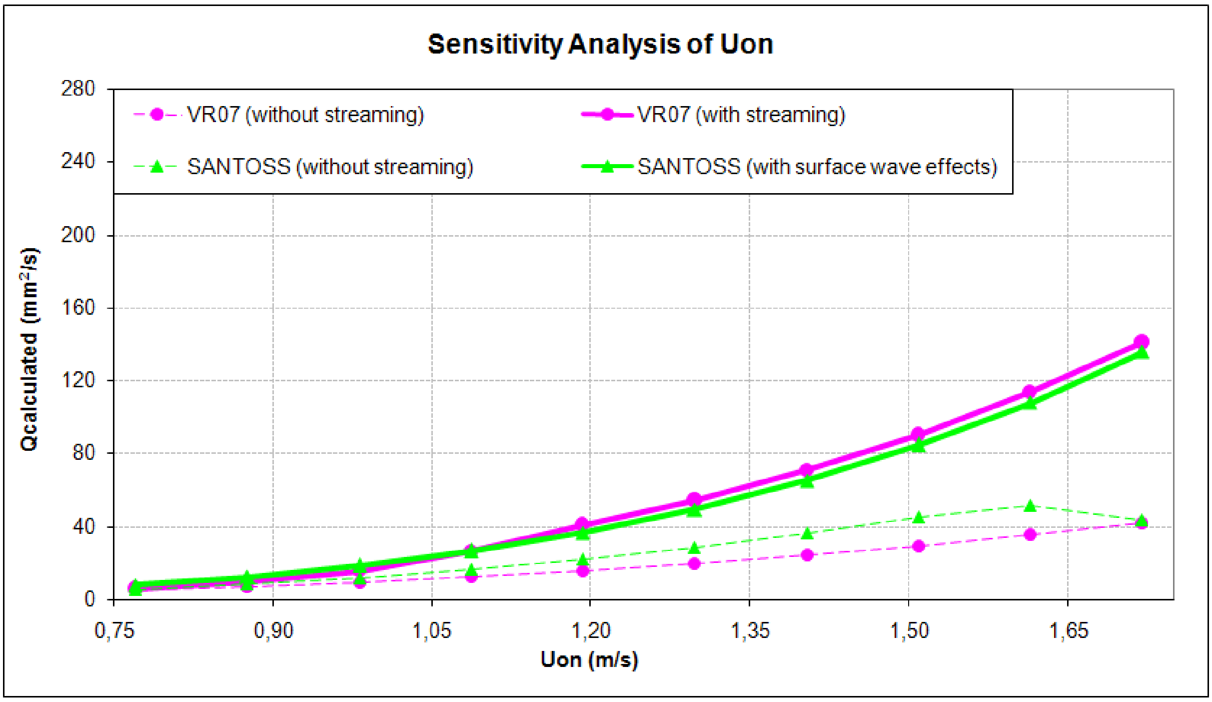

Figure 29: The calculated net transport rates as function of the peak orbital velocity. The dotted lines represent the sand transport calculations without the surface wave effects and the solid lines with the surface wave effects. The degree of velocity skewness has been remained on R = 0.6.

Appendix C : Generating time series

The SANTOSS model does not uses time series as input for the model. Instead of this, two representative values of the velocity are used for the calculation of the sand transport; the peak crest orbital velocity (U_{on}) and the peak trough orbital velocity (U_{off}). The SANTOSS-database therefore does not contain the time dependent velocities that the N06 and VR07 models require as input. To be able to use the database, time series are generated with the U_{on} and U_{off}. It may be noted that only formulas to generate a velocity skewed wave *or* an acceleration skewed wave is presented here. This also represents most of the data. In the used datasets of the SANTOSS database, only six conditions are velocity skewed as well as acceleration skewed. However, the degree of acceleration skewness is low. This will be neglected and the waves are assumed to be only velocity skewed.

Appendix C.1 Velocity skewed waves

An assumption is made that the near bed orbital velocity for the velocity skewed waves has the form of second-order Stokes waves. A second order Stokes wave can be generated with the following equation:

$$u(t) = u_1 \cos \omega t + u_2 \cos 2\omega t \qquad \text{(A.1)}$$

In which

$$u_1 = \frac{U_{on} + U_{off}}{2} \qquad \text{(A.2)}$$

$$u_2 = \frac{U_{on} - U_{off}}{2} \qquad \text{(A.3)}$$

$$\omega = \frac{2\pi}{T} \qquad \text{(A.4)}$$

Appendix C.2 Acceleration skewed waves

To generate acceleration skewed waves, the following formula is used (Van der A., 2008):

$$u_\infty(t) = \frac{U_{on} + U_{off}}{2} f(\beta) \sum_{i=1}^{6} \frac{(2\beta - 1)^{i-1} \sin(i\omega t)}{i} \qquad \text{(A.5)}$$

With:

$$f(\beta) \approx \frac{1}{\sum_{i=1}^{6} \frac{(2\beta - 1)^{i-1} \sin(i\omega t)}{i}} \qquad \text{(A.6)}$$

Appendix D : Depth averaged current velocity

For the calculations of the sand transport due to wave and current, the VR07 model requires a depth averaged current velocity as input for his model. This is not available in the SANTOSS database. For the wave with current conditions, only a current velocity at a specific reference water level is available in the database. The following method is used to calculate a depth averaged current velocity:

First a bed shear stress is calculated with a current velocity at a reference depth:

$$\tau'_{b,c} = 0.5\rho_w f_{cr}' u_\delta^2 \tag{B.1}$$

In which:

$$f_{cr}' = 2\left(\frac{0.4}{\ln \frac{\delta}{z0}}\right)^2 \tag{B.2}$$

Whereby $\tau'_{b,c}$ is the instantaneous grain-related bed-shear stress due to currents, u_δ is the current velocity at z = δ and f_{cr}' is the current related friction coefficient presented by Ribberink (1998).

A bed shear stress can also be calculated using a depth average current velocity. This can be calculated as:

$$\tau'_{b,c} = 0.5\rho_w f_{cvr}' u_c^2 \tag{B.3}$$

In which:

$$f_{cvr}' = \frac{8g}{[18\log(12h/k_{s,grain})]^2} \tag{B.4}$$

Whereby u_c is the depth averaged velocity and f_{cvr}' is the current-related grain friction coefficient based on $k_{s,grain} = d_{90}$ presented by van Rijn (2007). Combining the shear stress calculated with the friction factor of Ribberink (1998) and the equation to calculate it with the friction factor of van Rijn (2007), the following can be obtained:

$$u_c = \sqrt{\frac{\tau'_{b,c}}{0.5\rho_w f_{cvr}}} \tag{B.5}$$

It may be noted that for this depth averaged velocity a logarithmic profile is assumed. This might not be the case for the wave with current conditions. Since the database does not provide the required depth averaged current velocity, this method will be used.

Appendix E : SANTOSS without phase-lag

The SANTOSS model accounts for the influences of the phase-lag with equation (4.62) until equation (4.71). This appendix shows how this streaming component influences the model performance. The performance of the SANTOSS model without the streaming component is shown in Figure 30 and Table 18. The phase-lag effects are removed from the model by manually adjusting the values of P_t and P_s to 1. As seen in Figure 30 and Table 18, the model significantly decreases. Just like the N06 and the VR07 models, sand transport into the wrong direction can be observed for the rippled-bed conditions. For the rippled-bed conditions, 79% of the calculated transports are in the wrong direction.

Table 18 The performance of the SANTOSS model without the phase-lag component.

Total	N	Factor 2	Factor 5	Wrong direction
All wave dominated datasets	211	53%	72%	25%
Data subset: type of flow				
Velocity-skewed waves (without currents)	94	36%	43%	53%
Acceleration-skewed waves (without currents)	53	58%	98%	2%
Waves with a superimposed current	50	78%	90%	2%
Surface waves	14	50%	100%	0%
Data subset: type of bed form				
Flat bed (Sheet flow)	155	69%	92%	5%
Rippled-bed	56	7%	14%	79%

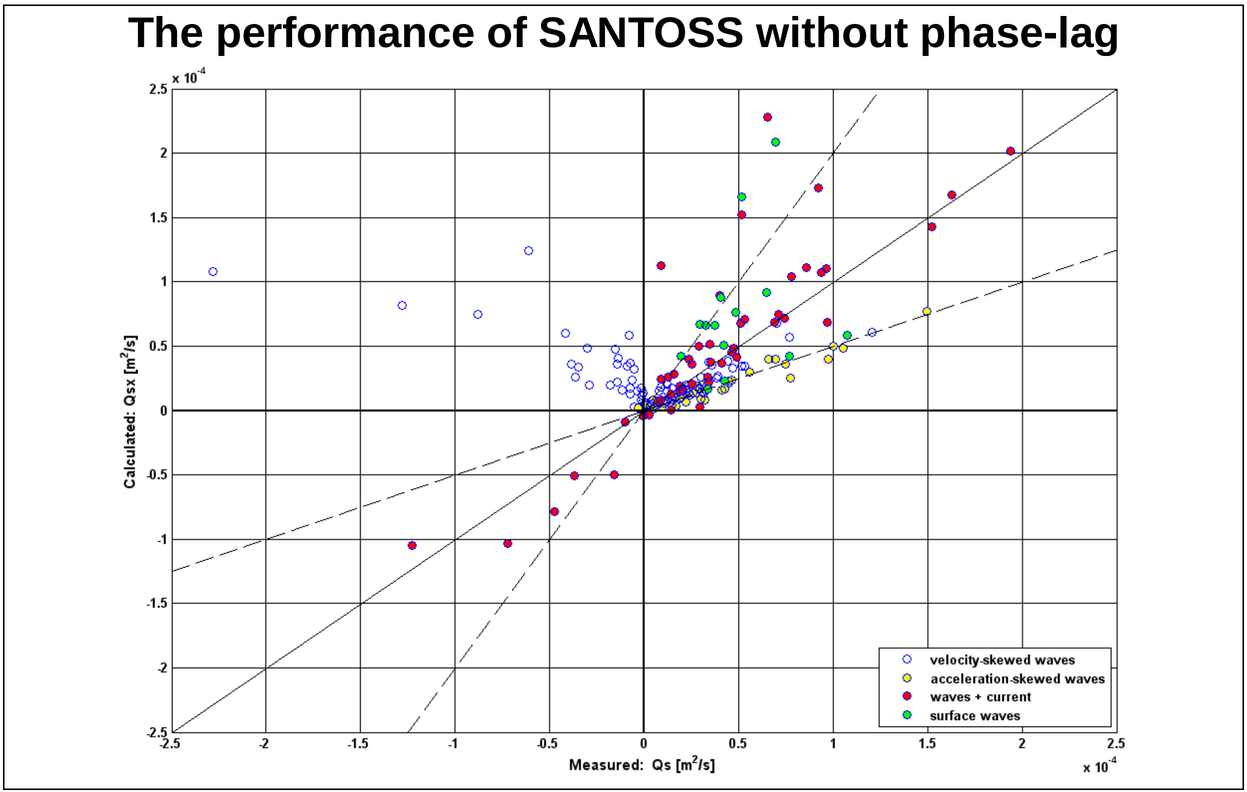

Figure 30: The transport calculated with SANTOSS without the component to account for the effects of phase-lag. The solid line indicates perfect agreement; the dashed lines a factor 2 difference.

Appendix F : N06 with phase-lag parameter for sheet flow and rippled-bed conditions

Chapter 8 shows that using the approach of the SANTOSS model to account for the influences of the phase-lag effects improves the performances of N06 and VR07. The phase-lag parameter is only applied to the rippled-bed conditions and not to the sheet flow conditions. This appendix shows an example of including the phase-lag parameter for rippled-bed conditions *and* sheet flow conditions. For this example, the adjusted N06 model is used (see Chapter 8). An example is presented with the calibration coefficients α_s =2 and α_r = 13.94. The phase-lag effects for sheet flow conditions are included in this example since $\alpha_s > 0$.

The measurements show that under fine sand sheet flow conditions with velocity skewed waves sand transports are offshore directed in OFT experiments and onshore directed in surface wave experiments. Table 19, Figure 31 and Figure 32 presents the results of the adjusted N06 with α_s =2 and α_r = 13.94. After the inclusion of the phase-lag parameters most of the transports of fine sand under sheet flow conditions are correctly predicted into the offshore direction. However, the transports under fine sand surface wave conditions are now also predicted into the offshore direction. The wrong prediction under surface wave condition is due to the fact that N06 does not account for the influences of vertical orbital velocity and Lagrangian motion. These two processes reduce the influences of the phase-lag effects under surface wave conditions. Since the performance of the surface wave conditions decreases, including the phase-lag effects for sheet flow conditions is not a useful adjustment.

Table 19 The performance of the adjusted N06 model with α_s =2 and α_r = 13.94.

Total	N	Factor 2	Factor 5	Wrong direction
All wave dominated datasets	211	67%	90%	7%
Data subset: type of flow				
Velocity-skewed waves (without currents)	94	64%	86%	9%
Acceleration-skewed waves (without currents)	53	55%	94%	2%
Waves with a superimposed current	50	86%	96%	4%
Surface waves	14	64%	79%	21%
Data subset: type of bed form				
Flat bed (Sheet flow)	155	73%	92%	5%
Rippled-bed	56	50%	84%	11%

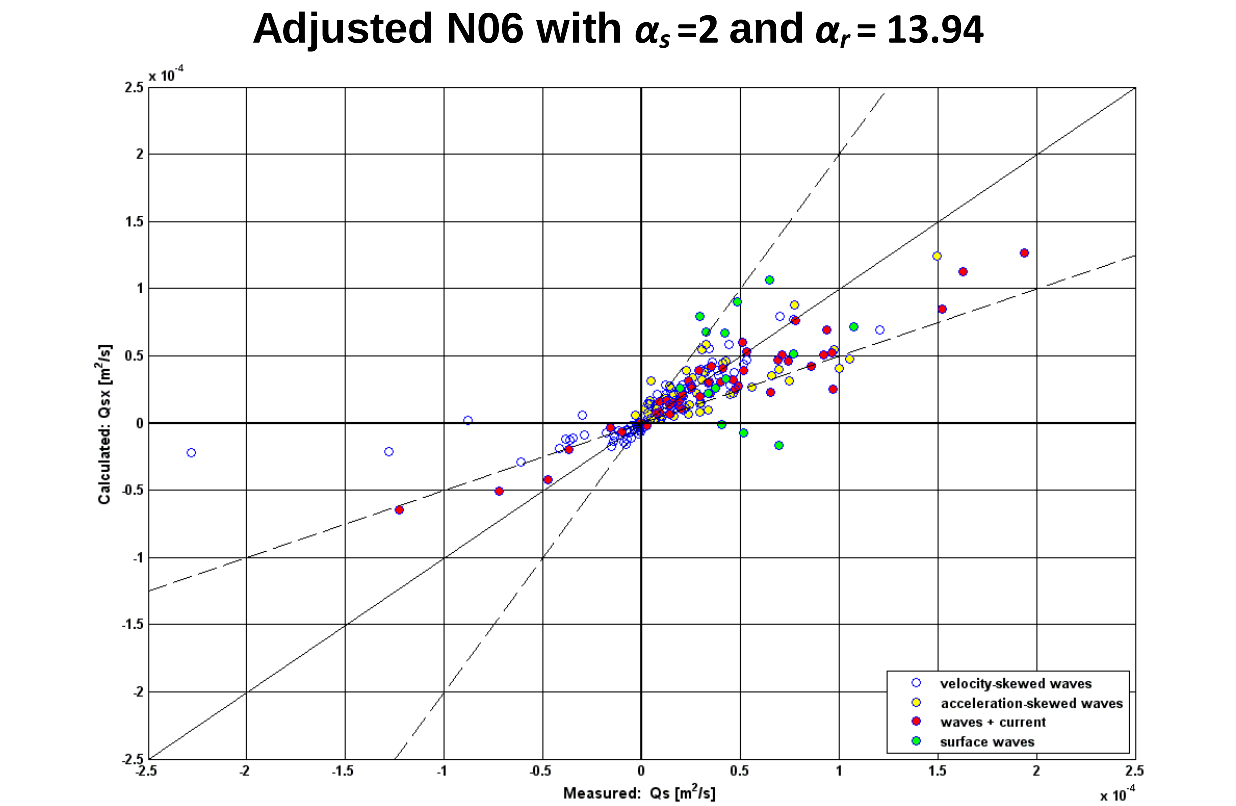

Figure 31: The adjusted N06 with α_s =2 and α_r = 13.94. The solid line indicates perfect agreement; the dashed lines a factor 2 difference.

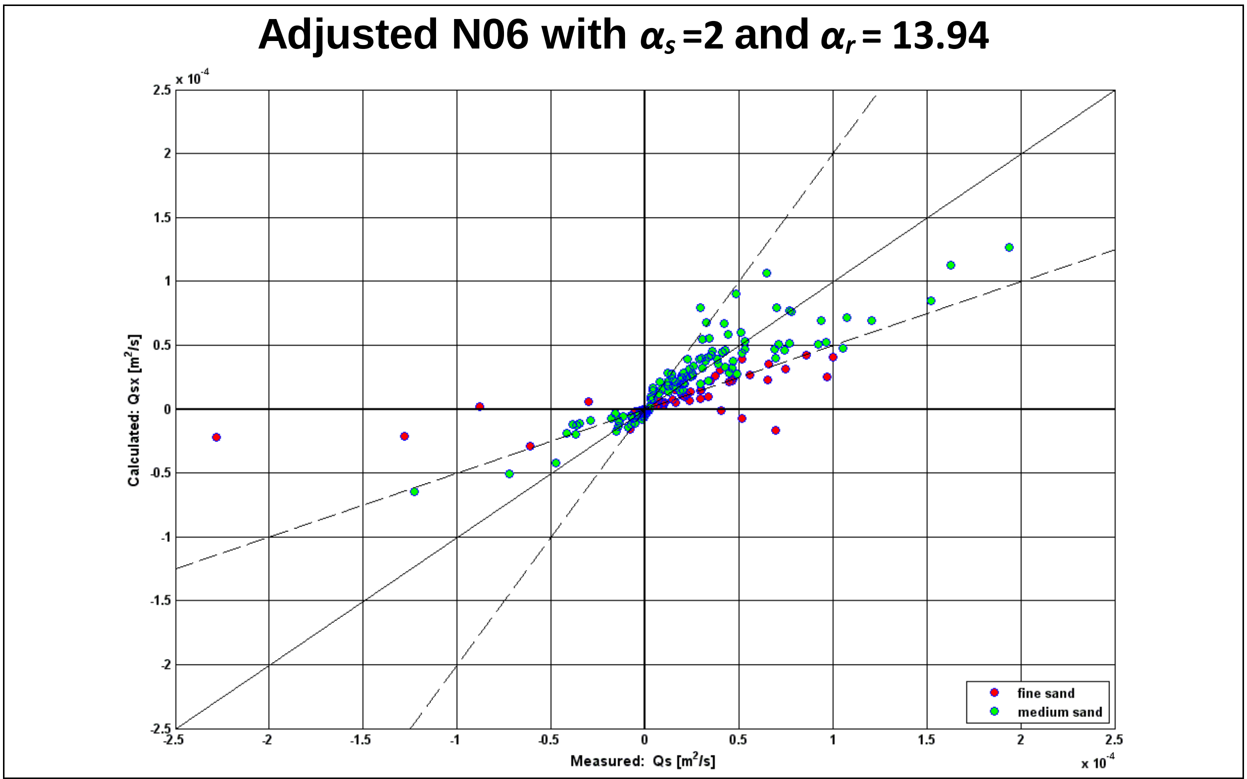

Figure 32: The adjusted N06 with α_s =2 and α_r = 13.94. The solid line indicates perfect agreement; the dashed lines a factor 2 difference. A distinction is made between fine sand with d50 ≤ 0.2mm and medium sand with d50 > 0.2 mm